November 2017

Robust Biosensors for Healthcare Applications: from High-Content Screening to Point-of-Care Testing

Ngoc D. B. Le
University of Massachusetts Amherst

ROBUST BIOSENSORS FOR HEALTHCARE APPLICATIONS: FROM HIGH-CONTENT SCREENING TO POINT-OF-CARE TESTING

A Dissertation Presented

By

NGOC D. B. LE

Submitted to the Graduate School of the
University of Massachusetts Amherst in partial fulfillment
Of the requirements for the degree of

DOCTOR OF PHILOSOPHY

September 2017
Chemistry

ROBUST BIOSENSORS FOR HEALTHCARE APPLICATIONS: FROM HIGH-CONTENT SCREENING TO POINT-OF-CARE TESTING

A Dissertation Presented

By

NGOC D. B. LE

Approved as to style and content by:

_____
Vincent M. Rotello, Chair

_____
Richard W. Vachet, Member

_____
Michael J. Maroney, Member

_____
Shelly Peyton, Member

_____
Richard W. Vachet, Head
Department of Chemistry

DEDICATION

To my parents, Han Le and Thanh Tran
and my beloved husband, Anthony Le
whose love and support made this possible

ACKNOWLEDGEMENTS

In the past six years of my PhD life, I have received tremendous support from all the people I mentioned here. Without their help and encouragement, it would be extremely difficult to complete my PhD journey.

I would like to first express my deep and sincere gratitude to my research advisor, Professor Vincent M. Rotello. He has taught me a great deal on how to approach and solve a scientific challenge. He is also a great writer from whom I have learned how to set up a scientific problem and address it with my inventions in writing. Throughout my PhD, professor Rotello has always been so patient with me in both my scientific and personal development. I will be forever indebted to him for his efforts and valuable guidance.

I am deeply grateful to my thesis committee members, Prof. Richard Vachet, Prof. Michael J. Maroney, and Prof. Shelly Peyton for their detailed and helpful suggestions during my PhD journey including prospectus and original research proposal (ORP). I am also very thankful for their constructive comments to help improve my thesis.

My dissertation is the result of numerous effective collaborations. Without all the efforts from all of my collaborators, either within or outside of the Rotello research group, I would not be able to complete my thesis. I would like to take this chance to thank Prof. Joseph D. Jerry, Prof. Karen A. Dunphy, Dr. Arvind Singla, Prof. Frank R. Jirik, Dr. Jinsong Han, Dr. Kai Seehafer, Prof. Uwe Bunz, Dr. Huda A. Jerri, Prof. Caren M. Rotello, and Ngoc Thai for successful and productive research collaborations throughout my time here. I would like to specifically thank Dr. Subinoy Rana and Dr. Chang Soo Kim for being my great mentors at the beginning of my PhD journey. I would

also like to acknowledge the help and support from all the past and present Rotello lab members including Yingying, Gulen, Rubul, Sung-Tae, Marcos, Daniel, Gyan, Tatsuyuki, Tsukasa, Moumita, Xian, Ziwen, Rui, Bradley, Colleen, Akash, Singyuk, Bo, Ying, Xiaoning, and Krishnendu. Additionally, I am thankful for administrative and technical support from Carol and JMS. I would also like to acknowledge all the funding sources that allowed me to conduct my research.

Finally, I am deeply grateful for my parents and family members who constantly give moral and financial support to make my dreams come true. Without their help, I would not have accomplished what I can today. I want to especially thank my parents for giving me a wonderful life and a good education in Vietnam, my big sister, Vietha Le, for taking care of me and supporting me during the first two years getting my college education in the US. I want to thank my host family, the Porter family, who took me in as their own daughter during my first year in America. I am also very grateful for the motivation from my parents-in-laws. Lastly, I am forever indebted to my beloved husband, Anthony Le, for his constant support and encouragement. He has always been there for me throughout my long and difficult journey. I am so thankful for his unconditional love, sacrifices, and life-long companionship.

ABSTRACT

ROBUST BIOSENSORS FOR HEALTHCARE APPLICATIONS: FROM HIGH-CONTENT SCREENING TO POINT-OF-CARE TESTING

SEPTEMBER 2017

NGOC D. B. LE

B.S., SHORTER UNIVERSITY

Ph.D., UNIVERSITY OF MASSACHUSETTS AMHERST

Directed by: Professor Vincent M. Rotello

Efficient detection of proteins, mammalian cells, microorganisms and other biological systems in complex mixture is essential in disease diagnosis and environmental health. Therefore, technological platforms that provide sensors of high sensitivity, selectivity and stability are greatly desired. Recently, the 'chemical-nose' sensing approach has proved to be an effective strategy for profiling bio-relevant targets in complex mixtures. Detecting analytes in complex mixture is a challenge that conventional *specificity*-based sensors are still trying to solve due to the requirement of prior knowledge of the analyte, which is unknown in many cases. This thesis focuses on how to develop simple and robust chemical-nose sensors for complex mixtures using supramolecular interactions between nanoparticles, fluorescent proteins, enzymes, and fluorescent polymers. We have successfully developed effective sensors for many healthcare applications including chemotherapeutic drug profiling, cancer diagnostics, environmental toxicity and bacterial detection. Throughout this dissertation, there is an emphasis on moving from high-content screening to point-of-care testing, especially in

cancer diagnostics. Overall, the chemical-nose sensors provide a simple generic tool for bio-relevant analyte profiling, avoiding additional processing steps prior to screening as seen in traditional methods. More importantly, chemical-nose sensors hold great promise for addressing the needs in personalized screening of disease states and environmental toxicology.

TABLE OF CONTENTS

LIST OF TABLES

Table Page

LIST OF FIGURES

Figure Page

CHAPTER 1

INTRODUCTION

1.1. Biosensor

Efficient detection of proteins, mammalian cells, microorganisms and other biological systems in complex mixture is essential in disease diagnosis, forensic, agricultural, and environmental toxicity. Early detection of diseases or identification of harmful chemicals in the environment provide the prospect of better health and alarm people to take appropriate actions in a timely manner. Therefore, technological platforms that provide sensors of high sensitivity, selectivity and stability are in high demand.

Biosensors have two functional components: recognition elements and transducers. Recognition elements are receptors used to recognize and bind to the target analytes. This interaction between the analyte and the receptor is designed to produce an effect that can be measured by a transducer. Receptors can be biological species, such as antibodies, enzymes, proteins, nucleic acid, or synthetic elements such as small molecules, nanoparticles, and polymers. To transduce the analyte-receptor binding event, a number of techniques are available including 1) optical (absorption, luminescence, fluorescence, and surface plasmon resonance), 2) electrochemical, and 3) mass-sensitive measurements (surface acoustic wave and microbalance).

The efficiency of a biosensor is critically related to the outcome of each process associating with each component, recognition and transducer, in term of the response time, signal-to-noise (S/N) characteristics, sensitivity, and selectivity of the system. Thus,

much attention in the field has been focusing on improving the recognition process as well as designing new signal transduction mechanisms. With the advent of nanostructures and new interface materials, the pursuit of new recognition and transduction processes is made possible for the development of novel biosensors.

1.2. Biosensor designs: Lock-and-key specificity *versus* chemical-nose selectivity

Biosensors can be broadly split into two types of sensing designs: highly specific sensing (lock-and-key approach), and array-based selective sensing (chemical-nose approach). The former is a sensor that in its strict definition would be completely specific to a single analyte and not recognize any other targets. In this context, the receptor is the lock and the analyte is the key. The notion leads to the concept of one key that is complementary to one lock, thereby opening up only one lock, recognizing only one target. This idea is approached by antibodies, lectins, aptamers and enzymes. As an example for using an antibody in identifying and capturing a target analyte, Sha and coworkers developed a sensor for cancer circulating cells (CTCs). This sensor was fabricated by combining capturing capability of a magnetic bead and specific labeling of surface enhanced Raman scattering (SERS) nanotags.[1] This bead was conjugated with anti-EpCAM antibody to capture SKBR3 cancer cells. These cells were then labeled for SERS detection by gold nanoparticles (AuNPs) functionalized with anti-HER2 antibody (human epidermal growth factor receptor-2) (Figure 1.1).[2] In a similar study, SERS-based systems were further employed for in vivo tumor targeting.[3]

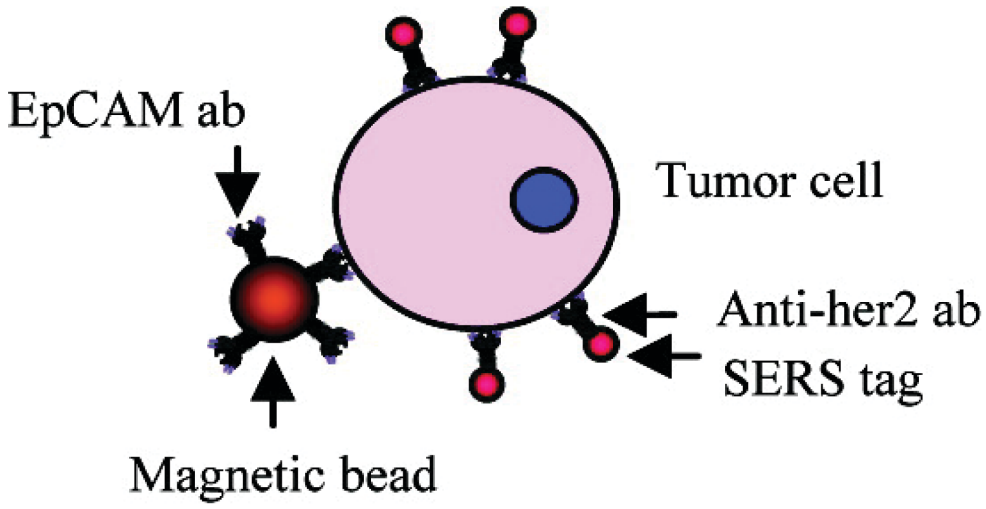

Figure 1.1. Schematic illustration of the immuno-complex formed by nanoplex biotags and magnetic bead conjugates binding to the model tumor cell. Republished with permission from ref. 1.

There are several advantages when using the lock-and-key approach such as the absence of false positive results and an ultrasensitive detection.[4] However, since specific recognition-based sensors require pre-identification of the biomarkers, they face certain limitations when the analytes are unknown and/or their structures are not fully characterized. In that case, detecting unknown analytes using lock-and-key sensing approach is impractical. In addition, even when the biomarker is known, the specific sensing approach would not be an ideal test for systems that contain multiple analytes with varied biomarker levels among cell populations. For example, cancer cells present multiple biomarkers on the cell surface and these markers coexist in normal cells at different levels, making the detection of a specific biomarker that is strictly associating with only cancer status nearly impossible. These subtle changes in the biomarker levels could be indicative of dramatic phenotypic differences. As an alternative, sensors using

selectivity-based modality do not require the knowledge of a specific biomarker. On the contrary, selectivity-based approaches capture the responses from complex analytes to generate a signature for each sample. In a typical array-based sensor, a set of recognition elements interacts with a number of different analytes or classes of analytes, providing a process reminiscent of mammalian olfaction.[5] This mechanistic similarity is why array-based sensors are often denoted as chemical ‘‘noses’’ or ‘‘tongues’’ (Figure 1.2).[6]

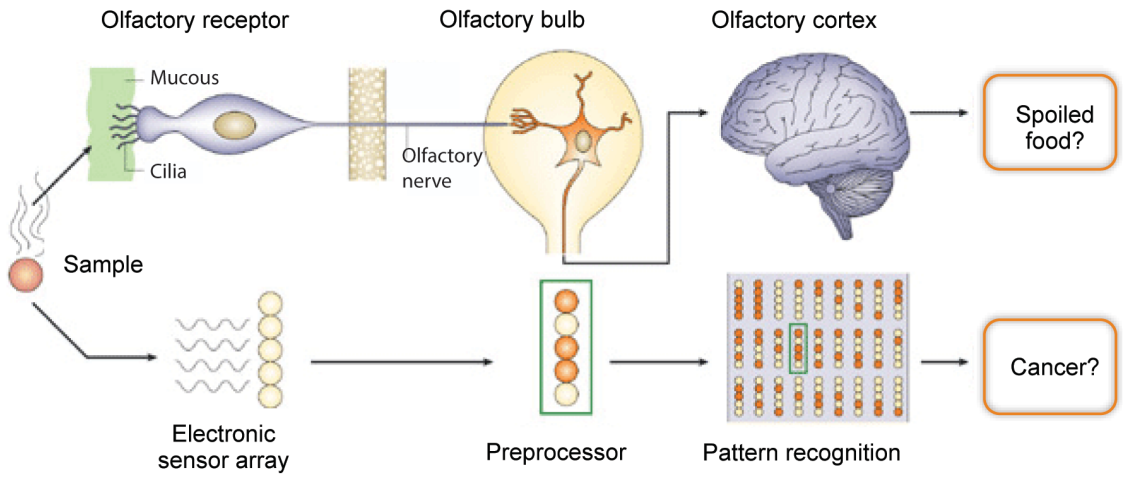

Figure 1.2. Electronic nose devices mimic the human olfactory system. Adapted from ref. 6.

Chemical-nose sensing approach mimics the mammalian olfactory system to recognize mixtures of analytes. Overall, there are about 1000 genes that encode olfactory receptors, and each olfactory receptor has multiple sites for odorant binding with different affinity levels. This characteristic is known as crossreactivity.[7,8] A generated unique signaling fingerprint for a specific odorant is then interpreted in the olfactory cortex by matching the signal with previously established patterns of analytes. This process makes it possible to distinguish between thousands of odorants using just much

fewer numbers of olfactory receptors (Figure 1.2). The effort of mimicking the olfactory system for analyte detection has led to the first model of an 'electronic nose', reported by Persaud and Dodd in 1982.[9] Their idea was to detect different volatile compounds by mimicking the three different stages of the human olfactory system, including interacting with the odorant, establishing the pattern of the odorant, and identifing what the odorant is using biochemical sensors.

The advantage of chemical-nose sensor is that it can be trained to recognize complex mixtures without the knowledge of what types of biomarkers the mixture contains. Chemical-nose approach is useful when the disease lacks an ideal biomarker or biomarkers are poorly characterized such as in cancer disease. This method has been used to sense calcium and metal ions, pH levels, sugars as well as cholesterol levels in blood, cocaine in urine, and toxins in water.[10,11] Chemical nose sensors can also recognize a wide range of volatile organic compounds,[12] amino acids,[13] proteins,[14] carbohydrates,[15] mammalian cells.[16]

One of the strengths of nose-based sensing is the versatility of the methodology. This versatility provides a challenge: array-based sensors need to be retrained and validated for each new analyte, and baseline profiles for known samples must be carefully examined to maximize accuracy.[17] Perhaps the greatest challenge of nose type sensing is the fundamental difference between this method and other biomarker-based strategies. Just like our sense of smell, sensing using olfaction mimics is inherently hypothesis-free, a situation with which many researchers are not yet comfortable. In this dissertation, we focus on the development of chemical-nose sensors for healthcare applications.

1.3. Gold nanoparticles and fluorescent polymers as efficient receptors for chemical-nose sensor designs

Gold nanoparticles (AuNPs) possess several distinctive physical and chemical attributes that make them promising synthetic scaffolds for creating novel biosensor systems.[18] First of all, the size of the NP core is tunable from 1 – 150 nm, an ideal size for the interaction of AuNPs with bio-relevant analytes.[19] The high surface area-to-volume ratio of AuNPs provides dense ligand loading, enhancing the interaction with analytes.[20] These particles typically have a hydrophobic core for stability. For biological applications, oligo(ethylene glycol) (OEG) is added in the linker to enhance biocompatibility and minimize non-specific adsorption of other materials. Lastly, recognition receptors on the surface of AuNPs are used for the interactions with bio-analytes. A common structure of ligands on a AuNP for biomolecular interactions is shown in Figure 1.3. Most importantly, AuNPs have excellent quenching ability for fluorophores, an ideal feature for biosensor design.

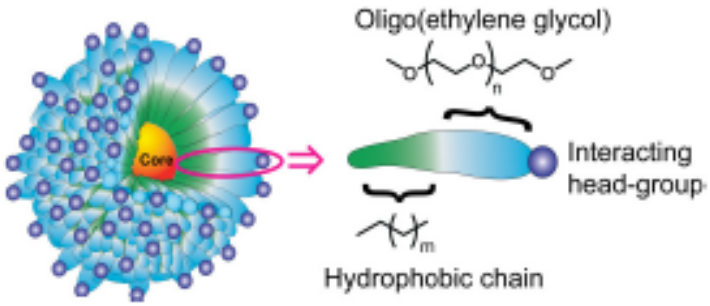

Figure 1.3. Schematic of common surface ligands on AuNPs used for interactions with biological systems. The multifunctional particle monolayers featuring a hydrophobic core for stability, OEG layer for biocompatibility, and recognition elements on the surface for interaction with biomolecules.

The diverse ligand functionalities enabled by the ease of AuNP synthesis, along with unique features of AuNPs as mentioned above provide a versatile scaffold for constructing biosensor using chemical-nose approach. Our group has pioneered the use of AuNPs for chemical-nose sensing systems by non-covalently assembling AuNPs with different types of transducers such as fluorescent proteins (including EBFP2, EGFP, and td Tomato) and conjugated fluorescent polymers. In this design, cationic AuNPs with various functional headgroups form supramolecular complexes with anionic fluorescent proteins or polymers (poly(p-phenyleneethynylene) (PPE) to quench their intrinsic fluorescence. Competitive bindings of the bio-analytes release the fluorescent proteins or polymers, resulting in their fluorescence recovery.[21,22] This approach has been used successfully for protein, cell, and tissue identification.

Another type of receptor that is suitable for the design of chemical-nose sensor is fluorescent polymer. Besides the use of fluorescent polymer as transducers as described previously, conjugated polymers can also act as receptor to recognize bio-analytes. Unlike small molecules and nonconjugated polymers, these conjugated polymers are more responsive to conformational or environmental changes due to its unity of delocalized electronic structure of the polymer backbones. Such behavior of conjugated polymers provides more dynamic interactions (either intra- or intermolecularly) that could lead to various changes in the fluorescence outputs, providing a rich signature profile for complex analytes, a requirement for chemical-nose approach. Conjugated polymers can be designed to have high fluorescence quantum yields in aqueous solution and ability to interact electrostatically with other charged species. These water-soluble

polymers are also attractive because of their easily tailoring multivalent functionalities, stability, and scalability properties. Some of the conjugated polymers that have been used for chemical nose sensing are poly(p-phenyleneethynylen) (PPEs) and poly(*p*-aryleneethynylene)s (PAE) for the detection of proteins, antibiotics, explosives, and fruit juices.[23-26]

1.4. High-content screening: ideal space for chemical-nose sensors

There is always high demand for rapid identification of mechanisms in drug discovery and detections of serious diseases. Thus, high-throughput screening (HTS) and high-content screening (HCS) have been extensively implemented to meet the demand. While HTS focuses on rapid examination of the effects of thousands of testing compounds in various *in vitro* and cell-based assays, HCS approaches might sacrifice some of the high-throughput speed to achieve more information in phenotypic complexity measured by the assay endpoints.

Whole cells have been the major target for many assays and have the potential to provide rapid sensing with minimal processing, in contrast to approaches that need to physically extract cell contents such as intracellular proteins, nucleic acids, or other markers buried inside the cells. The rich environment presented by the cell exterior also gives cell sensors the capability to read out the phenotypes of cells, a property that is the final outcome of multiple factors including both genetic and epigenetic variations. Taking advantage of the final phenotypic outcome of cells, HCS uses a set of analytical methods such as automated microscopy, multi-parameter image processing, and visualization tools

to extract data from different features of cell populations. These features include spatial distribution of targets, individual cell and organelle morphology. For example, Young and coworkers have developed a HCS method to profile mechanisms of action in drug discovery that combines signals from multiple fluorescence probes that show cells' features such as nuclear size, DNA replication, chromosome condensation, nuclear morphology, and nuclear ellipticity. Some of these features have obvious biological meaning such as the amount of DNA per nucleus. However, the biological importance of other features has much less obvious meaning such as the DNA texture or nuclear ellipticity. Biologists usually overlook these non-obvious features since they are not 'hypothesis-driven' markers, even though they may contribute some valuable insights. The goal of HCS is to create a unique fingerprint of cell phenotypes composed of multiple specific cell features using various fluorescence probes. These HCS approaches are very powerful in profiling mechanism/cell status of interested. However, as we can imagine, extracting numerous cell phenotypic features through staining, fixing and imaging, these HCS methods face the limitation of multi-step processing of cells prior to analyses. There are also challenges arising from limited dynamic range, time consuming steps, and expensive instrumentation that restrict the applicability of these methods for rapid screening.

As mentioned earlier, since chemical-nose sensor can create fingerprints for each analyte including all obvious and non-obvious features of cells in a very rapid manner, it presents an ideal method for minimizing number of cellular parameters typically found in HCS assays to greatly expedite drug development and disease diagnosis.

1.5. Chemical-nose sensors offer a new avenue for point-of-care testing

Changes in healthcare delivery trend have driven the widespread of point-of-care testing (PoC) in disease diagnosis. This change is partly due to economic pressures and the general recognition that cares need to be less fragmented and more patient-centered.[27] The concept of PoC testing is aimed at delivering less costly care, closer to the patient's home and not around the provider. Typically, the testing process is quite disconnected with the consultation process such that a patient has to deal with multiple doctor visits to complete the health assessment. This issue appears clearly for those who have chronic diseases such as diabetes where regular monitoring of glucose level by frequent blood test is necessary. As a result, the growth in self-monitoring of blood glucose up to date is the evidence for the need of more convenient and sometimes, more effective care.[28,29]

Table 1.1. The ASSURED guidelines that indicate the features that should be designed into all POC testing devices. Adapted from ref. 28.

Affordable - for those at risk of infection
Sensitive - minimal false negatives
Specific - minimal false positives
User-friendly - minimal steps to carry out test
Rapid & **R**obust - short turnaround time and no need for refrigerated storage
Equipment-free - no complex eqipment
Delivered - to end users

PoC testing can be divided into two categories: 1) small handheld devices and 2) larger bench-top devices. The former type usually provides qualitative or semi-quantitative determination of analyte concentrations. Some of the dominant technologies are glucose biosensor strips or lateral flow strips using immobilized antibodies for biomarker detections such as cardiac markers and infectious pathogens.[29] The second category includes larger devices to use in a laboratory setting but with reduced size and complexity. These devices are used to monitor 'critical care' analytes such as blood gases, electrolyte, and certain metabolites. Recently, molecular technique such as PCR was incorporated into a sufficiently small device for infectious disease testing at the point of care. The World Health Organization (WHO) determined desired features for PoC devices as listed in Table 1.1, a guideline known as ASSURED.[29] Of course, some features might be more important than others, depending on the final end-users and purposes (Figure 1.4). To further improve the concept of PoC testings to include the parameters of end-users and test purposes that are lacking in the ASSURED guideline, a recent PoC concept has been developed. This concept views PoC testing as multiple components including 1) the complexity of technologies that ranges from simplest to more sophisticated, 2) users including lay persons to highly trained workers, 3) settings in which the test is needed including home, communities, clinics, peripheral laboratory, and hospital. When we separate PoC need based on diverse settings, PoC tests do not need to meet all the requirements listed in the ASSURED guideline. For example, malaria rapid diagnostic tests used by community health workers in Africa or in-home pregnancy tests need to be very simple, instrument-free and straightforward because the goal here is self-assessment. At the other end of the spectrum showed in Figure 1.4, hospitals have

starting to implement more PoC testing programs. For example, emergency room doctors use handheld ultrasound devices to rapidly diagnose and treat pregnancy complications. Rapid tests are also being used in intensive care units to make timely decisions on patient treatments. In this setting of health care delivery system, tests do not need to be instrument-free or inexpensive. The users for these PoC tests are often well trained.

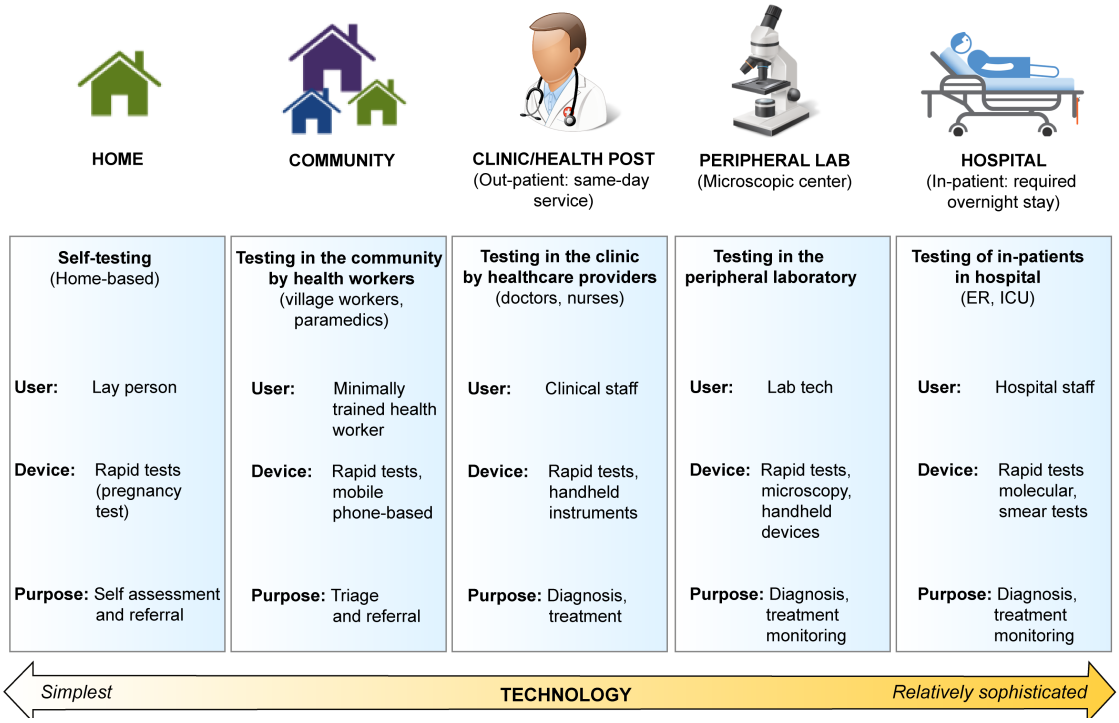

Figure 1.4. The spectrum of point-of-care testing. Adapted from ref. 30

The implementation of PoC devices will have tremendous healthcare and economic benefits, especially in developing countries where easy access to health providers is still limited. Looking through the lens of a global scale in both developing and developed countries, PoC testing will reduce the cost of disease diagnosis, improve survival and recovery rate of patients through more effective therapeutic treatments. This trait is the direct result of early detection, a blessing provided by PoC's ease of use.

Despite much success in PoC testing, there are clearly areas where new PoC technologies are lagging behind such as in cancer and infectious disease. The challenge of developing PoC testing for these areas lies in the identification of an ideal biomarker. For example, in cancer diagnosis, the search for the ideal biomarker that only associates with the presence and the progress of cancer status is poorly characterized. There is a wide baseline of biomarker in the population, even within the subpopulation of patients that have the same type of cancer. This observation triggered the development of personalized diagnostic devices for personalized medicine via patient-specific disease profiling.

Chemical-nose sensors have great potential to advance personalized medicine. The robustness of the system comes from the crossreactivity nature of nose sensors. They can be trained and retrained for any analyte, any disease status, and any specific patient with a simple design and no requirement of expensive and sophisticated instruments. In 2015, a perfect example of using the nose sensor for cancer diagnosis was reported in *The Guardian* newspaper about a dog, named Frankie, who could detect thyroid cancer with 88 % accuracy among patients. Frankie was trained to lie down in front of patients' urine samples if he detected metastatic cancer.[30]

Researchers have been focusing on developing biomimetic devices that capable of detecting cancer as seen in the dog, Frankie. Currently, the use of urine[31] and breath[32] as samples in cancer diagnosis has been employed due to their attractive noninvasiveness. When using urine samples as biofluids for analysis, one challenge is that the concentrations of naturally occurring biomarkers are typically low. To compensate for this limitation, an array of sensors with the ability to amplify biomarker concentration in

urine has been developed.[33] For this purpose, a class of engineered mass-encoded peptides with specific protease-sensitive moieties conjugated to iron oxide NPs were synthesized. These synthetic biomarkers passively accumulate in the cancer tissue after administration. Aberrantly active proteases in the tumor subsequently cleave the protease-sensitive agents of these NPs, with the resulting fragments excreted in the urine.[34] Using a library of different substrates as the protease-specific mass signatures, differentiation between different proteases was possible. The unique profiles of the isobar-coded reporters for each protease were identified.

Another noninvasive sample type for PoC testing in cancer diagnosis is breath obtained from patients. Perhaps, breath sensing is the least invasive of all diagnostic strategies. Metabolic reactions in the body generate different volatile organic compounds (VOCs). These VOCs include hydrocarbons, alcohols, aldehydes, ketones, esters, nitriles and aromatic compounds. VOCs can be detected in diverse biosamples, such as cancer cells, blood, urine, skin/sweat[35,36] and breath. In fact, besides cancer detection, VOCs are being used as new diagnostic-based biomarkers for detection of different diseases such as diabetes,[37] Alzheimer's, Parkinson's,[38] and chronic kidney disease.[39] Compared with healthy individuals, cancer patients express different VOC compositions in their breath due to the different activities of cancer cells.[32] These activities can generate very subtle changes in the concentration and composition of VOCs in the blood stream. Through constant exchange between the lung and bloodstream, these subtle changes in VOC compositions can be transported to the patient's breath, creating distinct breath signatures for each cancer type.[40] In a healthy breath, the concentrations of several VOCs are normally in the range of 1–20 p.p.b.[12] However, they can be detected in the levels of 10–

100 p.p.b. in some cancer types. These changes in concentration and composition mixture of VOCs have made it possible to not only distinguish between the breath of healthy individuals and cancerous patients, but also differentiate between different types of cancer.[12,32] Previously, VOCs have been detected using gas sensors such as gas chromatography,[41] and ion mobility spectrometry.[42] However, the downsides to these methods are that they are time consuming and require large size, expensive instrumentation and an expert operator. Moreover, to improve the detection in some of these devices, capturing and preconcentrating the breath sample is a prerequisite step.[43,44] Using the advantages of NPs, a nanoscale artificial nose has been designed by Haick and co-workers.[44] This simple, cost effective and portable sensor is able to detect cancer by analyzing the VOCs using pattern recognition methods. The nanoscale artificial nose is capable of identifying different odors even at very low concentrations and subtle differences.[44] The gas sensor is based on an array of highly cross-reactive chemiresistors made of AuNPs with different organic capping layers. In the resulting sensor, electrical conductivity was provided by the metallic particles and the organic capping layers create sites used to capture the analytes.[12]

Due to the chemical diversity of sensor materials, each sensor of the array shows a unique response to a certain group of VOCs. This means that the characteristic signal (electrical resistance) of each sensor in the array changes specifically when exposed to a specific VOC, which could be the cancer specific odor.[44] Consequently, for each cancer type, a distinct fingerprint is produced from the array of cross-reactive sensors. Using this gas sensor along with pattern recognition methods, it is possible to discriminate different cancer types and stages.[32,45] It is also worth mentioning that these sensor arrays have

detection limits of 1–5 p.p.b. or even down to approximately 10 p.p.t.[32] Breast, lung, colon, gastric, colorectal, head-and-neck and prostate cancer are the cancer types that have been detected using this sensor. Carbon nanotube arrays have been used in a similar fashion.[46,47]

It should also be mentioned that although breath sensing is a novel method for cancer detection, the approach has some limitations. First of all, there are not dramatic changes in VOCs in the early stages of cancer development; only certain stages will cause the expression of these VOCs. Second, the conditions and type of foods and drinks consumed by patients can influence results. The results can also be affected if the patients have other diseases and are using other medicines.[32] Therefore, having sufficient controls over sample collection is essential when using this type of noninvasive sample.

1.6. Chemometric analysis for data processing

In an array-based sensing strategy, each analyte produces a response from each of the sensor elements. A multivariate data matrix is obtained from different analytes. As a result, a large number of generated data has to be analyzed quickly and efficiently to establish high quantity of fingerprints for identification. These data can be analyzed using multivariate chemometrics methods. These methods consist of a collection of techniques that can be used when several measurements are done on each individual analyte. Among these techniques, principal component analysis (PCA) and linear discriminant analysis (LDA) are most commonly used. These methods reduce the dimensionality of the data

sets by extracting the most useful information into new and simpler components called principal components or canonical factors for LDA.

PCA is one of several multivariate methods that explore patterns in these data. PCA can determine the general relationship between these data by indicating which analytes behave similarly (in another words, which analytes belong to a similar group). While it is useful to know the pattern of these data, identifying which group a new unknown analyte belongs to is necessary. LDA as a classification (supervised pattern recognition) method is used for this purpose. In the classification methods, samples with known identities are used to define the groups (classes). These known sets of samples are referred to as a training set. The unknown analytes can then be assigned to the predefined groups using the appropriate classification algorithm.[48,49] In the present dissertation, we extensively utilized LDA for data analysis using SYSTAT software (version 11).

1.7. Dissertation overview

Chemical-nose sensing approach has proved to be an effective strategy for profiling biorelevant targets such as proteins, glycans, and mammalian cells. However, it is still a long haul to implement chemical-nose sensors in clinical applications due to certain challenges discussed in section 1.2. Addressing the challenges associated with chemical-nose approach is critical to close the gap from basic research to practical applications. Keeping this goal in mind, my research has focused on fabricating biocompatible sensor elements for healthcare applications using supramolecular chemistry of functionalized AuNPs, fluorescent proteins, fluorescent polymers and

enzymes. This dissertation covers three main themes: cancer therapeutic drug profiling and cancer diagnostics (Chapter 2-4), environmental toxicity (Chapter 5), and bacterial detection (Chapter 6) (Figure 1.5).

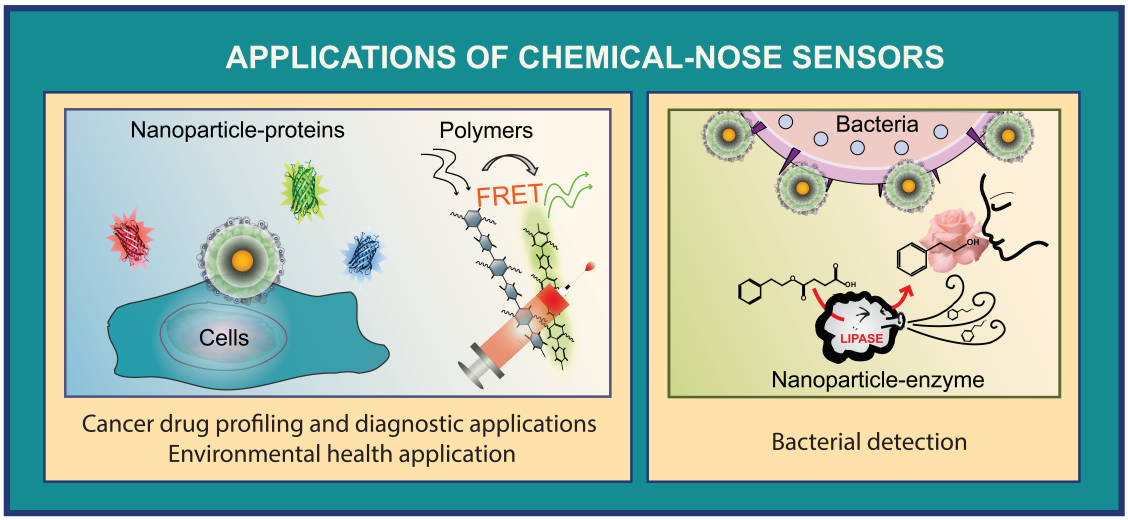

Figure 1.5. Overview of the dissertation, which includes the use of nanoparticle-proteins, fluorescent polymers, and nanoparticle-enzyme for healthcare applications.

In the first theme where cancer is the topic of interest, **Chapter 2** discusses the use of supramolecular complexes between cationic AuNPs and three fluorescent proteins (FPs) for mechanism profiling of chemotherapeutic drugs in a high-content screening manner. **Chapter 3** focuses on the improvement of chemical-nose sensors for cancer diagnostics based on the 3-channel platform established in Chapter 2. In this chapter, an innovative supramolecular interaction was used to double the output channels of a sensor array without additional synthesis. This simple approach provides single-well identification of cancer cell lysates and opens up a new dimension for array-based sensor design. The system also uses minimal sample quantity of cell lysates (200 ng, ~1000 cells), making the methodology compatible with microbiopsy technology, a step closer to

PoC testing. **Chapter 4** presents the transformation of chemical-nose sensor in the PoC testing field. This chapter discusses the use of a polymer-based sensor to rapidly detect cancer, based on changes in serum protein levels. Using this approach, only small quantity of serum sample is needed, allowing a rapid and simple test for cancer diagnostics. The system was validated using serum collected from different animal models. This polymer-based sensor holds the potential to stand at the forefront of the field as it solves the problem of multiple array components typically found in chemical-nose sensors, along with the ease of detection using serum. In this system, only two polymers were used while maintaining high sensitivity and specificity for cancer detection, exceeding the standard clinical benchmark.

In the second theme of environmental health, **Chapter 5** discusses the extended use of nanoparticle and green fluorescent protein complexes in a cell-based assay to detect cellular changes due to hormone disruptor exposures. The use of our sensor in this application offers a simple way of screening toxic chemicals released into the environment.

In the third theme of bacterial detection, **Chapter 6** discusses the need of a PoC test for bacteria that can be used in the field. The supramolecular complexes between nanoparticles and enzymes provide a highly efficient sensor platform for bacteria using human sense of smell as an output, a convenient way that promotes equipment-free sensing platform.

1.8. References

(1) Sha, M. Y.; Xu, H. X.; Natan, M. J.; Cromer, R. *J. Am. Chem. Soc.* **2008**, *130*, 17214-17215.

(2) Mulvaney, S. P.; Musick, M. D.; Keating, C. D.; Natan, M. J. *Langmuir* **2003**, *19*, 4784-4790.

(3) Qian, X. M.; Peng, X. H.; Ansari, D. O.; Yin-Goen, Q.; Chen, G. Z.; Shin, D. M.; Yang, L.; Young, A. N.; Wang, M. D.; Nie, S. M. *Nat. Biotechnol.* **2008**, *26*, 83-90.

(4) Rich, R. L.; Myszka, D. G. *J. Mol. Recogn.* **2008**, *21*, 355-400.

(5) Le, N. D. B.; Yazdani, M.; Rotello, V. M. *Nanomedicine* **2014**, *9*, 1487-1498.

(6) Turner, A. P. F.; Magan, N. *Nature Rev. Microbiol.* 2004, *2*, 161-166.

(7) Katada, S.; Hirokawa, T.; Oka, Y.; Suwa, M.; Touhara, K. *J. Neurosci.* **2005**, *25*, 1806-1815.

(8) Buck, L. B. *Angew*. *Chem*. *Int. Ed.* **2005**, *44*, 6128-6140.

(9) Persaud, K.; Dodd, G. *Nature* **1982**, *299*, 352-355.

(10) Wiskur, S. L.; Floriano, P. N.; Anslyn, E. V.; McDevitt, J. T. *Angew. Chem. Int. Ed.* **2003**, *42*, 2070-2072.

(11) Lavigne, J. J.; Savoy, S.; Clevenger, M. B.; Ritchie, J. E.; McDoniel, B.; Yoo, S. J.; Anslyn, E. V.; McDevitt, J. T.; Shear, J. B.; Neikirk, D. *J. Am. Chem. Soc.* **1998**, *120*, 6429-6430.

(12) Peng, G.; Tisch, U.; Adams, O.; Hakim, M.; Shehada, N.; Broza, Y. Y.; Billan, S.; Abdah-Bortnyak, R.; Kuten, A.; Haick, H. *Nat. Nanotechnol.* **2009**, *4*, 669-673.

(13) Folmer-Andersen, J. F.; Kitamura, M.; Anslyn, E. V. *J. Am. Chem. Soc.* **2006**, *128*, 5652-5653.

(14) De, M.; Rana, S.; Akpinar, H.; Miranda, O. R.; Arvizo, R. R.; Bunz, U. H. F.; Rotello, V. M. *Nat. Chem.* **2009**, *1*, 461-465.

(15) Wright, A. T.; Zhong, Z. L.; Anslyn, E. V. *Angew. Chem. Int. Ed.* **2005**, *44*, 5679-5682.

(16) Kong, H.; Liu, D.; Zhang, S. C.; Zhang, X. R. *Anal. Chem.* **2011**, *83*, 1867-1870.

(17) Srinivas, P. R.; Kramer, B. S.; Srivastava, S. *Lancet Oncol.* **2001**, *2*, 698-704.

(18) Rosi, N.; Mirkin, C. A. *Chem. Rev*. **2005**, *105*, 1547-1562.

(19) Hostetler, M. J.; Wingate, J. E.; Zhong, C. J.; Harris, J. E.; Vachet, R. W.; Clark, M.

R.; Londono, J. D.; Green, S. J.; Stokes, J. J.; Wignall, G. D. et al. *Langmuir* **1998**, *14*,

17-30.

(20) Love, J. C.; Estroff, L. A.; Kriebel, J. K.; Nuzzo, R. G.; Whitesides, G. M. *Chem. Rev.* **2005**, *105*, 1103-1169.

(21) Bajaj, A.; Miranda, O. R.; Kim, I. B.; Phillips, R. L.; Jerry, D. J.; Bunz, U. H. F.; Rotello, V. M. *Proc. Natl. Acad. Sci. U.S.A.* **2009**, *106*, 10912-10916.

(22) Bajaj, A.; Rana, S.; Miranda, O. R.; Yawe, J. C.; Jerry, D. J.; Bunz, U. H. F.; Rotello, V. M. *Chem. Sci.* **2010**, *1*, 134-138.

(23) O. R. Miranda, C. C. You, R. Phillips, I.-B. Kim, P. S. Ghosh, U. H. F. Bunz and V. M. Rotello, *J. Am. Chem. Soc.*, **2007**, *129*, 9856–9857.

(24) Han, J. S.; Wang, B. H.; Bender, M.; Pfisterer, J.; Huang, W.; Seehafer, K.; Yazdani, M.; Rotello, V. M.; Rotello, C. M.; Bunz, U. H. F. *Polym. Chem.* **2017**, *8*, 2723-2732.

(25) Wang, B.; Han, J.; Bender, M.; Seehafer, K.; Bunz, U. H. F. *Macromolecules* **2017**.

(26) Han, J. S.; Wang, B. H.; Bender, M.; Seehafer, K.; Bunz, U. H. F. *Analyst* **2017**, *142*, 537-543.

(27) Kemp, H. *Ann. Clin. Biochem.* **2013**, *50*, 632-632.

(28) Olansky, L.; Kennedy, L. *Diabetes Care* **2010**, *33*, 948-949.

(29) St John, A.; Price, C. P. *Clin. Biochem. Rev.* **2014**, *35*, 155-167.

(30) https://www.theguardian.com/us-news/2015/mar/09/dog-detects-thyroid-cancer-research

(31) Kwong, G. A.; von Maltzahn, G.; Murugappan, G.; Abudayyeh, O.; Mo, S.; Papayannopoulos, I. A.; Sverdlov, D. Y.; Liu, S. B.; Warren, A. D.; Popov, Y.; Schuppan, D.; Bhatia, S. N. *Nat. Biotechnol.* **2013**, *31*, 63-70.

(32) Peng, G.; Hakim, M.; Broza, Y. Y.; Billan, S.; Abdah-Bortnyak, R.; Kuten, A.; Tisch, U.; Haick, H. *Br. J. Cancer* **2010**, *103*, 542-551.

(33) Bamrungsap, S.; Chen, T.; Shukoor, M. I.; Chen, Z.; Sefah, K.; Chen, Y.; Tan, W. H. *Acs Nano* **2012**, *6*, 3974-3981.

(34) Choi, H. S.; Liu, W.; Misra, P.; Tanaka, E.; Zimmer, J. P.; Ipe, B. I.; Bawendi, M. G.; Frangioni, J. V. *Nat. Biotechnol.* **2007**, *25*, 1165-1170.

(35) Hakim, M.; Broza, Y. Y.; Barash, O.; Peled, N.; Phillips, M.; Amann, A.; Haick, H. *Chem. Rev.* **2012**, *112*, 5949-5966.

(36) Broza, Y. Y.; Haick, H. *Nanomedicine* **2013**, *8*, 785-806.

(37) Shin, J.; Choi, S. J.; Lee, I.; Youn, D. Y.; Park, C. O.; Lee, J. H.; Tuller, H. L.; Kim, I. D. *Adv. Funct. Mater.* **2013**, *23*, 2357-2367.

(38) Tisch, U.; Schlesinger, I.; Ionescu, R.; Nassar, M.; Axelrod, N.; Robertman, D.; Tessler, Y.; Azar, F.; Marmur, A.; Aharon-Peretz, J.; Haick, H. *Nanomedicine* **2013**, *8*, 43-56.

(39) Marom, O.; Nakhoul, F.; Tisch, U.; Shiban, A.; Abassi, Z.; Haick, H. *Nanomedicine* **2012**, *7*, 639-650.

(40) Tisch, U.; Haick, H. *Mrs Bulletin* **2010**, *35*, 797-803.

(41) Sanchez, J. M.; Sacks, R. D. *Anal. Chem.* **2003**, *75*, 2231-2236.

(42) Lord, H.; Yu, Y. F.; Segal, A.; Pawliszyn, J. *Anal. Chem.* **2002**, *74*, 5650-5657.

(43) Barash, O.; Peled, N.; Hirsch, F. R.; Haick, H. *Small* **2009**, *5*, 2618-2624.

(44) Shuster, G.; Gallimidi, Z.; Reiss, A. H.; Dovgolevsky, E.; Billan, S.; Abdah-Bortnyak, R.; Kuten, A.; Engel, A.; Shiban, A.; Tisch, U.; Haick, H. *Breast Cancer Res. Treat.* **2011**, *126*, 791-796.

(45) Barash, O.; Peled, N.; Tisch, U.; Bunn, P. A.; Hirsch, F. R.; Haick, H. *Nanomed.-Nanotech. Bio. Med.* **2012**, *8*, 580-589.

(46) Xu, Z. Q.; Broza, Y. Y.; Ionsecu, R.; Tisch, U.; Ding, L.; Liu, H.; Song, Q.; Pan, Y. Y.; Xiong, F. X.; Gu, K. S.; Sun, G. P.; Chen, Z. D.; Leja, M.; Haick, H. *Br. J. Cancer* **2013**, *108*, 941-950.

(47) Peng, G.; Trock, E.; Haick, H. *Nano Lett.* **2008**, *8*, 3631-3635.

(48) Brereton, R. G. Data analysis for the laboratory and chemical plant. John Wiley & Sons Ltd, England, UK (2003).

(49) Wold, S.; Esbensen, K.; Geladi, P. Principal component analysis. Chemom. *Intell. Lab. Syst.* 2(1–3), 37–52 (1987).

CHAPTER 2

A MULTICHANNEL NANOSENSOR FOR INSTANTANEOUS READOUT OF CANCER DRUG MECHANISMS

2.1. Abstract

Screening methods that use traditional genomic,[1-3] transcriptional,[4] proteomic,[5,6] and metabonomic[7] signatures to characterize drug mechanisms exist. However, they are time-consuming and require specialized equipment. Here, we present a high-throughput multi-channel sensor platform that can profile the mechanisms of various chemotherapeutic drugs in minutes. The sensor consists of a gold nanoparticle (AuNP) complexed with three different fluorescent proteins (FPs) that can sense drug-induced physicochemical changes on cell surfaces.[8-10] In the presence of cells, FPs are rapidly displaced from the AuNP surface and fluorescence restored. Fluorescence "turn on" of the FPs depends on the drug-induced cell surface changes, generating patterns that identify specific mechanisms of cell death induced by drugs. The nanosensor is generalisable to different cell types and does not require processing steps prior to analysis, offering an effective way to expedite research in drug discovery, toxicology and cell-based sensing.

2.2. Introduction

Rapid determination of the mechanism of drug candidates would greatly facilitate the discovery and optimisation of new therapeutics,[11] particularly in the emerging area of personalised medicine.[12] Recently, “signature”-based profiling of drug mechanisms has

provided a powerful strategy in drug discovery.[1,2,13-16] These screening methods measure a series of molecular/phenotypic changes of cells/multicellular organisms induced by chemotherapeutic agents and create a fingerprint that is used as a reference for uncharacterized compounds. Several signature-based drug screening studies using traditional intracellular biomarkers[1-7] require multi-step processing of cells such as extracting biomarker[1,2,4,5] or labeling cells[6,14] and specialized equipment, limiting adoption of these strategies in rapid drug screening.

Cell surface phenotypes have been utilized in sensing cell states using nanoparticle-based array sensors.[17,18] These sensors follow a hypothesis-free signature-based strategy[14,16,19-22] that allows them to be "trained" to identify diverse bioanalytes. However, the single channel output of these nanosensors required separate measurements for each array element, and were unable to differentiate between subtle cell surface phenotypic differences arising from different cell death mechanisms. We introduce a new multiplexed three-channel sensor platform created through supramolecular assembly/disassembly of a functionalised AuNP with three FPs. The simultaneous triple-channel fluorescence transduction provides a ratiometric output that enhances the accuracy of measurements. Moreover, the information-rich output allows determination of chemotherapeutic mechanism from a single measurement that provides answers far faster (minutes) than current methods, and using standard laboratory instrumentation.

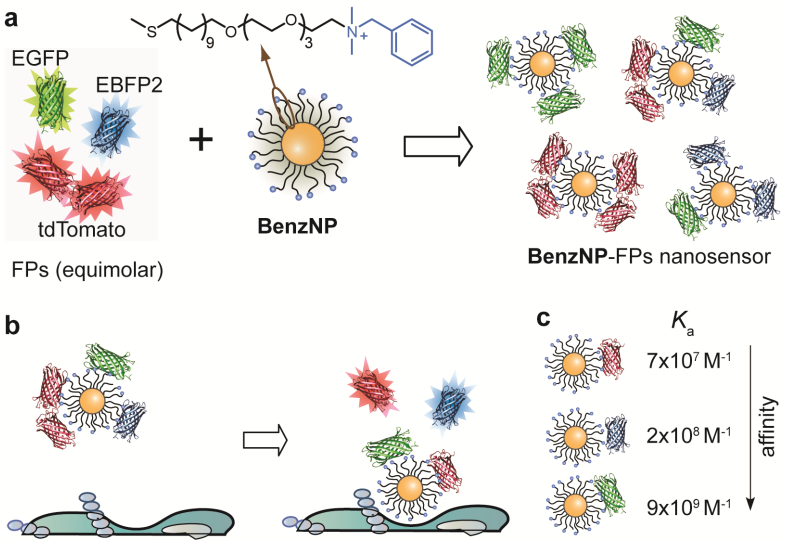

Figure 2.1. Assembly and working principle of the nanosensor. (a) Fabrication of the three-channel nanosensor (BenzNP–FPs complex). The sensor was prepared by incubating BenzNP to an equimolar mixture of three FPs at a ratio that was determined through fluorescence titration. (b) Schematic diagram illustrating the displacement and fluorescence turn-on of FPs by cell-surface functionalities. (c) Differential affinity of BenzNP to tdTomato (red), EBFP2 (blue) and EGFP (green) protein. The association constant (K_a) was determined through titration of equimolar mixture of FPs with BenzNP.

2.3. Results and Discussion

The sensor was generated by non-covalent conjugation of a benzyl headgroup-terminated AuNP (BenzNP, Fig. 2.1a) with three FPs (EBFP2, EGFP and tdTomato). The FPs serve dual roles of exhibiting differential supramolecular affinities with the particle, and transducing the binding events. BenzNPs were used in the sensor based on our previous studies that indicated its effectiveness in profiling cell surface phenotypes.[17] In these BenzNP-FP supramolecular complexes, the cationic AuNP binds strongly with the anionic FPs, resulting in quenching of the FP fluorescence by the particle core. The binding equilibria between BenzNP and the FPs are altered in presence of cells due to competitive binding to cell surfaces, resulting in rapid (seconds/minutes) displacement of FPs from the particle surface with consequent restoration of FP fluorescence (Fig. 2.1b).

The fluorescence "turn-on" of the three emission channels differs considerably depending on the signatures of drug-treated cell surfaces.

A key issue in the sensor design is selecting appropriate FPs from the broad range of variants[23] such that they provide reproducible sensor responses. Through tests with different FP variants we selected a three color FP set for the present study: blue (EBFP2), green (EGFP), and red (tdTomato). This optimized set of proteins was selected to: (i) bear net negative charge and feature minimum spectral 'crosstalk' with well-separated excitation and emission spectra, obtaining independent responses from each channel, (ii) exist as monomers or tandem dimers, simplifying their use in displacement assays relative to other multimeric analogs, (iii) be photostable, providing reliable outputs.

A second requirement for the FP transducer is differential and reversible interaction with BenzNP recognition element. We determined the binding parameters by fluorescence quenching studies that provided the complex stability constant and association stoichiometry for each FP. It was observed that the binding affinities of BenzNP and FPs varied over three orders of magnitude (Fig. 2.1c), providing the differential affinity required for multi-channel output.

We demonstrated the ability of the BenzNP-FP sensor platform to categorize chemotherapeutic mechanisms using a set of apoptosis- and necrosis-inducing chemical agents with established mechanisms. These clinical and experimental drugs cover common mechanisms of therapeutic action in cancer and include several groups with a common target (macromolecule/pathway). The necrotic agents induce cell death by rapid plasma membrane rupture,[24] which would be expected to generate a strong surface response. Apoptotic drugs cause programmed cell death that is associated with alterations

of the plasma membrane including translocation of molecules from the cytosol, as well as suppression of signaling macromolecules.[8-9,10,24] We tested the hypothesis that these drug-induced cell surface alterations could be rapidly discerned using the nanosensor. We used BT549 human breast cancer cells (triple negative) as a testbed for profiling chemotherapeutic mechanisms, since chemotherapy serves as the *only* systemic therapy for patients with this type of cancer.[25]

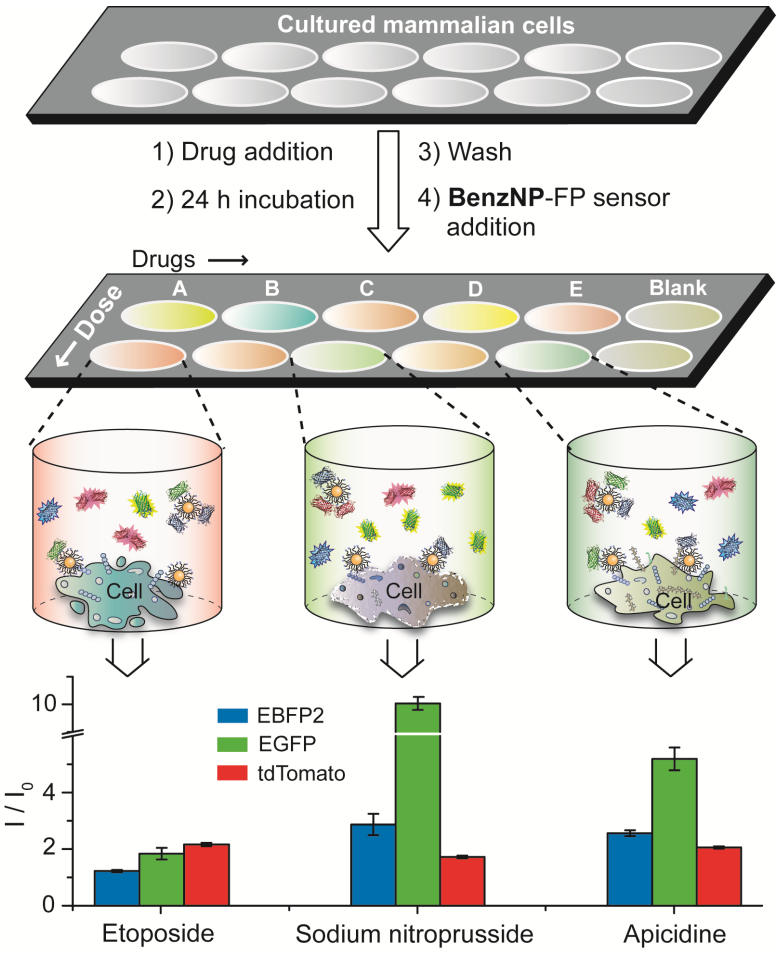

Figure 2.2. The nanosensor-based drug screening workflow. The Schematic diagram illustrates the drug screening workflow. Cells cultured in a 96-well microplate are treated with chemotherapeutic drugs at their IC50 concentrations for 24 h followed by washing and incubation the nanosensor. Different drug-treated cells result in distinct cell surface phenotypes and hence different FP displacement patterns as schematically shown for the three wells. The bar plot shows differential fluorescence responses for three representative drugs that may corroborate with the schematic of FP displacement. The

change in fluorescence along three channels was recorded simultaneously, where I0 and I are the fluorescence intensity before and after the addition of the sensor to the cells, respectively. The responses are averages of eight replicate data and the error bars represent ±standard deviation.

Drug screening studies followed the straightforward protocol shown in Fig. 2.2. Cell culture, drug treatment, and the sensing studies were carried out in a single well of a 96-well microplate. For consistency, the cells were treated with drugs at their half-maximal inhibitory concentrations (IC_{50}). We confirmed that the number of cells attached to the plate for each drug was consistent, ensuring that sensor differentiation arose from difference in cell surfaces. Notably, the sensor itself did not exhibit any cytotoxicity and cellular uptake of the particle is negligible within the short experimental time,[26] making our sensing strategy non-interfering in terms of cell behavior.

Initially, we used 15 chemotherapeutics that act through different molecular mechanisms (Fig. 2.3a) to generate a reference set based on fluorescence responses. Upon interaction with the drug-treated cells, the sensor generated characteristic fluorescence fingerprints for the three FPs. The distinct responses along each FP channel arise from the differential non-covalent interactions such as electrostatic and π–π stacking with the different biomolecules expressed on the drug-treated cell surfaces. Hierarchical clustering analysis (HCA) of the fluorescence responses produced seven distinct clusters (Fig. 2.3a), each corresponding to an individual molecular mechanism. The differential response pattern in the heat plot demonstrates the sensitivity of the sensor to drug-induced cell surface changes.

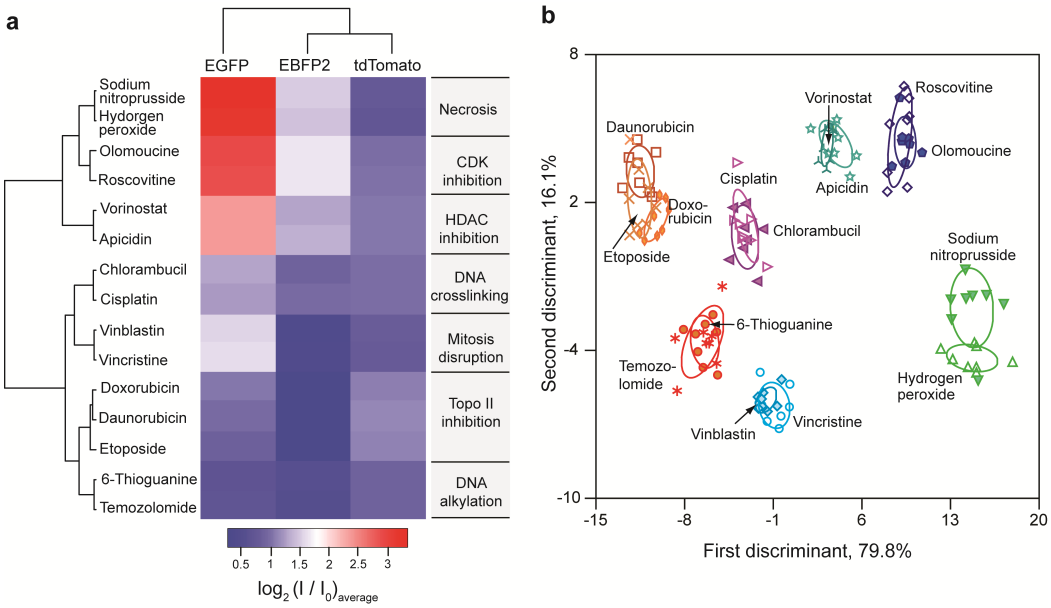

c

	Compound	Mechanism of action	*p* - value	Correct prediction
Similar mechanism as the reference set	Paclitaxel	mitosis disruption	0.06	yes
	Scriptaid	HDAC inhibition	0.75	yes
	Apigenin	topoisomerase II inhibition	0.24	yes
	Thio-TEPA	DNA alkylation	0.24	yes
	Purvalanol A	CDK inhibition	0.92	yes
	Oxaliplatin	DNA crosslinking	0.11	yes
	β-Lapachone	necrosis	0.14	yes
Mechanisms outside the reference set (Novel)	Topotecan	topoisomerase I inhibition	<0.0001	novel
	Irinotecan	topoisomerase I inhibition	<0.0001	novel
	MG-132	protein degradation	0.0027	novel
	ALLN	protein degradation	0.0064	novel
	Anisomycin	protein synthesis inhibition	<0.0001	novel
	Emetin	protein synthesis inhibition	<0.0001	novel
	Puromycin	protein synthesis inhibition	<0.0001	novel

Figure 2.3. Screening of chemotherapeutic drug mechanisms using fluorescence fingerprints. (a) Heat map of the fluorescence response patterns for the reference drug set. Hierarchical clustering was performed on the log-transformed average of the fluorescence responses using a correlation metric and average linkage. The resulting dendrograms show the degree of association of the drugs, as well as each FP. Literature-reported mechanisms of each drug are listed next to the heat map. (b) Clustering the reference drugs via LDA of the fluorescence responses. The canonical scores were obtained from LDA on the fluorescence responses, and were plotted with 95% confidence ellipses around the centroid of each group. (c) Probabilistic predictions of drug mechanisms utlising the fluorescence signatures. The *p*-values were calculated for the averages of eight replicates using the shortest Mahalanobis distance to the centroid of the nearest cluster in the reference set that was derived from LDA. A *p*-value of <0.01 was considered to be evidence of a "novel" drug mechanism.

The multidimensional sensor data was quantitatively interpreted using linear discriminant analysis (LDA). LDA classified the 15 drugs into seven distinct clusters according to the different pathways/targets of the drugs (Fig. 2.3b). Notably, drugs with similar molecular mechanisms showed overlapping clusters that were quantifiably distinguishable from other mechanistic categories. The distinctly separate region between the apoptotic and necrotic groups demonstrates the ability of the sensor to demarcate between broader classes of cell death mechanisms. It should be noted that the group size may determine the broadness of each drug category, with some categories amenable to further subdivisions.[27] We validated the robustness of the LDA method by leave-one-out cross-validation using a Jackknifed analysis. The between-group (mechanism) cross-validation accuracy was 99%, indicating the trained classifier to be a reliable and robust statistical tool. The generality of our strategy was assessed using another cell line with entirely different genotype/phenotype, for example, pTD cells (murine mammary cancer cells) that provide an important testbed for exploring therapeutics to regulate oncogenic epithelial-mesenchymal transition.[28] Characteristic fluorescence responses from the drug-treated pTD cells were generated and yielded distinct mechanism-based clusters. These clusters were somewhat different than that observed with BT549, as expected based on the geno/phenotypic difference between cell lines (Figure 2.4).

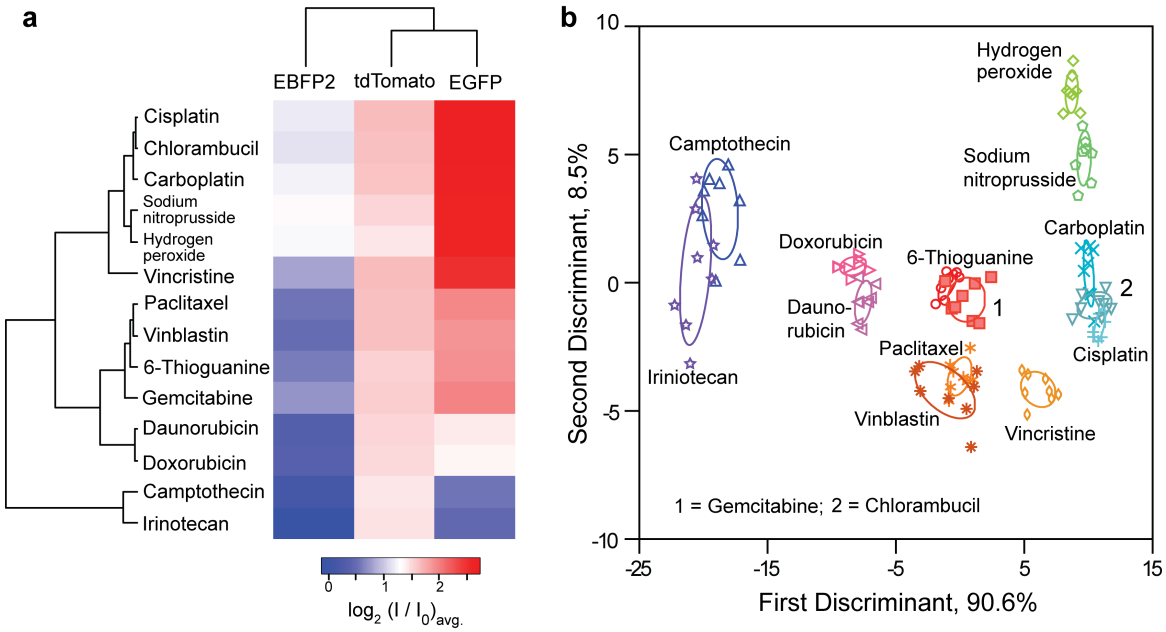

Figure 2. 4. Drug screening using pTD cells. (a) Heat map of the fluorescence responses pTD cells when treated with 11 reference drugs, where I_0 and I are respectively the fluorescence before and after the addition of the sensor to the cells. Agglomerative hierarchical analysis was performed on the averages of the fluorescence responses. The dendrogram shows degree of association. (b) Linear discriminant analysis of the fluorescence responses resulted in canonical scores with three discriminants explaining 90.6, 8.5, and 0.9% of total variance and plotted with 95% confidence ellipses around the centroid of each group (based on the standard error of the mean).

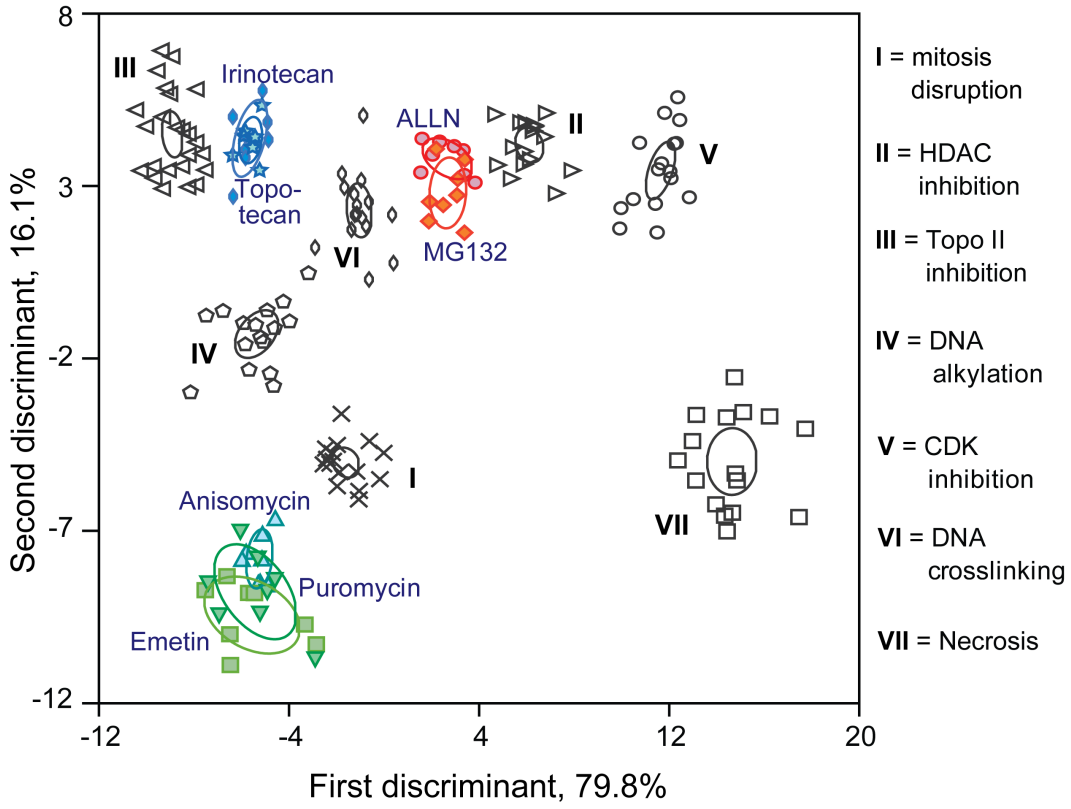

Figure 2.5. Classification of unknowns outside the initial reference set using BT549 cells. Updated canonical score plot was derived from LDA of the fluorescence responses from a combination of the initial reference set and the compounds with 'novel' mechanisms, and were plotted with 95% confidence ellipses around the centroid of each group (based on the standard error of the mean). The clusters corresponding to the 'novel' compounds are coloured, while the initial reference set compounds are presented in black.

The ability to identify the mechanism of lead compounds as either known or novel is a key issue in drug screening. In blinded experiments we assessed seven anticancer agents that exhibit mechanisms similar to the training set. We predicted the mechanism of the test compounds by determining the probability of a compound belonging to the closest reference group using an appropriate *F*-distribution for the minimum Mahalanobis distance obtained from LDA. Using a cutoff *p*-value of 0.01, the analysis correctly predicted the molecular mechanisms of the seven test compounds

(Figure 2.3c), demonstrating the capability of the sensor to screen 'real' unknowns. We next sought to examine if the sensor can identify compounds involving targets/pathways different from the reference set. Seven compounds with “novel” (i.e. outside the reference set) cell death mechanisms were tested using the nanosensor. Implementing the same probabilistic analysis, *p*-value for each compound was found to be less than 0.01 (Figure 2.3c), indicating that the compounds were far from all the training groups and could be readily classified as “novel”. Furthermore, a follow-up LDA solution space including the reference and novel compound set showed clearly distinct clusters, while the drugs with similar targets paired with each other correctly (Figure 2.5), indicating the ability to update the training set with ‘new’ mechanistic groups with sufficient resolution. We tested the robustness of prediction by studying eight parallel replicates of the blinded unknowns and the novel compounds that resulted in 87.5% (98 of 112 samples) correct prediction (Figure 2.6). The capability of the sensor to discriminate between learned and potentially new mechanisms demonstrates the ability of the system to avoid false positives of mechanism identification. The ability of the sensor to stratify molecularly targeted drugs such as the HDAC and CDK inhibitors suggests its applicability to broader class of modern targeted drugs (targeting EGFR, HER2, PDGFR, VEGF, proteasome, etc)[29] that cause up/downregulation of the receptors on cell surfaces.

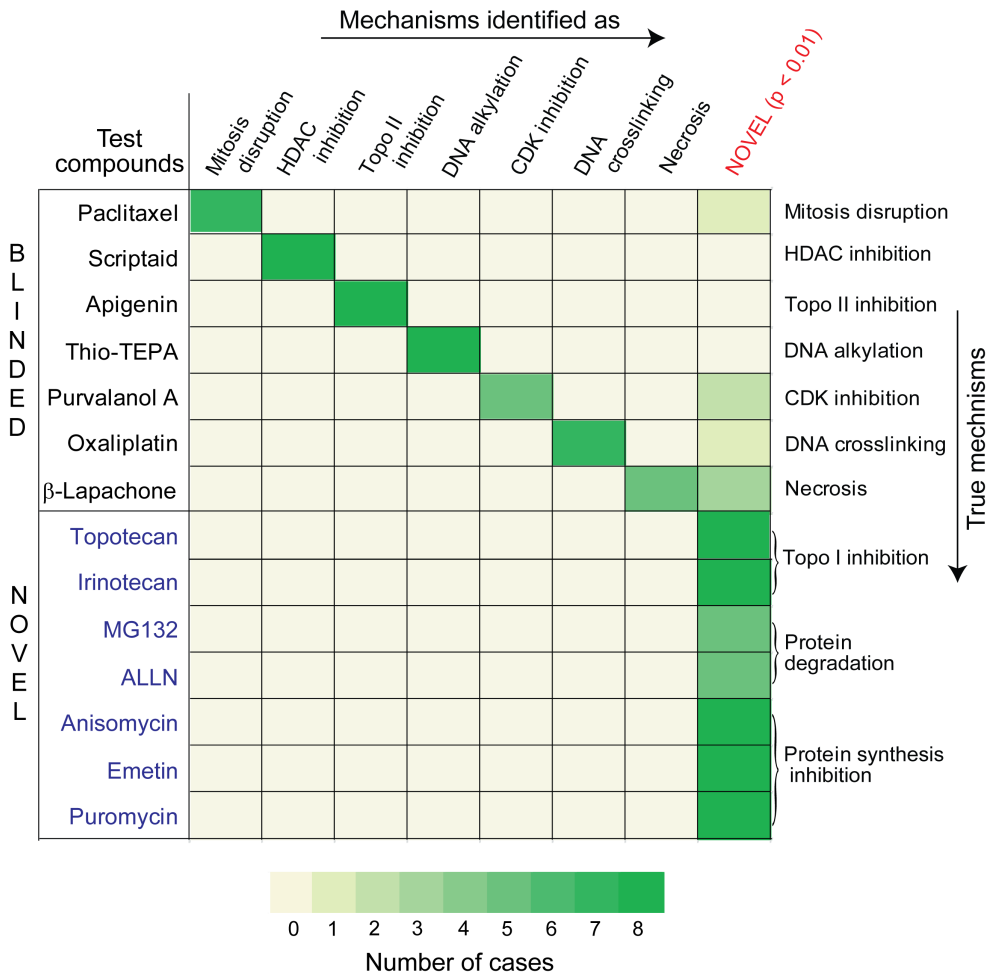

Figure 2. 6. Prediction of drug mechanisms on parallel replicates using the triple-channel sensor. Fluorescence responses from the EBFP2, EGFP, and tdTomato channels were utilised to perform the statistical analysis. The *p*-values were derived from *F*-distribution on the minimum Mahalanobis distance of each replicate to the centroid of reference groups calculated by LDA. Based on the *p*-values, each unknown case (parallel replicate) was assigned to a mechanistic group of the reference set or regarded as 'novel'. The blinded unknowns exhibits cell death mechanisms similar to the reference set, while the 'novel' unknowns involve mechanisms completely different from the reference set.

Combination therapy provides a complementary strategy to new drug discovery, greatly enhancing the efficacy of chemotherapeutics, e.g. by overcoming the drug resistance of cancer cells.[30] Drug combinations produce therapeutic activities (synergistic, additive, or antagonistic)[31] at different ratios of the individual components.

Thus, a cell surface-based quick screening of the therapeutic activities with respect to individual drug mechanisms should lead to predicting the contribution of each drug in their therapeutic combination.[32,33]

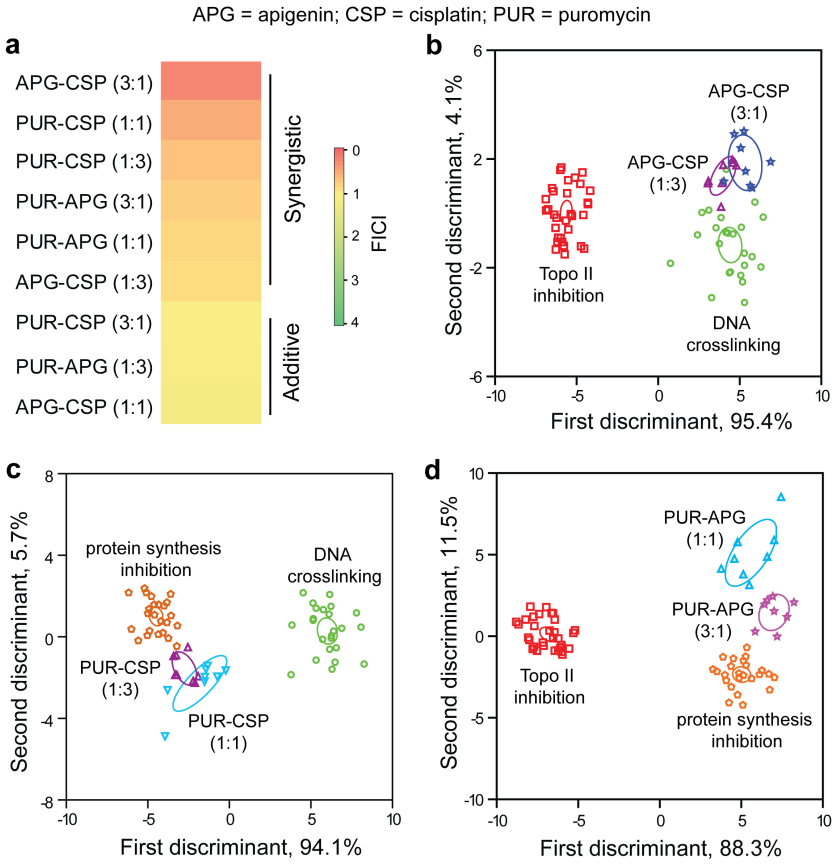

Figure 2.7. Profiling the mechanisms of drug combinations. (a) Determination of therapeutic activities of pairwise drug combinations using fractional inhibitory concentration index (FICI). Correlation of the synergistic combinations of (b) apigenin-cisplatin, (c) puromycin-cisplatin, and (d) puromycin-apigenin with the single-drug mechanistic categories. The canonical scores were calculated for the pairwise combinations with the mechanistic groups that contain the single-drug components forming the combinations. The LDA-derived scores from the fluorescence responses were plotted with 95% confidence ellipses around the centroid of each group. The mechanistic categories consist of several drugs with the same mechanism, Topo II inhibition: daunorubicin, etoposide, doxorubicin, and apigenin; DNA crosslinking: cisplatin, chlorambucil, and oxaliplatin; Protein synthesis inhibition: anisomycin, emetin, and puromycin. Each drug was used in eight replicates.

We demonstrated the ability of our sensor to determine mechanistic correlation between individual drugs and their combinations using three apoptotic drugs: apigenin (APG), puromycin (PUR), and cisplatin (CSP). We utilized fractional inhibitory concentration index[34] to select the synergistic drug combinations. Interestingly, pairwise interactions of the drugs showed synergy or additivity depending on the ratios of the individual drugs (Fig. 2.7a). Comparison of the APG-CSP synergistic pairs with the single-drug components indicated that both the combinations exhibited a DNA crosslinking-like mechanism, consistent with previous observations[35] of APG enhancing the cytotoxicity of CSP. The LDA scores quantified the similarity of the signatures of APG-CSP synergistic combinations to CSP with $p>0.01$ (Fig. 2.7b). Similarly, the signature of the PUR-CSP(1:3) combinations revealed its close proximity to protein synthesis inhibition-like mechanism (Fig. 2.7c), suggesting CSP potentiating the PUR-induced cytotoxicity. However, PUR-CSP(1:1) and the PUR-APG synergistic combinations were classified quite far ($p<0.01$) from their single-drug components (Fig. 2.7c,d), indicating a mechanistically distinct cell surface phenotypic change that provides a potentially new therapeutic strategy. These representative examples indicate that the sensor can provide an information-rich strategy for predicting the mechanisms of drug combinations.

2.4. Conclusions

In summary, we demonstrated the creation of a novel multichannel sensor based on non-covalent supramolecular complexes. This sensor uses an engineered nanoparticle and three different FPs to provide a three-channel sensor that can be “trained” to detect

subtle changes in cell surface properties. This biocompatible nanosensor can identify specific mechanisms induced by different chemotherapeutic agents, *using a single well* of a microplate, making this strategy applicable to massively high-throughput screening. The simplicity and effectiveness of the system underscores its potential to accelerate drug discovery, greatly facilitating the development of new therapeutics and drug "cocktails". This sensor system also provides a potential way forward for toxicology, providing a viable method to classify the tens of thousands of commercial chemicals for which no data are available.

2.5. Experimental section

2.5.1. Fluorescence titrations. In the fluorescence quenching experiment, an equimolar solution of the three FPs (100 nM each) was titrated with various concentrations of BenzNP ranging from 0 to 300 nM. The excitation/emission/cut-off wavelengths were 380/450/435, 475/510/495, and 550/585/570 nm for EBFP2, EGFP and tdTomato, respectively. The change of fluorescence intensity at the respective emission maxima was recorded on a Molecular Devices SpectraMax M3 microplate reader at 25 °C. Decay of fluorescence intensity of each FP was observed with increasing NP concentration. Nonlinear least-squares curve fitting analysis was employed to estimate the binding constant (K_a) and association stoichiometry (n) using a 1:1 binding model (Figure 2.8).[36,37]

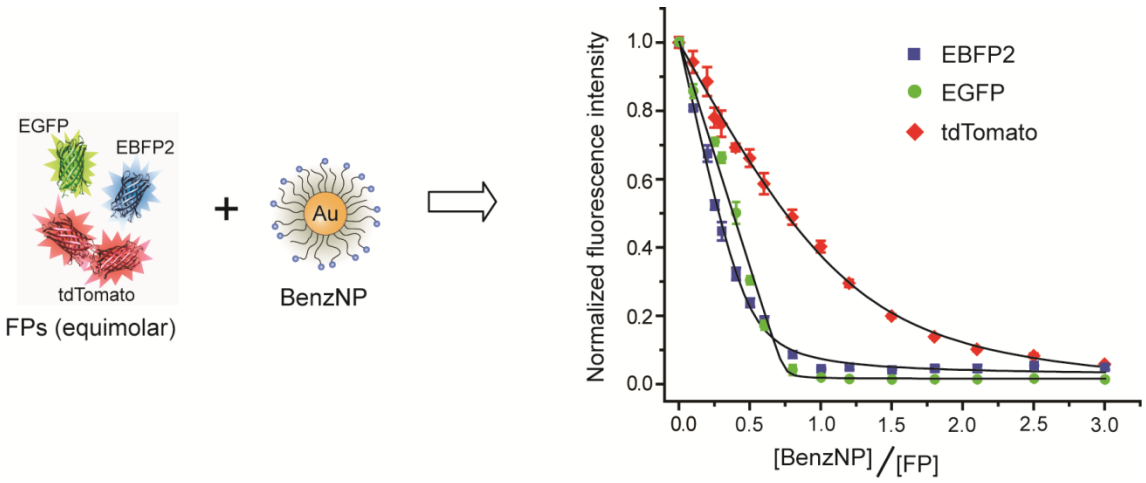

Figure 2.8. Titration of FPs with BenzNP. Fluorescence titration of an equimolar mixture of the three FPs by BenzNP. The emissions for each FP were measured independently at the corresponding emission wavelengths. The data points are averages of three replicates and the error bars represent the ±standard deviations. The black solid lines through the data points represent the best curve fitting using the model of single set of identical binding sites.

2.5.2. Sensor preparation. First, a FP solution was prepared by mixing the FPs at the final concentration of 100 nM (for each FP). The BenzNP-FP sensor was generated by incubating the FP solution with BenzNP (at the final concentration of 150 nM) for 30 min in 5 mM sodium phosphate buffer (pH 7.4). The FP and BenzNP-FP solutions were maintained in the dark to minimise photobleaching of the FPs, if any. This conjugate was then added to the drug-treated cells for screening studies.

2.5.3. Cell culture. BT549 cell line was purchased from ATCC (ATCC® HTB-122™). pTD cell line[38] was donated by Prof. D. Josph Jerry. BT549 cells were cultured in DMEM media supplemented with 10% FBS and 1% antibiotics. Cells were grown in a humidified atmosphere containing 5% CO_2 at 37 °C. The TD cells were cultured in DMEM high glucose media supplemented with 10% FBS and 1% antibiotics. At ~80%

confluence, cells were trypsinised and plated in 96-well plates (Greiner black-and-clear bottom) and cultured for the next studies.

2.5.4. IC50 of the drugs. The IC_{50} values of the drugs were determined by Alamar blue assay. Cells were seeded at 10,000 (BT549 cells) or 15,000 (pTD cells) per well in 96-well microplates (Greiner black-and-clear bottom). After 24 h, the cells were washed twice with phosphate buffered saline (PBS) and treated with drugs at different concentrations. The drug treatment was continued for 24 h for all the drugs except hydrogen peroxide and sodium nitroprusside for which 5 h treatment was effective. Drug treatment was done in cell culture media lacking antibiotics. After the drug treatments, cells were washed with PBS twice and the percentage cell viability was determined by using Alamar blue assay following the manufacturer's protocol (Invitrogen). The IC_{50} values were determined by fitting the data using a dose response model with variable Hill slope built in OriginPro 8.5 (Figure 2.9).

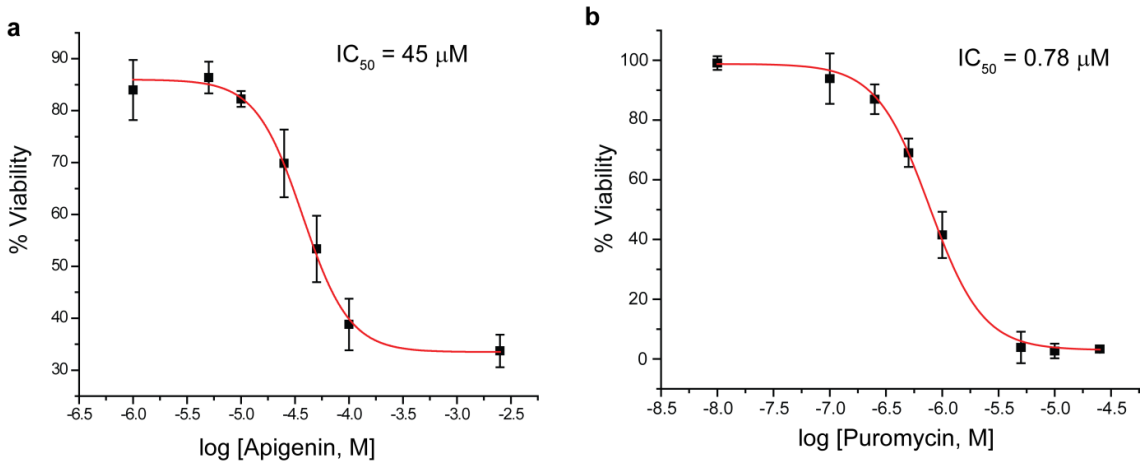

Figure 2.9. Determination of IC_{50} value of the single cytotoxic compounds. Representative dose response curves of (a), apigenin, and (b, puromycin using 10,000 BT549 cells following 24 h drug treatment. The IC_{50} values were determined by fitting the data (the red line) using dose response model with variable Hill slope built in OriginPro 8.5. The data are averages of three replicates and the error bars represent the ±standard deviation.

Dose response studies for combination of drugs were followed in a similar method of single drug. Three drugs (puromycin (PUR), cisplatin (CSP), and apigenin (APG)) were chosen arbitrarily to study the drug combinations (Fig. 4). To determine the IC_{50} values, two drugs of a combination were added to confluent cells one by one at 1:1, 1:3, and 3:1 ratio with varying concentrations (Supplementary Table 2). The concentrations of drugs used were same for all the different combinations (PUR-CSP, PUR-APG, and APG-CSP). The IC_{50} values were determined by fitting the data using the same dose response model (Figure 2.10).

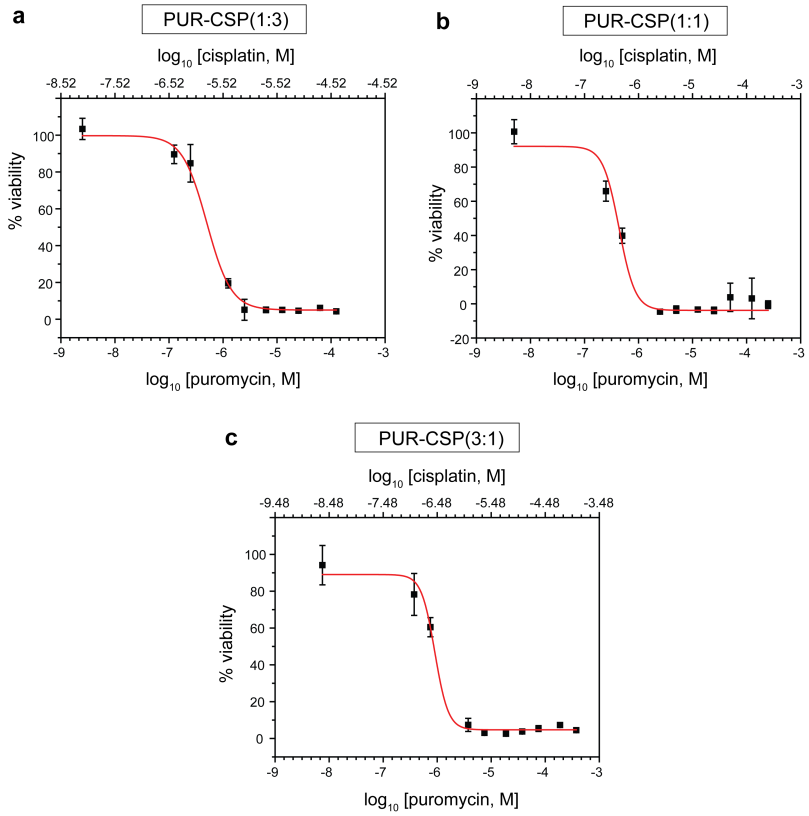

Figure 2.10. Determination of IC_{50} value of the combination of drugs. Representative dose response curves of the drug combinations (a), PUR-CSP(1:3), (b), PUR-CSP(1:1), and (c), PUR-CSP(3:1) using 10,000 BT549 cells after 24 h of drug treatment. The IC_{50} values were determined by fitting the data (the red line) using dose response model with variable Hill slope built in Origin 8.5 program. The data are averages of three replicates and the error bars represent the ±standard deviation.

2.5.5. Drug screening studies. The drugs were purchased from VWR International, Sigma-Aldrich, and Tocris Bioscience. First, 10,000 (for BT549 cells) or 15,000 (for pTD cells) cells/well were seeded in 96-well Greiner black-and-clear bottom microplates and allowed to grow in their respective culture media at 37 °C and 5% CO_2 for 24 h. Then, cells were washed twice with PBS and treated with the drugs at their respective IC_{50} concentrations. The drug treatment was continued for 24 h for the individual drugs as well as their combinations (except for hydrogen peroxide and sodium nitroprusside, which were treated for 5 h). Cells were then washed three times with PBS and incubated with the sensor for 15 min before taking the reading. Then, 200 μL of the BenzNP-FP conjugate was loaded into 96-well plates containing drug treated cells to be analyzed. After 15 min of incubation with the sensor, fluorescence intensities were monitored for each FP using a plate reader (Molecular Device Spectramax M3) at 25 °C. Appropriate filters were used to collect emissions from each FP. The excitation/emission/cut-off wavelengths were 380/450/435, 475/510/495, and 550/585/570 nm for EBFP2, EGFP and tdTomato, respectively. Fluorescence responses were $\log_2$-transformed before employing the statistical analyses.

2.5.6. Determination of FICI. The fractional inhibitory concentration index (FICI) was calculated using the following equation based on Loewe additivity:[39,40]

$$FICI = \frac{[A]_C}{[A]_E} + \frac{[B]_C}{[B]_E}$$

where, $[A]_C$ and $[B]_C$ are the concentrations of drug A and B in the combination associated with a particular level of effect, e.g., IC_{50}, and $[A]_E$ and $[B]_E$ are the concentrations of A and B when used singly to produce the same level of effect. FICI < 1

indicates synergism, while $1 \leq FICI < 4$ indicates additivity, and $FICI \geq 4$ indicates antagonism.

2.5.7. Hierarchical clustering analysis. Hierarchical clustering analysis (HCA) is an unbiased clustering approach. HCA of the average data set was performed using the *hclust* function of the stats package of R assuming a complete linkage method.[41] *hclust* begins with each case serving as its own cluster; at each step in the clustering process, the two most similar cases or clusters are joined; the process iterates until all cases fall into a single cluster. HCA allows cases with mechanisms outside the reference set to be identified as novel, if they are dissimilar from the other cases in the set; in this case, they are linked to the other cases/clusters relatively high in the dendrogram.

2.5.8. Linear discriminant analysis. The raw fluorescence response data matrix was processed by classical linear discriminant analysis (LDA) using SYSTAT software (version 11.0, SystatSoftware, Richmond, CA, USA). In LDA, all variables were used in the model (complete mode) and the tolerance was set as 0.001. The raw fluorescence response patterns were transformed to canonical patterns where the ratio of between-class variance to the within-class variance was maximized, where the classes were defined as the drug mechanisms in the reference set. This defines the LDA solution space. To identify the unknown (blinded) samples, we first re-ran LDA on the reference set using the *lda* function in the MASS package[42] of R; these results replicated the SYSTAT analysis. Predicted classifications for the blinded samples were then obtained using the *predict.lda* function that uses the fluorescence response patterns of each new case to compute the Mahalanobis distance of that case to the centroid of each mechanism cluster in the LDA solution space (Fig. 3b). Blinded cases are predicted to belong to the closest

mechanism class, defined by the shortest Mahalanobis distance. Because some distance is always shortest, LDA is incapable of identifying blinded or completely unknown samples as having novel mechanisms. However, by considering the expected distribution of Mahalanobis distances under these conditions, cases can be identified as outliers if they fall far from the closest centroid (i.e., have an associated p-value < 0.01).

2.6. References

(1) Lamb, J.; Crawford, E. D.; Peck, D.; Modell, J. W.; Blat, I. C.; Wrobel, M. J.; Lerner, J.; Brunet, J. P.; Subramanian, A.; Ross, K. N.; Reich, M.; Hieronymus, H.; Wei, G.; Armstrong, S. A.; Haggarty, S. J.; Clemons, P. A.; Wei, R.; Carr, S. A.; Lander, E. S.; Golub, T. R. *Science* **2006**, *313*, 1929-1935.

(2) Jiang, H.; Pritchard, J. R.; Williams, R. T.; Lauffenburger, D. A.; Hemann, M. T. *Nature Chem. Biol.* **2011**, *7*, 92-100.

(3) Parsons, A. B.; Lopez, A.; Givoni, I. E.; Williams, D. E.; Gray, C. A.; Porter, J.; Chua, G.; Sopko, R.; Brost, R. L.; Ho, C. H.; Wang, J. Y.; Ketela, T.; Brenner, C.; Brill, J. A.; Fernandez, G. E.; Lorenz, T. C.; Payne, G. S.; Ishihara, S.; Ohya, Y.; Andrews, B.; Hughes, T. R.; Frey, B. J.; Graham, T. R.; Andersen, R. J.; Boone, C. *Cell* **2006**, *126*, 611-625.

(4) Butcher, R. A.; Schreiber, S. L. *Curr. Opin. Chem. Biol.* **2005**, *9*, 25-30.

(5) Schirle, M.; Bantscheff, M.; Kuster, B. *Chem. Biol.* **2012**, *19*, 72-84.

(6) Krutzik, P. O.; Crane, J. M.; Clutter, M. R.; Nolan, G. P. *Nature Chem. Biol.* **2008**, *4*, 132-142.

(7) Nicholson, J. K.; Connelly, J.; Lindon, J. C.; Holmes, E. *Nature Rev. Drug Discov.* **2002**, *1*, 153-161.

(8) Chuah, B. Y. S.; Putti, T.; Salto-Tellez, M.; Charlton, A.; Iau, P.; Buhari, S. A.; Wong, C. I.; Tan, S. H.; Wong, A. L. A.; Chan, C. W.; Goh, B. C.; Lee, S. C. *Ann. Oncol.* **2011**, *22*, 1748-1754.

(9) Obeid, M.; Tesniere, A.; Ghiringhelli, F.; Fimia, G. M.; Apetoh, L.; Perfettini, J. L.; Castedo, M.; Mignot, G.; Panaretakis, T.; Casares, N.; Metivier, D.; Larochette, N.; van Endert, P.; Ciccosanti, F.; Piacentini, M.; Zitvogel, L.; Kroemer, G. *Nature Med.* **2007**, *13*, 54-61.

(10) Azuma, Y.; Taniguchi, A.; Matsumoto, K. *Glycoconj. J.* **2000**, *17*, 301-306.

(11) *Nature Med.* **2010**, *16*, 347-347.

(12) De Castro, D. G.; Clarke, P. A.; Al-Lazikani, B.; Workman, P. *Clin. Pharm. Ther.* **2013**, *93*, 252-259.

(13) Feng, Y.; Mitchison, T. J.; Bender, A.; Young, D. W.; Tallarico, J. A. *Nature Rev. Drug Discov.* **2009**, *8*, 567-578.

(14) Perlman, Z. E.; Slack, M. D.; Feng, Y.; Mitchison, T. J.; Wu, L. F.; Altschuler, S. J. *Science* **2004**, *306*, 1194-1198.

(15) Rihel, J.; Prober, D. A.; Arvanites, A.; Lam, K.; Zimmerman, S.; Jang, S.; Haggarty, S. J.; Kokel, D.; Rubin, L. L.; Peterson, R. T.; Schier, A. F. *Science* **2010**, *327*, 348-351.

(16) Young, D. W.; Bender, A.; Hoyt, J.; McWhinnie, E.; Chirn, G. W.; Tao, C. Y.; Tallarico, J. A.; Labow, M.; Jenkins, J. L.; Mitchison, T. J.; Feng, Y. *Nature Chem. Biol.* **2008**, *4*, 59-68.

(17) Bajaj, A.; Miranda, O. R.; Kim, I. B.; Phillips, R. L.; Jerry, D. J.; Bunz, U. H. F.; Rotello, V. M. *Proc. Natl. Acad. Sci. U.S.A.* **2009**, *106*, 10912-10916.

(18) El-Boubbou, K.; Zhu, D. C.; Vasileiou, C.; Borhan, B.; Prosperi, D.; Li, W.; Huang, X. F. *J. Am. Chem. Soc.* **2010**, *132*, 4490-4499.

(19) Wright, A. T.; Anslyn, E. V. *Chem. Soc. Rev.* **2006**, *35*, 14-28.

(20) Peng, G.; Tisch, U.; Adams, O.; Hakim, M.; Shehada, N.; Broza, Y. Y.; Billan, S.; Abdah-Bortnyak, R.; Kuten, A.; Haick, H. *Nature Nanotech.* **2009**, *4*, 669-673.

(21) Tanaka, M.; Bateman, R.; Rauh, D.; Vaisberg, E.; Ramachandani, S.; Zhang, C.; Hansen, K. C.; Burlingame, A. L.; Trautman, J. K.; Shokat, K. M.; Adams, C. L. *PLoS Biol.* **2005**, *3*, 764-776.

(22) Rana, S.; Singla, A. K.; Bajaj, A.; Elci, S. G.; Miranda, O. R.; Mout, R.; Yan, B.; Jirik, F. R.; Rotello, V. M. *Acs Nano* **2012**, *6*, 8233-8240.

(23) Shaner, N. C.; Steinbach, P. A.; Tsien, R. Y. *Nature Methods* **2005**, *2*, 905-909.

(24) Vermes, I.; Haanen, C.; Reutelingsperger, C. *J. Immunol. Methods* **2000**, *243*, 167-190.

(25) Reis-Filho, J. S.; Tutt, A. N. J. *Histopathology* **2008**, *52*, 108-118.

(26) Saha, K.; Kim, S. T.; Yan, B.; Miranda, O. R.; Alfonso, F. S.; Shlosman, D.; Rotello, V. M. *Small* **2013**, *9*, 300-305.

(27) Pritchard, J. R.; Bruno, P. M.; Hemann, M. T.; Lauffenburger, D. A. *Mol. Biosyst.* **2013**, *9*, 1604-1619.

(28) Dunphy, K. A.; Seo, J. H.; Kim, D. J.; Roberts, A. L.; Tao, L. W.; DiRenzo, J.; Balboni, A. L.; Crisi, G. M.; Hagen, M. J.; Chandrasekaran, T.; Gauger, K. J.; Schneider, S. S.; Jerry, D. J. *Cancer Cell Int.* **2013**, *13*.

(29) Dancey, J. E.; Chen, H. X. *Nature Rev. Drug Discov.* **2006**, *5*, 649-659.

(30) Gottesman, M. M. *Ann. Rev. Med.* **2002**, *53*, 615-627.

(31) Jia, J.; Zhu, F.; Ma, X. H.; Cao, Z. W. W.; Li, Y. X. X.; Chen, Y. Z. *Nature Rev. Drug Discov.* **2009**, *8*, 111-128.

(32) Pritchard, J. R.; Bruno, P. M.; Gilbert, L. A.; Capron, K. L.; Lauffenburger, D. A.; Hemann, M. T. *Proc. Natl. Acad. Sci. U.S.A.* **2013**, *110*, E170-E179.

(33) Geva-Zatorsky, N.; Dekel, E.; Cohen, A. A.; Danon, T.; Cohen, L.; Alon, U. *Cell* **2010**, *140*, 643-651.

(34) Nandakumar, D. N.; Nagaraj, V. A.; Vathsala, P. G.; Rangarajan, P.; Padmanaban, G. *Antimicrob. Agents Chemother.* **2006**, *50*, 1859-1860.

(35) Chan, L. P.; Chou, T. H.; Ding, H. Y.; Chen, P. R.; Chiang, F. Y.; Kuo, P. L.; Liang, C. H. *BBA-Gen. Subjects* **2012**, *1820*, 1081-1091.

(36) You, C. C.; De, M.; Han, G.; Rotello, V. M. *J. Am. Chem. Soc.* **2005**, *127*, 12873-12881.

(37) Phillips, R. L.; Miranda, O. R.; Mortenson, D. E.; Subramani, C.; Rotello, V. M.; Bunz, U. H. F. *Soft Matter* **2009**, *5*, 607-612.

(38) Dunphy, K. A.; Seo, J. H.; Kim, D. J.; Roberts, A. L.; Tao, L. W.; DiRenzo, J.; Balboni, A. L.; Crisi, G. M.; Hagen, M. J.; Chandrasekaran, T.; Gauger, K. J.; Schneider, S. S.; Jerry, D. J. *Cancer Cell Int.* **2013**, *13*.

(39) Loewe, S. *Arzneimittelforschung* **1953**, *3*, 285-290.

(40) Greco, W. R.; Bravo, G.; Parsons, J. C. *Pharmacol. Rev.* **1995**, *47*, 331-385.

(41) R Development Core Team (2010). *R: A language and environment for statistical computing. R Foundation for Statistical Computing*, Vienna, Austria. ISBN 3-900051-07-0, URL http://www.R-project.org.

(42) Venables, W. N. & Ripley, B. D. (2002). *Modern Applied Statistics with S.* Fourth Edition. Springer, New York. ISBN 0-387-95457-0.

CHAPTER 3

CANCER CELL DISCRIMINATION USING HOST-GUEST 'DOUBLED' ARRAYS

3.1. Abstract

We report a nanosensor that uses cell lysates to rapidly profile the tumorigenicity of cancer cells. This sensing platform uses host-guest interactions between cucurbit[7]uril (CB[7]) and the cationic headgroup of a gold nanoparticle (AuNP) to non-covalently modify the binding of three fluorescent proteins of a multichannel sensor *in situ*. This approach doubles the number of output channels to six, providing single-well identification of cell lysates with 100 % accuracy. Significantly, this classification could be extended beyond the training set, determining the invasiveness of novel cell lines. The unique fingerprint of these cell lysates required minimal sample quantity (200 ng, ~1000 cells), making the methodology compatible with microbiopsy technology.

3.2. Introduction

Rapid methods for geno- and phenotyping cells are crucial for cancer prognosis and the design of therapeutic strategies for precision medicine.[1,2] Discrimination between healthy and cancerous cells, and then geno/phenotyping to determine whether the cancer is a slow-growing variant or a highly aggressive form are all important for optimal treatment.[3,4] The cell proteome provides a significant resource for determining cell tumorigenicity.[5,6] Traditionally, biomarker-based approaches employing proteomics techniques such as electrophoresis and mass spectrometry have been used to detect

changes in cell state.[7-9] These methods, however, require prior knowledge of the tumor, and are often not sensitive to subtle changes in proteomic signatures. In contrast, array-based 'chemical nose' sensing provides an alternative strategy uses selective receptors to generate multiple output channels that are used to create patterns (training sets), analogous to olfaction.[10-12] These outputs are then used to build a global diagnostic pattern that can be used to rapidly identify individual small molecule[13-15] and biomacromolecular analytes.[16,17] More recently, array-based sensing has been used to profile complex biosystems,[18-20] including the use of cell lysates to rapidly profile geno/phenotype of cells and tissues for cancer diagnosis.[21]

The traditional application of array-based sensing protocols uses spatially separated sensor units each with their own recognition element to provide the multiple outputs required for pattern generation.[22-26] Some studies report materials that have multiple optical properties that can be employed to give multiple channels within a single receptor;[27-31] however, even in this format, each optical signal must still be measured separately. In recent research, an alternative strategy employing a single nanoparticle recognition element with three different transducers (red, green, and blue fluorescent proteins (FPs)) was used to generate multi-channel outputs. This approach greatly simplifies the sensor system physically, facilitating 'one-well' discrimination of complex biosystems, including identification of bacterial biofilms,[32] mammalian cells,[33,34] and determination of drug mechanisms.[35] A key challenge with this strategy, however, is generation of sufficient non-interfering channels (e.g. fluorescent emission wavelengths) for effective pattern generation.

Host-guest chemistry is a versatile tool for noncovalent modification of polymers and nanomaterials, altering the structure and concomitantly the behavior of these materials.[36-39] This approach has been widely used in many applications, including imaging,[40] therapeutic delivery,[41] and sensing.[42] We hypothesized that a host-guest strategy could be used to increase the information content of array-based sensing platforms, facilitating their use in cancer identification and typing. In our approach, we used noncovalent modification of a cationic benzylammonium-functionalized nanoparticle with a complementary cucurbit[7]uril (CB[7]) moiety (Figure 3.1).[43,44] This binding modulates the interaction of the particle with both the fluorescent protein transduction elements and the cell lysate analytes. This change in competitive binding effectively doubles the number of output channels from three to six while maintaining the one-well configuration. This increased information content allowed facile discrimination of cells by their tumorigenicity. Significantly, this classification could be extended beyond the training set, determining the invasiveness of novel cell lines. Full differentiation of cell types was achieved with as little as 200 ng of protein (~1000 cells), demonstrating the potential of this method for microbiopsy-based cancer diagnostics.[45]

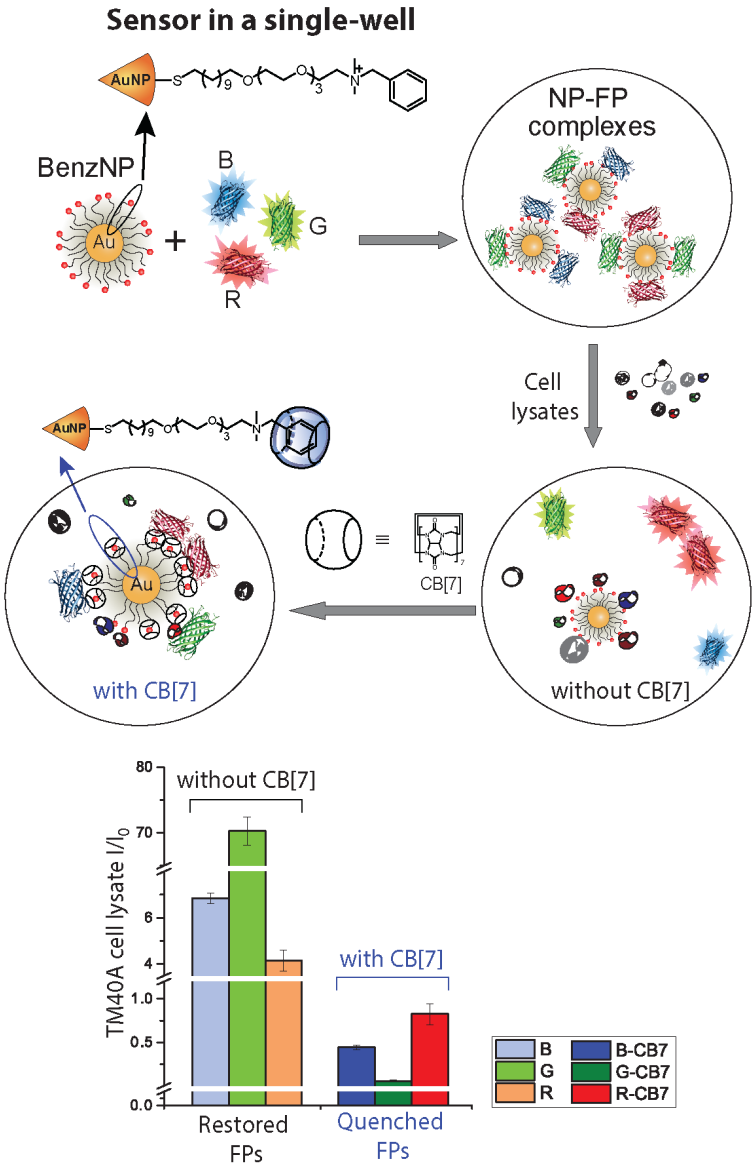

Figure 3.1. Six channel-output in a single well. The fluorescence of FPs is quenched when the BenzNP-FP complexes are formed. Upon addition of cell lysates, three emission channels are obtained from the released FPs. In the same well, CB[7] is added to obtain three additional channels from the three FPs as a result of changed interactions between the analyte and newly formed complex, BenzNP-CB[7].

3.3. Results and Discussion

The sensor consists of two supramolecularly-related recognition receptors: BenzNP and BenzNP-CB[7]. BenzNP can bind to the CB[7] host molecule to rapidly form host-guest complexes.[46] The binding events of BenzNP and BenzNP-CB[7] with the lysates are transduced by three fluorescent proteins: blue (EBFP2) (B), green (EGFP) (G), and red (tdTomato) (R). In the presence of BenzNP, the fluorescence intensity of FPs is quenched. Different amounts of FPs are then released after the addition of cell lysates due to their competitive binding for the particles, generating channels 1-3. Host-guest interactions between CB[7] and BenzNP[47] create the second recognition receptor.[48,49] The addition of CB[7] triggered a drastic change in fluorescence intensity of the three FPs, indicating a stronger interaction of BenzNP-CB[7] complexes to FPs than the BenzNP,[50-52] generating channel 4-6. CB[7] is a good synthetic receptor for peptides and proteins, which might contribute to the enhanced quenching ability of BenzNP–CB[7] toward FPs in the presence of lysates.[53] To ensure that the fluorescence changes are induced by the interaction of BenzNP-CB[7] with cell lysates and not from any changes of FPs themselves, we tested the effect of CB[7] and lysates on FPs alone and found that they do not affect fluorescence intensity of FPs (Figure 3.2).

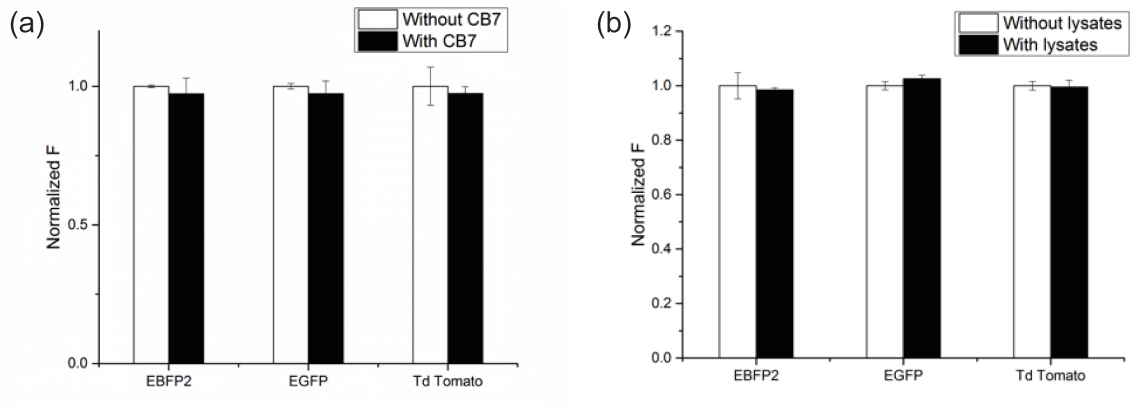

Figure 3.2. Effects of (a) CB[7] and (b) cell lysates on three fluorescence proteins. Both CB[7] and 200 ng of cell lysates did not change the fluorescence intensities of the three fluorescence proteins significantly. Each value is an average of three replicates.

The first step in our sensing was to determine the appropriate conditions for converting Benz-NP to BenzNP-CB[7]. The appropriate stoichiometry of CB[7] and BenzNP was determined by isothermal titration calorimetry (ITC) and the 100/1 ratio of CB[7]/BenzNP was used throughout our sensing experiments (Figure 3.3). We also measured the saturation point of CB[7]/BenzNP using fluorescence titration assay of BenzNP-FP complexes preincubated with 200 ng cell lysates and varied concentrations of CB[7]. The same ratio of 100/1 of CB[7]/BenzNP was observed for this assay (Figure 3.4).

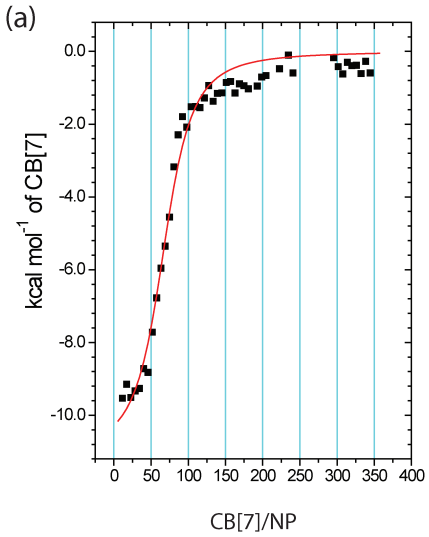

Figure 3.3. Isothermal titration calorimetry (ITC) measurements of BenzNP with CB[7]. The saturation ratio of CB[7]/BenzNP was determined to be 100/1.

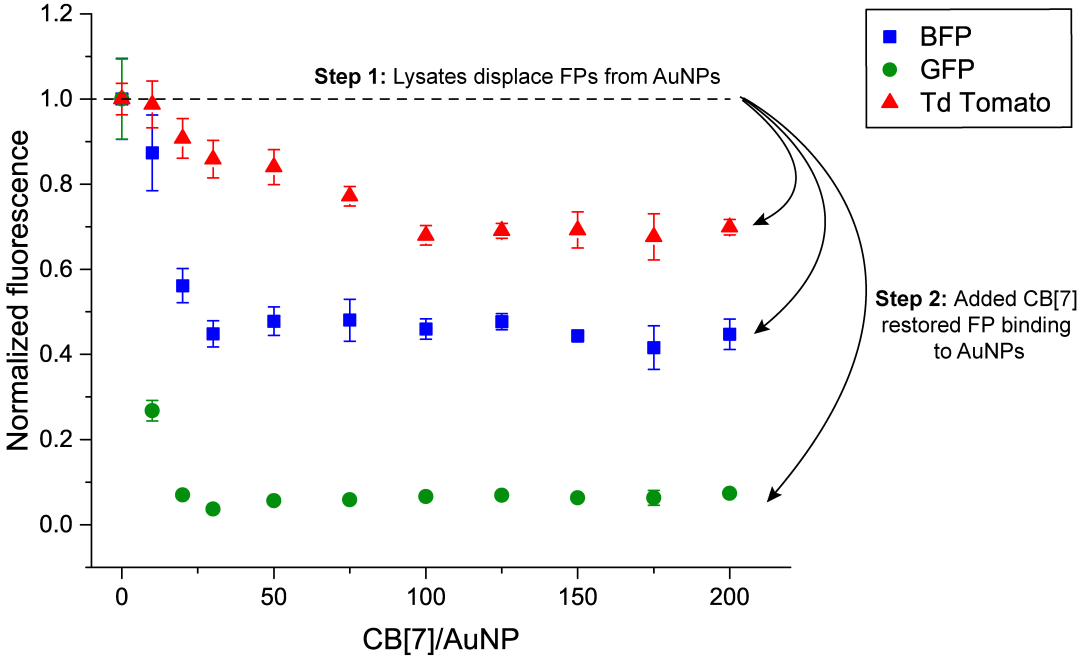

Figure 3.4. Fluorescence titration of BnzNP-FPs with lysates with varying concentrations of CB[7]. The saturation ratio of CB[7]/BenzNP was determined to be 100/1.

As an initial test of our method, five human cancer cell lines with different tissue/organ origins were used: MCF-7 (breast), SKOV3 (ovarian), Raji (blood), NCI-H1299 (lung), HEK239T (kidney) (Table 1). We used fluorescence spectroscopy to generate "fingerprints" for the cell lysates obtained from the cultured cell lines. In practice, cell lysates were added to the BenzNP−FPs complex, readings taken, then CB[7] was added to generate BenzNP−CB[7] in situ, with subsequent readout. These fluorescence outputs were analyzed by linear discriminant analysis (LDA). Cluster separation on an LDA plot was generated based on their standardized Mahalanobis distance: the greater the distance the lower the probability of misclassification. When only three channels are used, there is substantial overlap among different cell lines, especially NCI-H1299, SKOV3, MCF7, and Raji for the BenzNP-FPs channels (Figure 3.5a), and overlaps between NCI-H1299 with HEK-239T, and SKOV3 with MCF-7 for the BenzNP-CB[7] channels (Figure 3.5b). However, when all 6 channels are combined, all five cell lines are well separated (Figure 3.5c).

Table 3.1. Features of five cancerous human cell lines with different tissue origins.

#	Cell line	Tissue origin	Cell status
1	MCF-7	Breast	Cancerous
2	SKOV3	Ovarian	Cancerous
3	Raji	Blood	Cancerous
4	NCI-H1299	Lung	Cancerous
5	HEK239T	kidney	Cancerous

One critical step in chemical-nose sensing is to challenge its reproducibility. For this purpose, we revalidated our sensor by using an unknown set of all five cell lines (5

cell lines × 8 replicates = 40 unknown cases). We were able to predict the identities of the 38 out of 40 unknown cases with 95 % correct unknown identification (% CUI) in a single-well configuration using 6-channel system. When there are only three channels, the % CUI drops drastically (Figure 3.5d).

An important challenge in cancer therapy is determining whether tissue/cells are benign or cancerous; if they are cancerous, then whether or not it has the ability to metastasize to other organs. We chose three different human breast cell lines to test our host-guest doubled array sensor: MCF10A (normal), MCF-7 (cancerous), MDA-MB-231 (metastatic) (Figure 3.6a). The three cell lines also show differential fluorescence patterns that are clustered separately by LDA when 6 channels are used (Figure 3.6b). Similar trend is observed in the % CUI of these three human breast cell lines where the six channel system gives much better unknown identification of 96 % (23 out of 24 samples) compared to the three channels (Figure 3.6c).

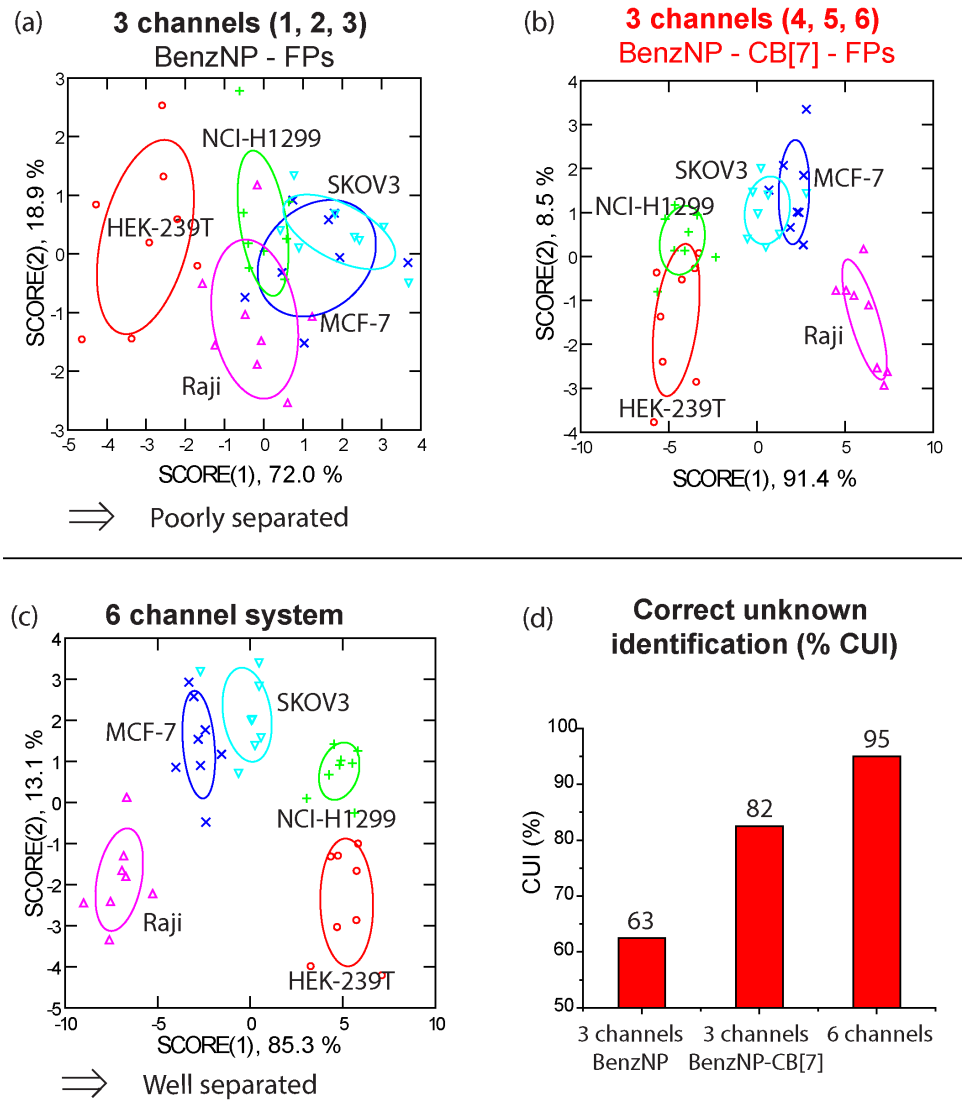

Figure 3.5. Five human cancerous cell lines were clustered using Linear Discriminant Analysis (LDA) with the fluorescence responses from a) only three channels: BenzNP-FPs and b) BenzNP-CB[7], c) all six channels. d) Correct unknown identification percentage of three sensing systems. Unknown population is 40 samples for five cell lines.

To further validate our sensor with a more stringent test, we employed isogenic cell lines derived from BALB/c mice. These cells can provide a testbed for our sensor by avoiding the issue of individual-to-individual geo/phenotypic variation since they share the same genetic background but have different histological stages, as characterized in

vivo. TM40A has undetectable tumorigenicity (0 %), TM9 generated tumors in 38 % of the cases, while MC7-L1 quickly developed tumors and became highly metastatic in 100% of tested mice (100% tumor) (Table 3.2). These challenging isogenic cell lines are also differentiated using our six channel system (Figure 3.7a). However, when only three channels are used, there is always some level of overlap between the non-tumorigenic (TM40A) and the low-tumorigenic group (TM9), while the high tumorigenic cluster is highly separated from the others. This indicates biological similarity between the non-tumorigenic and the low-tumorigenic samples. This same trend is also observed in the fluorescence heat map, analyzed by hierarchical clustering analysis (HCA) using six channels, where TM40A while is separated from TM9, they still share the same sub branch with each other and are much more different than the high-tumorigenic cell line MC7-L1 (Figure 3.7b). These results of 10 cell lines confirm the benefit of increasing the number of channels in chemical-nose sensing system, not just for the classification of each group but most importantly, the accuracy in unknown identification (Figure 3.7c).

(a)

#	Cell line	Tissue origin	Cell status
1	MCF10A	Human breast	Normal immortalized
2	MCF-7	Human breast	Cancerous
3	MDA-MB-231	Human breast	Metastatic

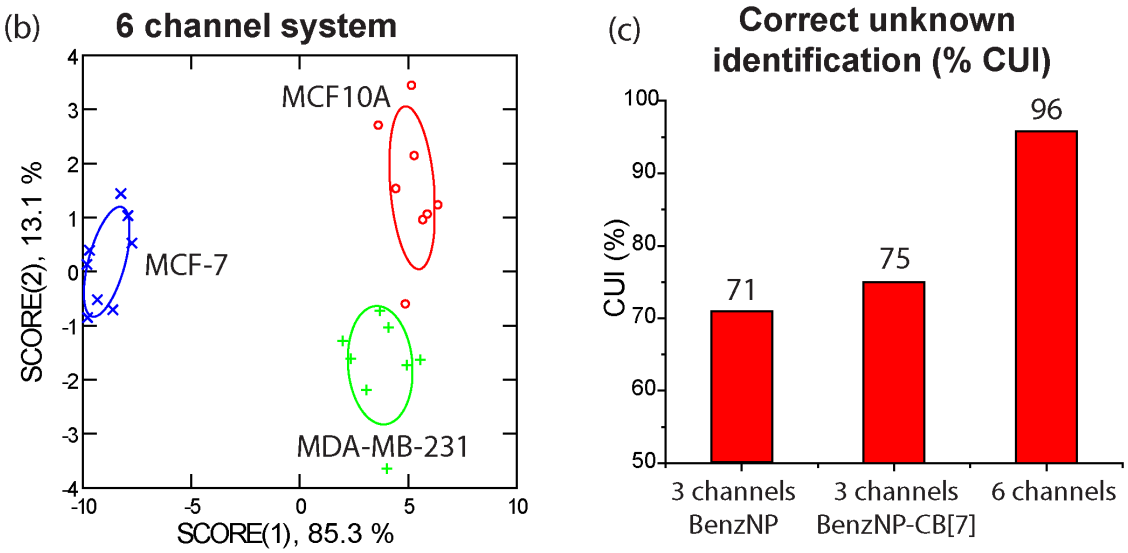

Figure 3.6. Three human breast cell lines with (a) different cell status were clustered using Linear Discriminant Analysis (LDA) with the fluorescence responses from (b) six channels. (c) Correct unknown identification percentage of three sensing systems. Unknown population is 24 samples for three cell lines.

Table 3.2. Features of five breast cell lines.

	#	Cell line	Tissue origin	Cell status
Reference cell lines	1	TM40A	Breast	Normal
	2	TM9	Breast	Low-tumorigenic
	3	MC7-L1	Breast	High-tumorigenic
Cell lines outside	4	FSK7	Breast	Low-tumorigenic

To further validate the versatility of our 6-channel system, we cultured two additional cell lines that have similar histological outcomes with the cell lines in our reference set but different identities. These cell lines are FSK7 (low-tumorigenic) and

MC4-L2 (high-tumorigenic).[54,55] The fingerprints of these two cell lines were compared to the reference set to predict their histological outcomes. LDA plots show the overlap of each unknown cell line with their corresponding tumorigenicity with 100 % accuracy (Figure 4, Table S6). This result strengthens the sensor reliability in identifying clinically relevant features of cells. Notably, translating results from one cell line to use as reference for other novel cell lines has not been achieved previously with chemical-nose sensors.

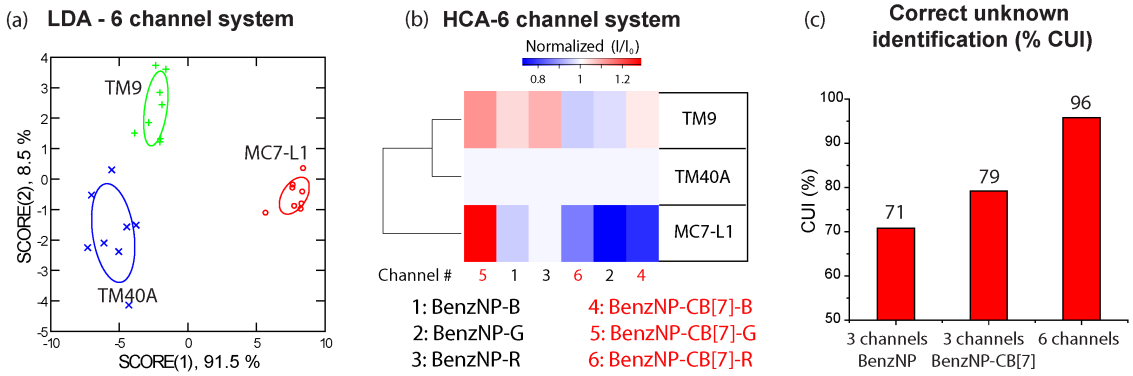

Figure 3.7. Three isogenic breast cell lines derived from BALB/c mice were clustered using Linear Discriminant Analysis (LDA) with the fluorescence responses from a) six channels. b) Heat map of the fluorescence response patterns for the reference set using six channels. Hierarchical clustering was performed on the normalized average of the fluorescence responses, where I_0 is the initial fluorescence intensity of the sensor and I is the final fluorescence intensity of the sensor after lysate incubation. c) Correct unknown identification percentage of three sensing systems. Unknown population is 24 samples for three cell lines.

(a)

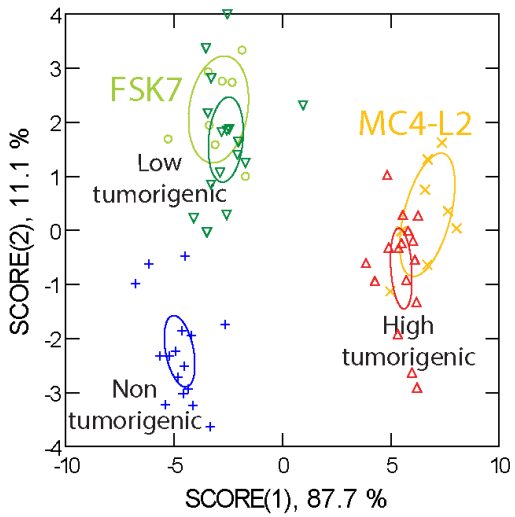

(b)

Cell lines outside of reference set	Type	Number of samples	Correctly identified	% Correct unknown identification (%CUI)
FSK7	Low-tumorigenic	8	8	100
MC4-L2	High-tumorigenic	8	8	100

Figure 3.8. (a) Unknown cell lines were clustered with the established reference cell lines via LDA by using the fluorescence responses from all six channels. (b) The correct unknown identification percentage of FSK7 and MC4-L2 are both 100 %.

3.4. Conclusions

In summary, we have used host-guest chemistry to double the information content of an array-based sensor for cancer diagnostics. The sensor was able to readily discriminate phenotypic changes among cells based on their complex proteomic signatures associated with different histological outcomes. The unique fingerprint of complex cell lysates can be obtained in a single well with minimal sample quantity (200 ng of total proteins), minimizing biopsy size, reducing the invasiveness of the methodology. Significantly, the classification of this host-guest-based sensor could be extended beyond the training set, determining the invasiveness of unknown cell lines that

have similar histological outcomes. In a broader context, this host-guest-based chemical nose sensor presents a general means of increasing dimensionality in array-based sensors.

3.5. Experimental section

3.5.1. Cell culture. Raji cell line was donated by Professor Rachel M. Gerstein (Department of Microbiology and Physiological Systems, University of Massachusetts Medical School). MCF10A, TM40A, TM9, MC7-L1, FSK7, and MC4-L2 cell lines were donated by Professor Joseph Jerry (Department of Veterinary and Animal Science, University of Massachusetts Amherst). Raji was cultured in RPMI-1640 media supplemented with 1% glutamine, 1% non essential amino acid, 1% Sodium Pyruvate, 50 μM β-mercaptoethanol, 10% FBS, and 1% antibiotic solution. MCF10A was cultured in DMEM/F-12 media supplemented with 5% horse serum, 1% penicillin/streptomycin,10 μg/ml insulin, 20 ng/ml EGF, 0.5 μg/ml hydrocortisone, and 100 ng/ml cholera toxin. TM40A, TM9, MC7-L1, FSK7, MC4-L2 were cultured in DMEM:Ham's F12 (1:1) media supplemented with 2% ABS, 25 mM HEPES, 10μg/ml insulin, 5 ng/ml EGF, and 1% antibiotics. MCF-7, SKOV3, HEK239T were cultured in DMEM media supplemented with 10% FBS and 1% antibiotics. MDA-MB-231 was cultured in DMEM/High Glucose media supplemented with 10% FBS and 1% antibiotics. NCI-H1299 was cultured in RPMI-1640 media supplemented with 10% FBS and 1% antibiotic solution. All cells were grown in a humidified atmosphere containing 5% CO2 at 37 °C.

3.5.2. Cell lysate preparation. At about 80% confluence, cells were washed with ice cold PBS to remove all the loosely bound serum proteins in the media before adding

1mL of protease inhibitor-contained lysis buffer (0.15 mmol/L NaCl, 5 mmol/L EDTA, 1% Triton-X 100, 10 mmol/L Tris-HCl (pH 7.4), plus half a tablet of complete protease inhibitor cocktail in 50 mL of buffer (Roche Diagnostics GmbH)). These cell flasks were stored at 4 oC for 15 minutes to ensure the lysis of the cell membrane. After 15 minutes, the cells were scraped with a sterile scraper, transferred to an eppendorf tube to be centrifuged down at 4 oC for 20 minutes at 14,000 rpm. The supernatant which contains cellular proteins were then quantified using BCA assay. For cell lysate sensing experiment, 200 ng of total protein from each cell line was used.

3.5.3. Fluorescence titrations. In the fluorescence quenching experiment with BenzNP, an equimolar solution of the three FPs (100 nM each) was titrated with various concentrations of BenzNP ranging from 0 to 300 nM. The excitation/emission/cut-off wavelengths were 380/450/435, 475/510/495, and 550/585/570 nm for EBFP2, EGFP and tdTomato, respectively. The change of fluorescence intensity at the respective emission maxima was recorded on a Molecular Devices SpectraMax M3 microplate reader at 25 °C. For the CB[7] titration with BenzNP-FPs complex, the optimized concentration of the sensor complex (150 nM BenzNP and 100 nM each FPs) was first mixed together and 200 μL of this mixture was added into the 96 well plate. To test the releasing capability of FPs, 200 ng of Lipase (prepared in the same lysis buffer as other cell lysates) was added into BenzNP-FPs mixture and this mixture was incubated for 15 minutes. Then, 10μL of a series of CB[7] concentrations was added into the previous mixture to determine the ratio of CB[7] and BenzNP that can quench FPs. Nonlinear least-squares curve fitting analysis was employed to estimate the binding constant (K_a) and association stoichiometry (n) using a 1:1 binding model.

3.5.4. Sensing studies. BenzNP-FPs conjugates were generated by mixing 150 nM of BenzNP and each FPs (100 nM) in 5 mM sodium phosphate buffer (pH 7.4). Then, 200 μL of BenzNP-FPs complex solution was loaded into a 96-well microplate, and initial fluorescence intensities (I_0) of the quenched complexes were measured at 450/510/585 nm. Then, 200 ng of each cell lysates was incubated with these complexes to determine the changes in fluorescence of the BenzNP-FPs complexes and establish the first three channels. After that, 10 μL of CB[7] was added into the 96 well plate using a Molecular Devices SpectraMax M3 microplate reader (at 25 ^{o}C).

3.6. References

(1) Van de Stolpe, A.; Den Toonder, J. M. J. *Cancers* **2014**, *6*, 1195-1207.

(2) Reil, A.; Wesche, J.; Greinacher, A.; Bux, J. *Transfusion* **2011**, *51*, 18-24.

(3) Peng, G.; Tisch, U.; Adams, O.; Hakim, M.; Shehada, N.; Broza, Y. Y.; Billan, S.; Abdah-Bortnyak, R.; Kuten, A.; Haick, H. *Nat. Nanotechnol.* **2009**, *4*, 669 – 673.

(4) Diamandis, E. P. *Mol. Cell. Proteomics* **2004***, 3*, 367–378.

(5) Everley, P. A.; Krijgsveld, J.; Zetter, B. R.; Gygi, S. P. *Mol. Cell. Proteomics* **2004**, *3*, 729-735.

(6) Gharbi, S.; Gaffney, P.; Yang, A.; M. J. Zvelebil, Cramer, R.; Waterfield, M. D.; Timms, J. F. *Mol. Cell. Proteomics* **2002**,*1*, 91-98.

(7) O'Dwyer, D.; Ralton, L. D.; O'Shea, A.; Murray, G. I. *Plos One* **2011**, *6*.

(8) Abbani, M. A.; Mallick, P.; Vogelsang, M. S. *Mass Spectrometry Based Proteomics in Cancer Research*, Springer, New York, **2010**.

(9) Hanash, S.; Taguchi, A. *Nature Reviews Cancer* **2010**, *10*, 652-660.

(10) Miranda, O. R.; Creran, B.; Rotello, V. M. *Curr. Opin. Chem. Biol.* **2010**, *14*, 728–736.

(11) Wright, A. T.; Anslyn, E. V. *Chem. Soc. Rev.* **2006**, *35*, 14–28.

(12) Tao, Y.; Ran, X.; Ren, J.; Qu, X. *Small* **2014**, *10*, 3667–3671.

(13) Peng, G.; Tisch, U.; Adams, O.; Hakim, M.; Shehada, N.; Broza, Y. Y.; Billan, S.; Abdah-Bortnyak, R.; Kuten, A.; Haick, H. *Nat. Nanotechnol.* **2009**, *4*, 669–673.

(14) Palacios, M. A.; Nishiyabu, R.; Marquez, M.; Anzenbacher, P. *J. Am. Chem. Soc.* **2007**, *129*, 7538–7544.

(15) Kumar, V.; Anslyn, E. V. *J. Am. Chem. Soc.* **2013**, *135*, 6338–6344.

(16) Zhou, H.; Baldini, L.; Hong, J.; Wilson, A. J.; Hamilton, A. D. *J. Am. Chem. Soc.* **2006**, *128*, 2421–2425.

(17) De, M.; Rana, S.; Akpinar, H.; Miranda, O. R.; Arvizo, R. R.; Bunz, U. H. F.; Rotello, V. M. *Nat. Chem.* **2009**, *1*, 461–465.

(18) Bajaj, A.; Miranda, O. R., Kim, I.-B.; Phillips, R. L.; Jerry, D. J.; Bunz, U. H. F.; Rotello, V. M. *Proc. Natl. Acad. Sci.* **2009**, *106*, 10912–10916.

(19) El-Boubbou, K.; Zhu, D. C.; Vasileiou, C.; Borhan, B.; Prosperi, D.; Li, W.; Huang, X. *J. Am. Chem. Soc.* **2010**, *132*, 4490–4499.

(20) Phillips, R. L. ; Miranda, O. R.; You, C.-C.; Rotello, V. M.; Bunz, U. H. F. *Angew. Chem. Int. Ed.* **2008**, *47*, 2590–2594.

(21) Rana, S.; Singla, A. K.; Bajaj, A.; Elci, S. G.; Miranda, O. R.; Mout, R.; Yan, B.; Jirik, F. R.; Rotello, V. M. *ACS Nano* **2012**, *6*, 8233–8240.

(22) You, C-C.; Miranda, O. R.; Gider, B.; Ghosh, P. S.; Kim, IK-B.; Erdogan, B.; Krovi, S. A.; Bunz, U. H. F.; Rotello, V. M. *Nat. Nanotechnol.* **2007**, *2*, 318–323.

(23) Chou, S. S.; De, M.; Luo, J.; Rotello, V. M.; Huang, J.; Dravid, V. P. *J. Am. Chem. Soc.* **2012**, *134*, 16725–16733.

(24) Pei, H.; Li, H. J.; Lv., M.; Wang, J.; Gao, J.; Lu, J.; Li, Y.; Huang, Q.; Hu, J.; Fan, C. *J. Am. Chem. Soc.* **2012**, *134*, 13843–13849.

(25) Yuan, Z.; Du, Y.; Tseng, Y.-T.; Peng, M.; Cai, N.; He, Y.; Chang, H.-T.; Yeung, E. S. *Anal. Chem.* **2015**, *87*, 4253–4259.

(26) Kong, H.; Liu, D.; Zhang, S. C.; Zhang, X. R. *Anal. Chem.* **2011**, *83*, 1867–1870.

(27) Jiménez, D.; Martínez-Máñez, R.; Sancenón, F.; Ros-Lis, J. V.; Soto, J.; Benito, Á.; García-Breijo, E. *Eur. J. Inorg. Chem.* **2005,** *2005***,** 2393–2403.

(28) Ábalos, T.; Jiménez, D.; Martínez-Máñez, R.; Ros-Lis, J. V.; Royo, S.; Sancenóna, F.; Soto, J.; Costero, A. M.; Gil, S.; Parra, M. *Tetrahedron Lett.* **2009**, *50*, 3885–3888.

(29) Jiménez, D.; Martínez-Máñez, R.; Sancenón, F.; Soto, J. *Tetrahedron Lett.* **2004**, *45*, 1257–1259.

(30) Wu, P.; Miao, L.-N.; Wang, H.-F.; Shao, X.-G.; Yan, X.-P. *Angew. Chem. Int. Ed.* **2011**, *50*, 8118–8121.

(31) Schmittel, M.; Lin, H.-W. *Angew. Chem. Int. Ed.* **2007**, *46*, 893–896.

(32) Li, X.; Kong, H.; Mout, R.; Saha, K.; Moyano, D. F.; Robinson, S. M.; Rana, S.; Zhang, X.; Riley, M. A.; Rotello, V. M. *ACS Nano* **2014**, *8*, 12014-12019.

(33) Rana, S.; Le, N.D. B.; Mout, R.; Duncan, B.; Elci, S. G.; Saha, K.; Rotello, V. M. *ACS Cent. Sci.* **2015**, *1*, 191–197.

(34) Xu, Q.; Zhang, Y.; Tang, B.; Zhang, C.-Y. *Anal. Chem.* **2016**, *88*, 2051-2058.

(35) Rana, S.; Le, N. D. B.; Mout, R.; Saha, K.; Tonga, G. Y.; Bain, R. E. S.; Miranda, O. R.; Rotello, C. M.; Rotello, V. M. *Nat. Nanotechnol.* **2015**, *10*, 65–69.

(36) Grana-Suarez, L.; Verboom, W.; Huskens, J. *Chem. Commun.* **2014**, *50*, 7280-7282.

(37) Yang, S. K.; Ambade, A. V.; Weck, M. *J. Am. Chem. Soc.* **2010**, *132*, 1637-1645.

(38) Chandler, D. *Nature* **2005**, *437*, 640−647.

(39) Wenz, G.; Han, B. H.; Müller, A. *Chem. Rev.* **2006**, *106*, 782−817.

(40 Xu, X.-D.; Zhao, L.; Qu, Q.; Wang, J.-G.; Shi, H.; Zhao, Y. *ACS Appl. Mater. Interfaces* **2015**, *7*, 17371–17380.

(41) Hu, Q.-D.; Tang, G.-P.; Chu, P. K. *Acc. Chem. Res.* **2014**, *47*, 2017–2025.

(42) Esser, B.; Swager, T. M. *Angew. Chem., Int. Ed.* **2010**, *49*, 8872–8875.

(43) Lee, J. W.; Samal, S.; Selvapalam, N.; Kim, H.-J.; Kim, K. *Acc. Chem. Res.* **2003**, *36*, 621–630.

(44) Masson, E.; Ling, X.; Joseph, R.; Kyeremeh-Mensah, L.; Lu, X. *RSC Adv.* **2012**, *2*, 1213–1247.

(45) Le, N. D. B.; Tonga, G. Y.; Mout, R.; Kim, S. T.; Wille, M. E.; Rana, S.; Dunphy, K. A.; Jerry, D. J.; Yazdani, M.; Ramanathan, R.; Rotello, C. M.; Rotello V. M. *J. Am. Chem. Soc.* **2017**, *139*, 8008-8012.

(46 Kim, C.; Tonga, G. Y.; Yan, B.; Kim, C. S.; Kim, S. T.; Park, M.-H.; Zhu, Z.; Duncan, B.; Creran, B.; Rotello, V. M. *Org. Biomol. Chem.* **2015**, *13*, 2474-2479.

(47) Freeman, W. A.; Mock, W. L.; Shih, N.-Y. *J. Am. Chem. Soc.* **1981**, *103*, 7367-7368.

(48) Cao, L.; Isaacs, L. *Supramol. Chem.* **2014**, *26*, 251-258.

(49) Zhao, J.; Zhang, Y. M.; Sun, H. L.; Chang, X. Y.; Liu, Y. *Chem. Eur. J.* **2014**, *20*, 15108-15115.

(50) Yeh, Y.-C.; Rana, S.; Mout, R.; Yan, B.; Alfonso, F. S.; Rotello, V. M. *Chem. Commun.* **2014**, 50, 5565-5568.

(51) Bhasikuttan, A. C.; Mohanty, J.; Nau, W. M.; Pal, H. *Angew.Chem.* **2007**, 119, 4198–4200.

(52) Chinai, J. M.; Taylor, A. B.; Ryno, L. M.; Hargreaves, N. D.; Morris, C. A.; Hart, P. J. Urbach, A. R. *J. Am. Chem. Soc.* **2011**, 133, 8810–8813.

(53) Logsdon, L. A.; Schardon, C. L.; Ramalingam, V.; Kwee, S. K.; Urbach, A. R. *J. Am. Chem. Soc.* **2011**, *133*, 17087-17092.

(54) Kittrell, F. S.; Oborn, C. J.; Medina, D. *Cancer Res.* **1992**, *52*, 1924-1932.

(55) Medina, D. *J. Cell. Biochem.* **1993**, 155–155.

CHAPTER 4

SIMPLE AND ROBUST POLYMER-BASED SENSOR FOR RAPID CANCER DETECTION USING SERUM

4.1. Abstract

We report a polymer-based sensor that rapidly detects cancer, based on changes in serum protein levels. This sensing platform utilizes the fluorescence signals from two charge-complementary polymers, and their fluorescence resonance energy transfer (FRET) to provide three ratiometric outputs. This simple system rapidly identifies cancer-bearing mice in transgenic and xenograft mouse models. This sensor was validated by accurate prediction on blinded unknown samples, demonstrating the robustness of the approach. Taken together, this polymer-sensing platform provides an attractive strategy for point-of-care testing.

4.2. Introduction

Effective treatment of cancer requires early detection, making the creation of rapid and inexpensive sensing systems important for both health and healthcare cost reasons.[1-3] Serum presents a minimally invasive target for the design of cancer diagnostics. A broad range of protein level in serum changes during tumor development.[3-5] Most techniques used for detection of cancer using serum focus on specific biomarkers. Enzyme-linked immunosorbent assay (ELISA) remains the method of choice.[6,7] ELISA, however, has limitations in sensitivity for low-abundance biomarkers. Most importantly, many cancer types do not have ideal biomarkers, due to widely different baseline

expressions of targeted biomarkers in the population, often leading to false positives and negatives in these tests.[1b,8-10] Serum analysis can also be done by gel electrophoresis, coupled with mass spectrometry, but analysis time, quantification challenges, and expensive instrumentation are an issue.[11-13]

'Chemical noses/tongues' provide an alternative to biomarker-based sensing and do not require previous knowledge of the analytes; instead they 'train' the sensor system to recognize analytes based on the overall subtle changes in complex mixtures.[14-16] Array-based sensors are composed of recognition and transduction elements, work hand in hand to establish a fingerprint for each analyte. An array of five gold nanoparticles detects proteins in human serum. Their binding was transduced by green fluorescent proteins (GFPs).[17] Array-based sensors combine recognition and transduction, such as magnetic glyconanoparticle (MGNP) arrays[18] and nanomaterial-assisted chemiluminescence.[19] Overall, chemical noses and tongues are able to identify proteins,[17] carbohydrates,[20] and mammalian cells[21-23] in addition to white wines, fruit juices and non-steroidal antiinflammatories.[24-26]

Simplicity and scalability are important attributes for point of care (POC) diagnostics.[27] To address this concern, we have directed our focus on a simple but robust polymer-based sensor system for profiling serum for cancer diagnostics. This system is based on the fluorescence signals of two charge-complementary conjugated fluorescent polymers and their fluorescence resonance energy transfer (FRET) to provide three ratiometric outputs. This polymer-only platform utilizes the structural diversity, fluorescence efficiency, stability, and scalability of conjugated polymer "molecular wires"[28-32] to detect cancer in sera of cancer-bearing mice. The transgenic and xenograft

animal models used in this study plausibly recapitulate some of the clinically relevant events seen in individuals with cancer.

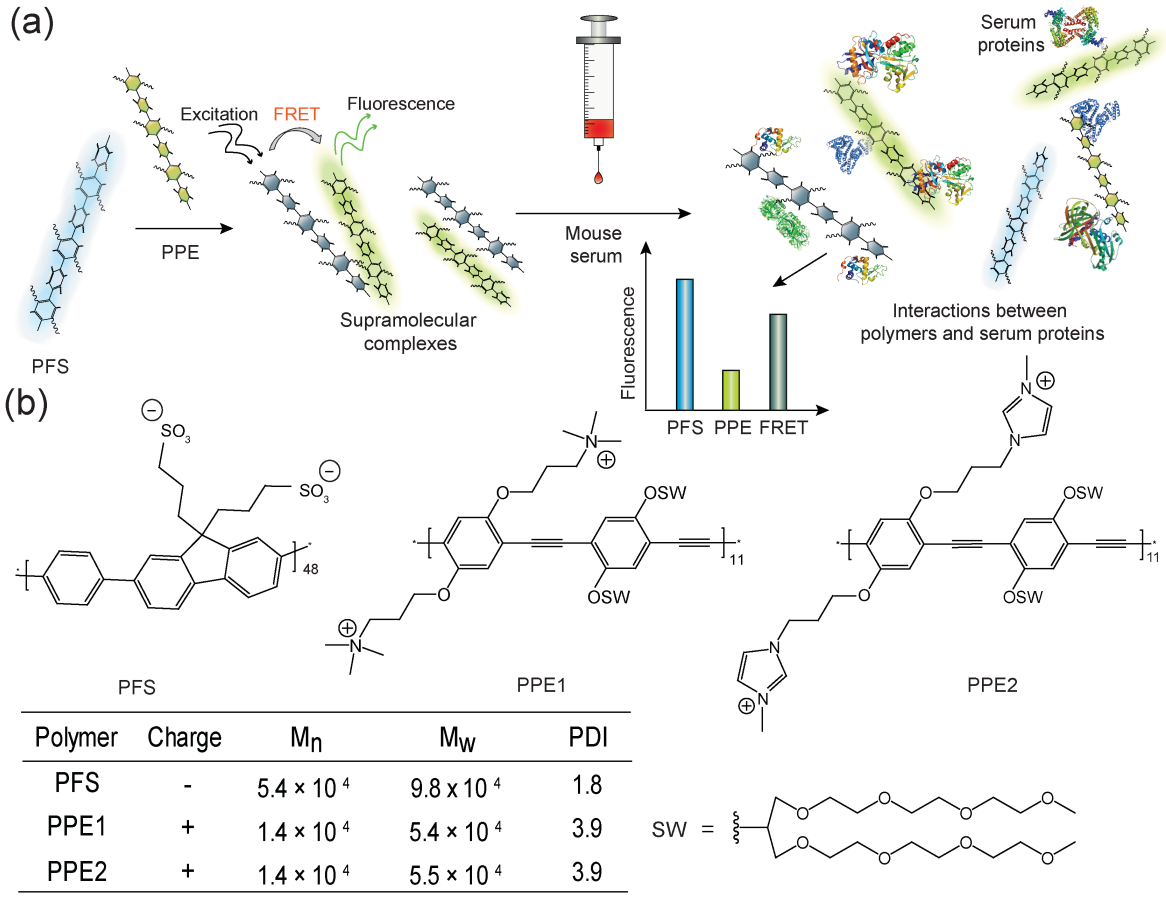

Polymer	Charge	M_n	M_w	PDI
PFS	-	5.4×10^4	9.8×10^4	1.8
PPE1	+	1.4×10^4	5.4×10^4	3.9
PPE2	+	1.4×10^4	5.5×10^4	3.9

Figure 4.1. Schematic illustration of FRET-based polymer sensor for serum sensing. (a) Two polymers with opposite charges form supramolecular complexes through electrostatic interactions, generating FRET responses. The fluorescence intensities of two polymers and FRET responses are interfered with the addition of serum proteins. (b) Chemical structures and characteristics of polymers used in the study. M_n: number-average molecular weight; M_w: weight-average molecular weight; PDI: polydispersity index.

4.3. Results and Discussion

We designed two different backbones for our donor and acceptor polymers to provide an optimum FRET-based sensor, which is composed of polyfluorene sulfonate (PFS) and poly(p-phenyleneethynylen) (PPEs), respectively. Upon addition of serum, the fluorescence of each polymer, as well as their FRET process, are modulated due to the binding of serum proteins to the polymers. These fluorescence fingerprints are analyzed by linear discriminant analysis (LDA) to create a reference set (training set) and predict future unknown samples (Figure 4.1). Upon excitation at the PFS absorbance band of 365 nm, the complexes PFS-PPE1 and PFS-PPE2 exhibit efficient FRET from PFS to PPEs. We observed the decreased fluorescence emission at 420 nm and sensitized emission at 480 nm for PPE1 and 482 nm for PPE2 (Figure 4.2).

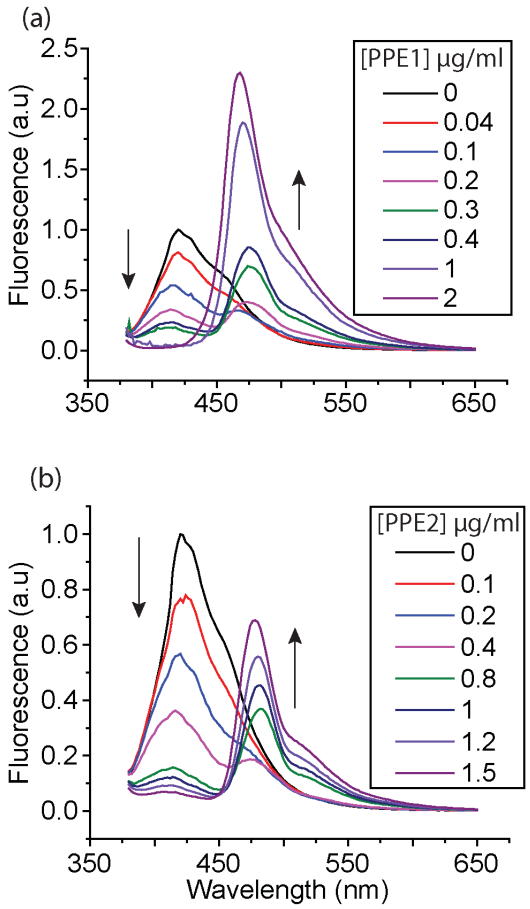

Figure 4.2. Emission spectra as a function of concentration of (a) PPE1 for the PFS-PPE1 pair and (b) PPE2 for the PFS-PPE2 pair. Spectra were recorded at an excitation of 356 nm for each pair in phosphate buffer saline (PBS), at pH 7.4.

Table 4.1. Characteristics of eight proteins in PBS

#	Proteins	Charge at pH 7.4	Isoelectric point	Molecular weight (kDa)
1	Transferrin	Neutral	6.1	80
2	Fibrinogen	-	5.5	340
3	Human Serum Albumin	-	5.2	69.4
4	α1-antitrypsin	-	4.6	52
5	Myoglobin	Neutral	7.2	17
6	Lipase	-	5.6	58
7	Alkaline Phosphatase	-	5.7	140
8	Cytochrome C	+	10.7	12.3

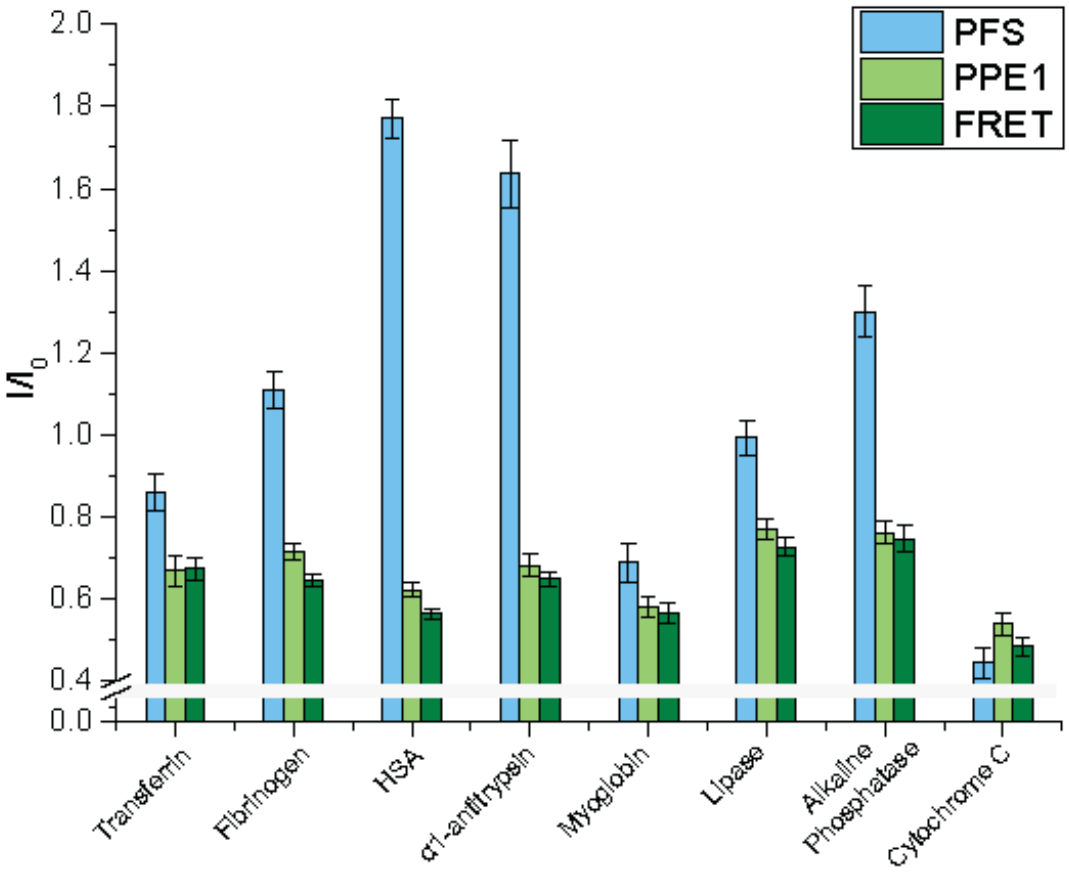

Figure 4.3. Fluorescence response from PFS-PPE1 sensor after eight protein incubation in PBS.

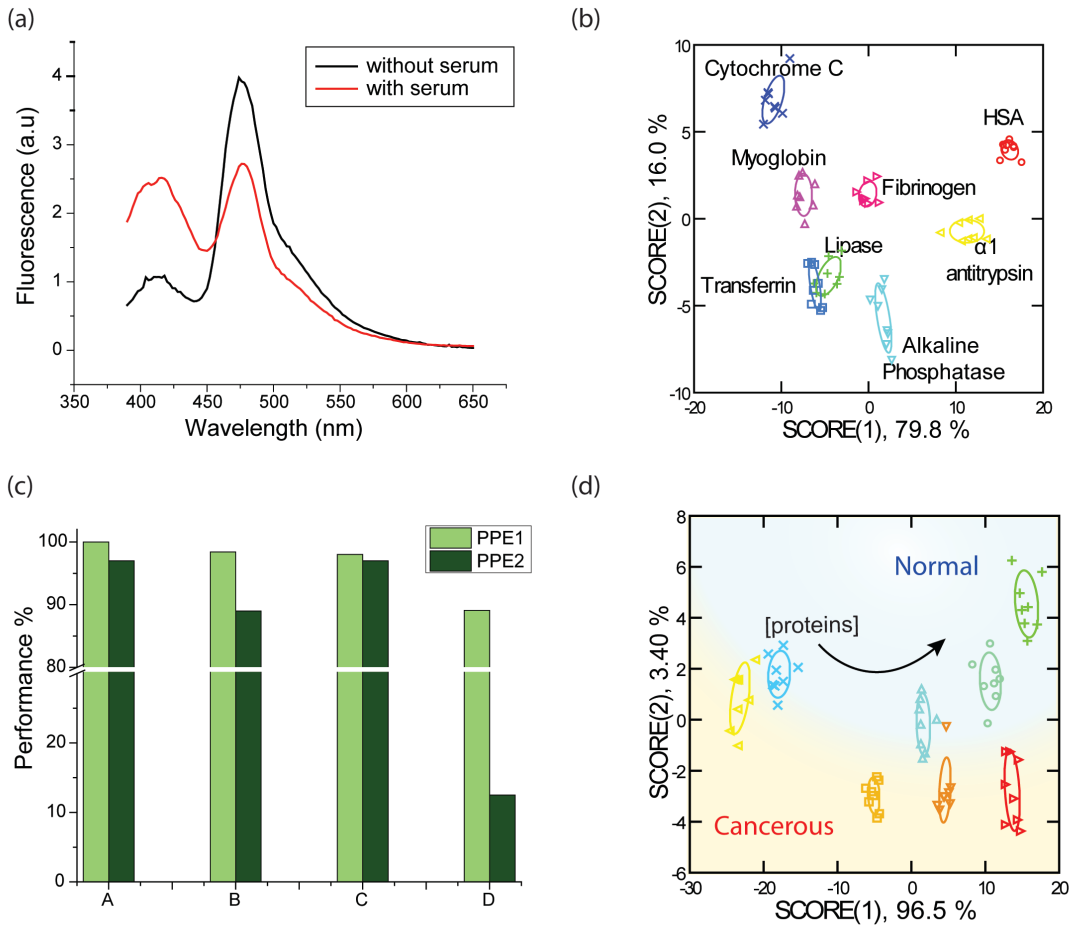

Figure 4.4. Comparison between two polymer pairs: PFS-PPE1 and PFS-PPE2. (a) Initial fluorescence spectrum (black) of the PFS-PPE1 complex and final spectrum upon incubation with pure calf serum (red). (b) LDA plot of the PFS-PPE1 complex responses to eight proteins in PBS at 10 µg/ml with a 100 % correct classification. HSA is Human Serum Albumin. The analysis resulted in canonical scores with two discriminants explaining 79.8 %, and 16.0 % of total variance and was plotted with 95% confidence ellipses around the centroid of each group. (c) Performance comparison between PFS-PPE1 and PFS-PPE2 FRET pairs, where A is the classification accuracy of eight proteins detected in PBS, B is the correct unknown identification (CUI %) of these eight proteins in PBS, C is the classification accuracy of normal and cancerous mouse serum samples from the transgenic lung cancer model at different concentrations, and D is the CUI % of these mouse serum samples at different concentrations. (d) Limit of detection of PFS-PPE1 complex in detecting normal and cancerous mouse serum samples from the transgenic cancer model at 1, 5, 10, and 20 mg/ml total protein concentrations, in the order from left to right.

After we determined the ratio of PFS and PPEs with a suitable FRET response, each pair was tested in calf serum, the addition of which caused a decrease in sensitized PPE fluorescence and an increase in the donor PFS fluorescence. This observation indicated dissociation of the complexes due to binding of serum proteins towards these polymers. These FRET-based sensors identify eight different proteins dissolved in phosphate buffer saline (PBS, pH 7.4) (Table 4.1). We observed distinct fluorescence changes for all eight proteins from each polymer pair, PFS-PPE1 and PFS-PPE2 (Figure 4.3). LDA plots show correct classifications of different proteins (100 % and 97.0 %, respectively) but also successfully identified blinded unknown samples (98.4 % and 89.0 %, respectively) (Figure 4.4b, c) and that in a matter of minutes.

Table 4.2. Characteristics of tumor mouse models

Model type	**Mouse strain**	**Cell line**	**Injection location**	**Tumor induction time (days)**	**# Controls**	**# Cancer-bearing mice**
Transgenic lung cancer model	129/Sv $p53^{R172HAg/+}$ $K\text{-}ras^{LA1/+}$ mice	N/A	N/A	100-300	5	5
Experimental lung cancer model	NIH-III (*nu/nu; beige/beige*) mice	H1299	Intracardiac route	55-120	5	5

We validated the sensor using a more challenging test bed: cancer-bearing mice and healthy controls from a transgenic lung model (Table 4.2), established by mutations

in the *Kras* and *p53* genes. We determined the total serum protein concentration necessary for the assay. Four different concentrations of normal and cancerous sera from the transgenic lung model were prepared and titrated with each sensor. The LDA plot shows separation of normal (upper) versus cancerous (lower) serum samples with a shift from left to right that associates with low to high concentrations of total proteins: 1, 5, 10, and 20 mg/ml (Figure 4.4d). Although sera from normal controls and cancer-bearing mice were differentiated at all four concentrations, we chose 5 mg/ml total serum proteins for further experiments because of its stable and differentiable fluorescence responses. Both sensors were able to classify all 8 clusters of 64 samples (4 concentrations × 2 serum types (normal and cancerous) × 8 replicates). PFS-PPE1 performed better than PFS-PPE2 with 89.1 % versus 12.5 % (Figure 4.4c) in unknown identification and we chose the PFS-PPE1 pair for all of our mouse serum experiments.

Serum protein levels vary from patient to patient even when they have the same type of cancer, one challenge for cancer diagnostics.[33] This motivates us to examine the effect of individual differences from cancer-bearing mice of the same cancer model. We prepared five normal healthy controls (M1 to M5) and five transgenic cancerous mice (M6 to M10). The LDA plot shows distinct clusters for the control versus cancerous groups, with all five healthy controls and all five cancerous mice clustering together within their respective groups with 100 % accuracy (Figure 4.5a). To test the reproducibility of our PFS-PPE1 sensor, we generated 80 blinded cases (5 mice × 2 types (normal and cancerous) × 8 replicates) for unknown prediction (Figure 4.5b), results in 98.7 % of correct unknown identification of normal and cancerous samples from the transgenic lung model (Figure 4.5c).

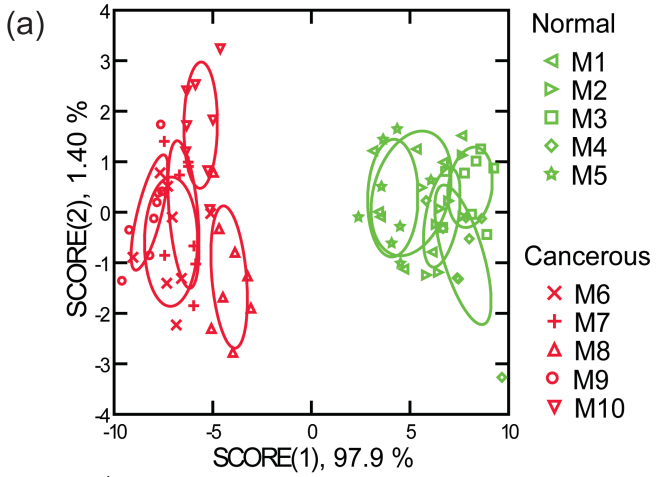

(c)

#	Status	# Samples	Correctly identified	Accuracy %
M1	Normal	8	8	100
M2	Normal	8	8	100
M3	Normal	8	8	100
M4	Normal	8	8	100
M5	Normal	8	7	87.5
M6	Cancerous	8	8	100
M7	Cancerous	8	8	100
M8	Cancerous	8	8	100
M9	Cancerous	8	8	100
M10	Cancerous	8	8	100
Total		80	79	**98.7**

Figure 4.5. Detection of mouse serum samples from the transgenic lung cancer model using PFS-PPE1 complex. (a) LDA plot of the PFS-PPE1 complex responses to serum samples of five normal and five cancerous mice. The analysis resulted in canonical scores with two discriminants explaining 97.9 %, and 1.4 % of total variance and was plotted with 95% confidence ellipses around the centroid of each group. (b) Unknown mouse serum samples were clustered with the established reference serum via LDA using the fluorescence responses. (c) Results of unknown identification of 80 mouse serum samples using LDA algorithm.

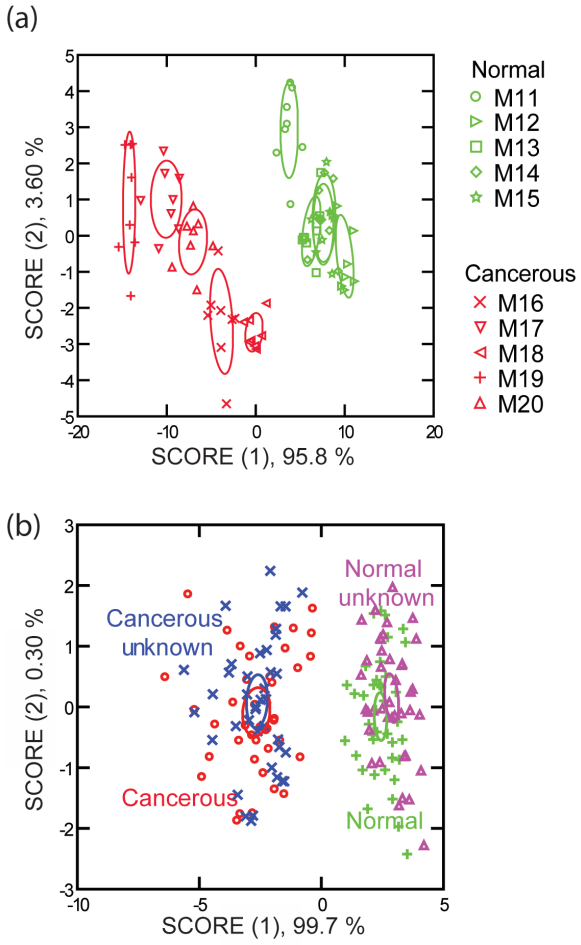

Figure 4.6. Detection of mouse serum samples from lung cancer model using PFS-PPE1 complex. (a) LDA plot of the PFS-PPE1 complex responses to serum samples of five normal and five cancerous mice. The analysis resulted in canonical scores with two discriminants explaining 95.8 %, and 3.6 % of total variance and was plotted with 95% confidence ellipses around the centroid of each group. (b) Unknown mouse serum samples were clustered with the established reference sera via LDA by using the fluorescence responses, resulted in a 100 % CUI.

We tested the generality of the PFS-PPE1 sensor using another mouse model: a lung tumor model induced by H1299-EGFP-luc2 cells. This model includes 10 mice (5 normal healthy mice and 5 cancerous mice) (Table 4.2). Similar to the transgenic cancer model, the LDA plot of this model differentiates between normal and cancerous mice

with 100 % classification accuracy (Figure 4.6). Our assay also picks up the heterogeneity in different cancerous mice within the same tumor model. In all the mouse models, there are more variations among cancerous mouse samples than the normal controls.

(a)

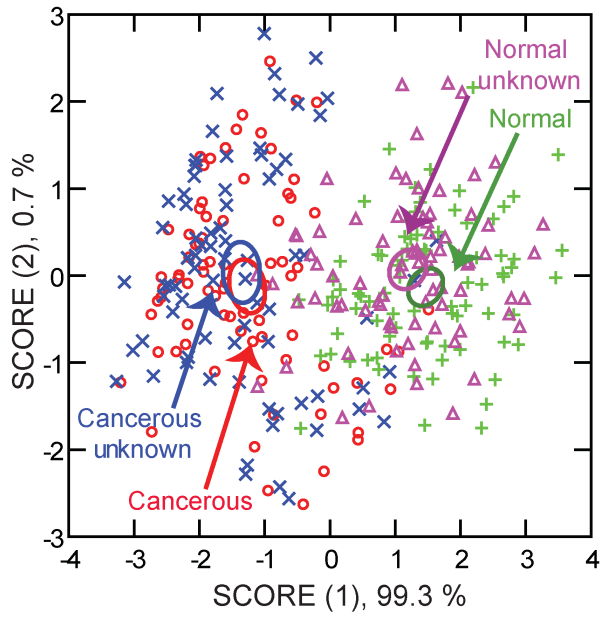

(b)

Model	True ID	# Samples	# Correctly identified	Accuracy %
Transgenic Lung Experimental Lung	Cancer	80	73	91
Transgenic Lung Experimental Lung	Normal	80	66	83
TOTAL		160	139	**87**

Figure 4.7. Combined serum data from both models: transgenic and experimental lung models. (a) LDA plot of the PFS-PPE1 complex responses to combined cancerous serum samples and combined normal serum samples. The analysis resulted in canonical scores with two discriminants explaining 99.3 %, and 0.7 % of total variance and was plotted with 95% confidence ellipses around the centroid of each group. (b) Unknown mouse serum samples were clustered with the established reference sera via LDA by using the fluorescence responses, resulted in a 87 % CUI.

The ultimate goal of a diagnostic test is to answer the question of whether or not the patient has cancer. For this purpose, we combined all control samples from both transgenic lung and experimental lung models to serve as the reference for normal healthy mice, and cancerous samples from both models as the reference for cancer-bearing mice. LDA analysis shows 91 % of classification accuracy between normal and cancerous samples from both cancer models. Unknown prediction for this combined-model data set is also very effective, 87 % (Figure 4.7).

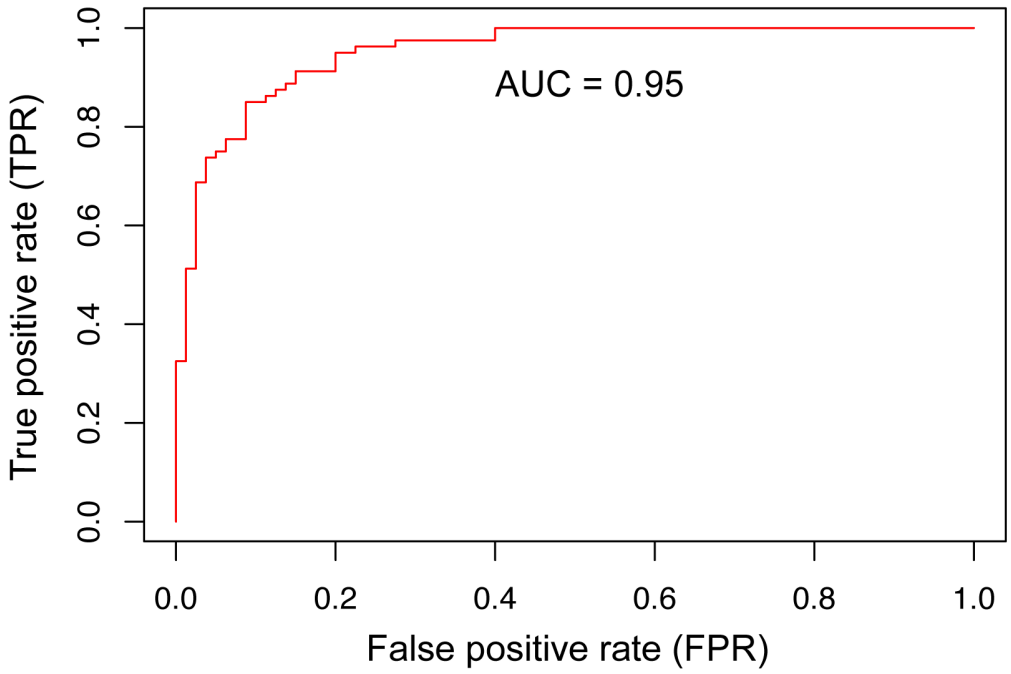

Figure 4.8. Receiver operating characteristic (ROC) analysis of the combined data from both transgenic lung and experimental lung models. The accuracy of the test depends on how well the test separates the group being tested into those with and without cancer. An ideal diagnostic test would have the true-positive rate equals one and the false-positive rate equals zero. AUC was calculated to be 0.95 with a sensitivity of 91.2 % and a specificity of 85.0 % using the cut-off level at 0.27. Cut-off level is the optimal threshold to maximize TPR while minimizing FPR.

An important and useful technique for evaluating the performance of diagnostic tests is the receiver operating characteristic (ROC) curve.[34] Conventionally, the performance of a diagnostic test is usually summarized by two quantities related to the two types of errors: true-positive rate and false-positive rate. The true-positive rate is the probability that a patient with cancer is correctly classified as having cancer, and the false-positive rate is the probability that a patient without cancer is incorrectly classified as having cancer. In other word, the true-positive rate reflects sensitivity and one minus the false-positive rate reflects specificity. An ideal diagnostic test would have the true-positive rate equals one and the false-positive rate equals zero. For cancer screening, the false-positive rate needs to be very low; otherwise, an inordinate number of screened healthy subjects will have unnecessary harmful therapies.[35] Figure 4.8 shows the ROC analysis of the sensor when using the combined data from both transgenic lung and experimental lung models in the unknown identification. The AUC was calculated to be 0.95 (95 % confidence level: 0.92-0.98) with a sensitivity of 91.2 % and a specificity of 85.0 % using the cut-off level at 0.27. The AUC value obtained in our study is well within the excellent diagnostic accuracy range (AUC = 0.9-1.0).[36] Our test is also well above the standard accuracy range required for most diagnostic tests[37] and is more accurate compared to most tests using single specific biomarker.[38-40]

4.4. Conclusions

We demonstrated a robust FRET-based polymer assay, which rapidly differentiated healthy controls and cancer-bearing mice using their sera. In total, 224

cases from 20 mice were accurately and readily identified within only minutes. This sensor benefits from the highly responsive conjugated fluorescent polymers as well as the simplicity of minimal sensor elements (only two polymers). In addition, the stability and scalability of this polymer-based sensor make it an attractive strategy for point-of-care testing.[27] More importantly, serum is an easy accessed biofluid, which allows a simple diagnostic and prognostic approach that poses low level of inconvenience to patients.

4.5. Experimental section

4.5.1. FRET optimization. A series of concentrations of PPE1 and PPE2 were mixed independently with a constant concentration of the donor PFS at 0.2 μg/ml in 96 well plate. All fluorescent spectra were recorded at room temperature using Molecular Devices Spectramax M5 plate reader with an excitation wavelength of 356 nm. PPE1 and PPE2 concentrations were varied between 0.04 to 2 μg/ml and 0.1 to 1.5 μg/ml, respectively. For the calf serum incubation study, each condition of each polymer pair was incubated with 10 μL of undiluted calf serum for 30 minutes. The optimized ratios of PPE1/PFS and PPE2/PFS were 1.5 and 5, respectively. To enhance the fluorescence intensity of PPE1 and PFS, we kept the same ratio for this pair but increased their concentrations to 0.75 and 0.5 μg/ml, respectively.

4.5.2. Animal models. Mice were maintained on standard mouse chow, and housed in a specific pathogen-free barrier facility with ethics approval from the University of Calgary Animal Care Committee and in accordance with Canadian Council on Animal Care guidelines. Use of the non-small cell lung cancer model harboring

p53R172HΔg/+ and K-rasLA1/+ transgenes has been described earlier.[41] Experimental Xenograft lung cancer model using H1299-EGFP-luc2 cells was previously described.[42] Following necropsy, organs were fixed in 10% formalin for an average of 24 to 48 hours. Skeletal tissue was then selected and placed into 88% formic acid for decalcification for an average of 4-6 hours. All tissue was then subject to routine processing (8 hour protocol) where tissue is sequentially placed into formalin then a series of graded alcohols (70% to 100%) followed by xylene and then paraffin wax infiltration. Tissues were then paraffin-embedded prior to sectioning and hematoxylin and eosin (H&E) staining.

4.5.3. Mouse serum preparation. Blood was collected from hearts of mice using syringes and carefully transferred to 1.5 ml eppendorf tube. These blood-contained tubes were kept at room temperature for 45-60 minutes to induce blood clotting. After that, samples were centrifuged at 13,000 rpm for 15 min at 4° C. After centrifugation, supernatant was carefully aliquot into new eppendorf tubes for long-term storage at - 80° C. Sterile PBS (pH 7.4) was added to dilute each serum sample in the amount of 200 μL, in order to minimize serum lost after filtration. Each diluted serum sample was filtered using a sterile 4 mm diameter syringe filter purchased from Corning®, with 0.2μm pore RC membrane. The total serum protein concentration was determined by bicinchoninic acid assay (BCA) and normalized by diluting to the same concentration with PBS before sensing.

4.5.4. Sensing studies. Appropriate concentration of each polymer was mixed together in PBS (pH 7.4) based on previous optimizations. Each of the PFS-PPE complexes was loaded (200 μL) into a black 96-well untreated plate (Costar), followed

by the addition of 10 μL of 210 μg/ml protein solution in PBS or 5 mg/ml total serum protein concentration of each mouse. The mixture was incubated for 30 minutes before their fluorescence intensities were recorded at EX/EM (nm) of 356/420, 408/480, 356/480 for PFS-PPE1 pair, and 356/420, 418/482, 356/482 for PFS-PPE2 pair. The fluorescence intensities of the sensor only (without any analyte) is I_0, while the intensities of the sensor with analytes after 30 minutes of incubation is I. Normalized fluorescence of each sample is I/I_0.

4.5.5. Receiver operating characteristic analysis (ROC). To evaluate how well LDA predicts the unknown samples, we ran ROC analysis. We used *lda* function in *MASS* package[43] of R to train set 1 then use algorithm trained in set 1 to predict set 2. The ROC curve is created by plotting the true positive rate (TPR) against the false positive rate (FPR) at various threshold (cut-off level) settings using *ROCR* package. Cut-off level is the optimal threshold to maximize TPR while minimizing FPR to achieve the most effective diagnostic test. The accuracy of the test depends on how well the test separates the group being tested into those with and without cancer. Accuracy is measured by the area under the ROC curve, also known as AUC (the area under the curve). An area of 1 represents a perfect test; an area of .5 represents a less accurate test. AUC was obtained by the *auc* function in *pROC* package. Sensitivity and specificity were weighted equally in the prediction.

4.6. References

(1) Misek, D. E.; Kim, E. H. *Int. J. Proteomics* **2011**, *2011*, 343582.

(2) Zhu, J. J.; Djukovic, D.; Deng, L. L.; Gu, H. W.; Himmati, F.; Chiorean, E. G.; Raftery, D. *J. Proteome Res.* **2014**, *13*, 4120-4130.

(3) Chinen, A. B.; Guan, C. M.; Ferrer, J. R.; Barnaby, S. N.; Merkel, T. J.; Mirkin, C. A. *Chem. Rev.* **2015**, *115*, 10530-10574. **2014**, *13*, 4120-4130.

(4) Acimovic, S. S.; Ortega, M. A.; Sanz, V.; Berthelot, J.; Garcia-Cordero, J. L.; Renger, J.; Maerkl, S. J.; Kreuzer, M. P.; Quidant, R. *Nano Lett.* **2014**, *14*, 2636-2641.

(5) Kosaka, P. M.; Pini, V.; Ruz, J. J.; da Silva, R. A.; Gonzalez, M. U.; Ramos, D.; Calleja, M.; Tamayo, J. *Nat. Nanotechnol.* **2014**, *9*, 1047-1053

(6) Lilja, H.; Ulmert, D.; Vickers, A. J. *Nat. Rev. Cancer* **2008**, *8*.

(7) Kingsmore, S. F. *Nat. Rev. Drug Discov.* **2006**, *5*, 310-320.

(8) Fernández-Olavarría, A.; Mosquera-Pérez, R.; Díaz-Sánchez, R.-M.; Serrera-Figallo, M.-A.; Gutiérrez-Pérez, J.-L.; Torres-Lagares, D. *J. Clin. Exp. Dent.* **2016**, *8*, e184-e193.

(9) Choi, Y. E.; Kwak, J. W.; Park, J. W. *Sensors* **2010**, *10*, 428-455.

(10) Rusling, J. F.; Kumar, C. V.; Gutkind, J. S.; Patel, V. *Analyst* **2010**, *135*, 2496-2511.

(11) Hanash, S. M. *Electrophoresis* **2000**, *21*, 1202-1209.

(12) Baggerly, K. A.; Morris, J. S.; Coombes, K. R. *Bioinformatics* **2004**, *20*, 777-U710.

(13) Wulfkuhle, J. D.; Liotta, L. A.; Petricoin, E. F. *Nat. Rev. Cancer* **2003**, *3*, 267-275.

(14) Le, N. D. B.; Rana, S.; Rotello, V. M. *Expert Rev. Mol. Diagn.* **2013**, *13*, 111-113.

(15) Le, N. D. B.; Yazdani, M.; Rotello, V. M. *Nanomedicine* **2014**, *9*, 1487-1498.

(16) Wright, A. T.; Anslyn, E. V. *Chem. Soc. Rev.* **2006**, *35*, 14-28. (d) Tao, Y.; Ran, X.; Ren, J. S.; Qu, X. G. *Small* **2014**, *10*, 3667-3671.

(17) De, M.; Rana, S.; Akpinar, H.; Miranda, O. R.; Arvizo, R. R.; Bunz, U. H. F.; Rotello, V. M. *Nat. Chem.* **2009**, *1*, 461-465.

(18) El-Boubbou, K.; Zhu, D. C.; Vasileiou, C.; Borhan, B.; Prosperi, D.; Li, W.; Huang, X. *J. Am. Chem. Soc.* **2010**, *132*, 4490-4499.

(19) Kong, H.; Liu, D.; Zhang, S. C.; Zhang, X. R. *Anal. Chem.* **2011**, *83*, 1867-1870.

(20) Wright, A. T.; Zhong, Z. L.; Anslyn, E. V. *Angew. Chem. Int. Ed.* **2005**, *44*, 5679-5682.

(21) Bajaj, A.; Miranda, O. R.; Kim, I. B.; Phillips, R. L.; Jerry, D. J.; Bunz, U. H. F.; Rotello, V. M. *Proc. Natl. Acad. Sci. USA* **2009**, *106*, 10912-10916.

(22) Rana, S.; Elci, S. G.; Mout, R.; Singla, A. K.; Yazdani, M.; Bender, M.; Bajaj, A.; Saha, K.; Bunz, U. H. F.; Jirik, F. R.; Rotello, V. M. *J. Am. Chem. Soc.* **2016**, *138*, 4522-4529.

(23) Bajaj, A.; Miranda, O. R.; Phillips, R.; Kim, I. B.; Jerry, D. J.; Bunz, U. H. F.; Rotello, V. M. *J. Am. Chem. Soc.* **2010**, *132*, 1018-1022.

(24) Han, J.; Bender, M.; Seehafer, K.; Bunz, U. H. F. *Angew. Chem. Int. Ed.* **2016**, *55*, 7689-7692.

(25) Han, J. S.; Wang, B. H.; Bender, M.; Kushida, S.; Seehafer, K.; Bunz, U. H. F. *ACS Appl. Mater. Interf.* **2017**, *9*, 790-797.

(26) Han, J. S.; Wang, B. H.; Bender, M.; Seehafer, K.; Bunz, U. H. F. *Analyst* **2017**, *142*, 537-543.

(27) St John, A.; Price, C. P. *Clin. Biochem. Rev.* **2014**, *35*, 155-167.

(28) Han, J. S.; Bender, M.; Hahn, S.; Seehafer, K.; Bunz, U. H. F. *Chem. Eur. J.* **2016**, *22*, 3230-3233.

(29) Han, J. S.; Wang, B. H.; Bender, M.; Seehafer, K.; Bunz, U. H. F. *ACS Appl. Mater. Interfaces* **2016**, *8*, 20415-20421.

(30) McQuade, D. T.; Pullen, A. E.; Swager, T. M. *Chem. Rev.* **2000**, *100*, 2537-2574.

(31) Liu, B.; Bazan, G. C. *Chem. Mater.* **2004**, *16*, 4467-4476.

(32) Chen, L. H.; Xu, S.; McBranch, D.; Whitten, D. *J. Am. Chem. Soc.* **2000**, *122*, 9302-9303.

(33) Heilig, B.; Hufner, M.; Dorken, B.; Schmidtgayk, H. *Klin. Wochenschr.* **1986**, *64*, 776-780.

(34) Shapiro, D. E. *Statistical Methods in Medical Research* **1999**, *8*, 113-134.

(35) Baker, S. G. *Journal of the National Cancer Institute* **2003**, *95*, 511-515.

(36) Šimundić, A.-M. *EJIFCC* **2009**, *19*, 203-211.

(37) Maibach, Howard I., Farzam Gorouhi, and Maibach. *Evidence Based Dermatology*. N.p.: People's Medical House USA Ltd (PMPH), 2011. Print.

(38) Werner, S.; Chen, H.; Butt, J.; Michel, A.; Knebel, P.; Holleczek, B.; Zornig, I.; Eichmuller, S. B.; Jager, D.; Pawlita, M.; Waterboer, T.; Brenner, H. *Scientific Reports* **2016**, *6*.

(39) Yoon, H. I.; Kwon, O.-R.; Kang, K. N.; Shin, Y. S.; Shin, H. S.; Yeon, E. H.; Kwon, K. Y.; Hwang, I.; Jeon, Y. K.; Kim, Y.; Kim, C. W. *Journal of Cancer Prevention* **2016**, *21*, 187-193.

(40) Wang, P.; Song, C. H.; Xie, W. H.; Ye, H.; Wang, K. J.; Dai, L. P.; Zhang, Y.; Zhang, J. Y. *Journal of Immunology Research* **2014**.

(41) Downey, C. M.; Aghaei, M.; Schwendener, R. A.; Jirik, F. R. *Plos One* **2014**, *9*. e99988.

(42) Singla, A. K.; Downey, C. M.; Bebb, G. D.; Jirik, F. R. *Oncoscience* **2015**, *2*, 263-271.

(43) Venables, W. N. & Ripley, B. D. (2002). *Modern Applied Statistics with S*. Fourth Edition. Springer, New York. ISBN 0-387-95457-0.

CHAPTER 5

RAPID DETECTION OF ENDOCRINE DISRUPTING CHEMICALS BY A NANOSENSOR AT ULTRA-SENSITIVE LEVEL

5.1. Abstract

Endocrine disrupting chemicals (EDCs) interact with estrogen receptors (ERs), causing a range of adverse health effects. Current assays for EDC activity are slow and often lack sensitivity. We report here an ultra-sensitive nanosensor that can detect estrogenic cellular changes in ER(+) MCF-7 cells rapidly (minutes) at levels orders of magnitude lower than generally used assays. Notably, the sensor responses at these ultra-low EDC levels correlate with an increased synthesis phase (S-phase) cell population of EDC-treated cells. The nanosensor was also able to detect binary EDC mixture effects, with synergism observed for bisphenol A (BPA) - 17β-Estradiol (E2) and antagonism for Dicyclohexylphthalate (DCHP) - E2, and Benzo(a)pyrene (BaP) - E2.

5.2. Introduction

Endocrine disrupting chemicals (EDCs) are structurally diverse compounds that interfere with the endocrine system, cause a broad range of adverse effects.[1-4] EDCs featuring estrogenic activity are of particular importance, posing a significant threat to reproduction and developmental processes in human and wildlife,[5] In common with other toxicological threats, there are tens of thousands of chemicals in use whose estrogenic effects are unknown.

Proliferative assays that rely on increased cell reproduction upon exposure to EDCs are by far the most widely used test for estrogenic activity. The widely used E-screen proliferative assay requires a six-day exposure period. The inability of this protocol to detect low-dose effects in the pico-and femtomolar range causes many false negatives.[6-8] Recently, flow cytometry assay has been used to detect estrogenic responses arising from lower EDC concentration exposures by detecting the percentage of cells in the S-phase.6 This assay, however, requires substantial sample preparation and specialized instrumentation, limiting its ability to address the high throughput demands of environmental toxicology. Recently, engineered bacterial sensor was developed to screen estrogenic EDCs at low concentrations. However, while this technique is quite rapid and convenient, it does not measure the direct phenotypic changes after EDC exposures that are relevant at a cellular level. Therefore, this design is more susceptible to false positives.[9]

The wide range of health issues generated by EDCs suggests that there is likewise a range of phenotypic consequences of EDC exposure at the cellular level. Predicting these changes on the molecular level is, however, quite challenging.[10,11] To address this issue, we report here the use of a hypothesis-free nanosensor to detect estrogenic EDC response of cells at pico- and femtomolar levels. This sensor system uses a gold nanoparticle (AuNP) as a recognition element and green fluorescence protein (GFP) as a transducer.[12] This sensor platform can capture the overall chemicophysical changes of the EDC-treated cells in minutes, avoiding false negatives due to the limitation of the typical single endpoint readout of current assays.[13] The simplicity of this method makes it

likewise a practical tool for addressing the real-world challenge arising from mixtures of EDCs.

5.3. Results and Discussion

We used a sensor system composed of non-covalent complexes of AuNPs and GFPs. We chose the benzyl nanoparticle (BenzNP) due to its sensitivity to differences in cell surfaces.[14] The fluorescence of the GFP is quenched when bound to BenzNP, with fluorescence restored upon displacement by cell surface functionality (Figure 5.1).[15-17] Human breast cancer MCF-7 cells were used in our study. This cell line is widely employed in EDC studies[5,6,8] due to their high level sensitivity to estrogenic agents.[18,19]

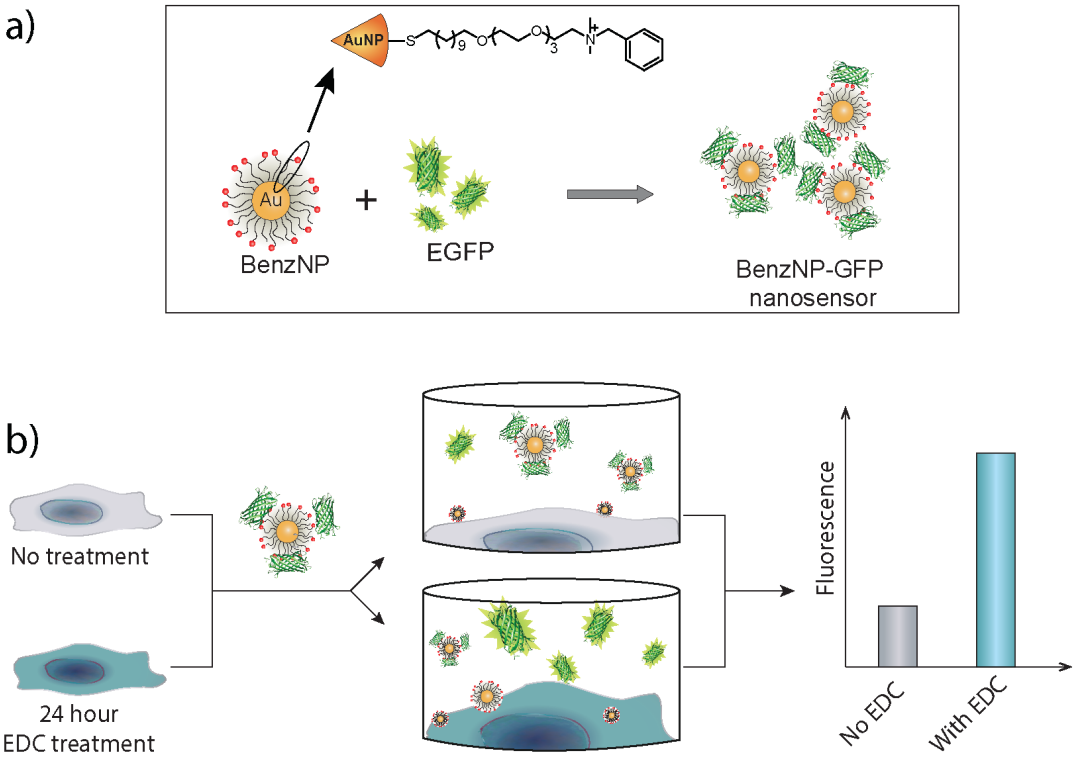

Figure 5.1. Schematic illustration of the nanosensor. (a) The sensor consists of BenzNP and green fluorescence proteins (GFPs). The fluorescence of GFP is quenched when the

BenzNP–GFPs complexes are formed. (b) When nanosensor is added to cells with and without EDC treatment, due to the different phenotypes of untreated and treated cells, BenzNP interacts differently with the cell surface and releases different amount of GFP, generating signal output.

Our initial experiments focused on establishing the response of our sensor to E2 as a positive control. MCF-7 cells were plated in 96-well plate overnight before being treated with E2, using 10,000 cells/well. After 24-hour treatment, cells were washed with Phosphate Buffer Saline (PBS), followed by the addition of the nanosensor BenzNP-GFP. The sensor detected significant cellular changes of E2-treated cells at femtomolar concentration (5×10^{-15} M). In contrast, there was no proliferative effect observed using Hoechst dye at even five orders of magnitude higher in E2 concentration. Significantly, co-incubation of cells with E2 and the anti-estrogen ICI 182,780 generated a response identical to that of control (untreated) cells, verifying that the sensor was responding to estrogenic changes in cell phenotype (Figure 5.2a). Our nanosensor was able to detect cellular changes induced by femtomolar concentration of E2, a four order of magnitude more sensitive than the conventional E-screen assay.[6,19]

We next tested our system on bisphenol A (BPA), an EDC that has generated considerable controversy.[20,21] The cells were treated with BPA for 24 hours prior to sensing. A significant increase in fluorescence signal from the sensor is observed at picomolar range (5×10^{-11} M, Figure 5.2b), while no significant response from Hoechst dye. Two other reported EDC agents, Dicyclohexylphthalate (DCHP), and Benzo(a)pyrene (BaP), likewise showed a positive response (Figure 5.2c).[5,6,22] Significantly, BaP was successfully detected by our nanosensor at the concentration of 1

× 10^{-11} M, even though no significant proliferative effect was observed with this EDC using a standard E-screen assay.[6]

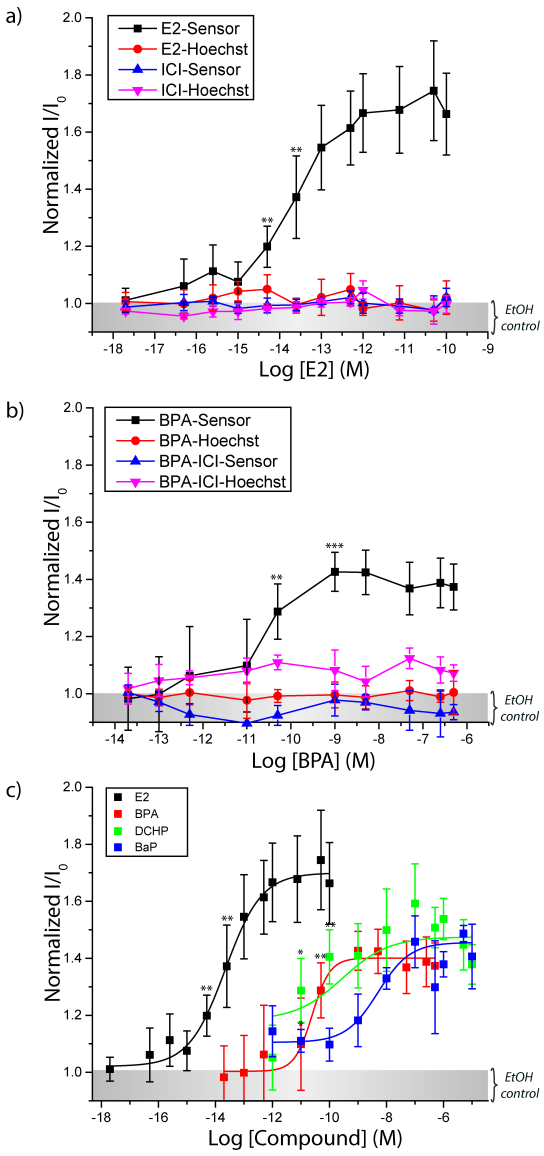

Figure 5.2. Fluorescence response from nanosensor BenzNP-GFP and Hoechst 33342 with and without co-incubation of estrogen receptor inhibitor ICI 182,780 with (a) 17β-Estradiol (E2) and (b) Bisphenol A (BPA). Fluorescence response of BenzNP-GFP sensor is significantly increased in the absence of ER inhibitor ICI 182,780 in both E2 and BPA treated cells at 10^{-15} M and 10^{-11} M respectively. (c) Fluorescence response from nanosensor BenzNP-GFP for all tested compounds: E2, BPA, Dicyclohexylphthalate (DCHP) and Benzo(a)pyrene (BaP). Each data point is the mean value of four replicates per treatment (n=4).

In reality, when we are being exposed to EDCs, it is usually a mixture of compounds and not a single agent. Therefore, it motivates us to investigate the low dose effect of EDC mixtures, starting with the binary mixtures of each tested compound described previously with a non-significant concentration of E2 at 1 fM. We used a sub-threshold dosing of E2 with the purpose of making the effects of binary mixtures more apparent by eliminating the potential affect of E2 alone in higher concentrations. Series of BPA, DCHP and BaP concentrations were prepared with and without co-incubation of 1 fM E2 to treat the cells for 24 hours before the detection by the nanosensor. To allow comparison across different compounds, equipotent concentrations (PC_{50}) need to be calculated. PC_{50} indicates the concentration of compound x that evokes 50% activity of the positive control, E2. This approach is more suitable for comparison than EC_{50} due to the fact that not all compounds reach a relative proliferation effect of 100%.[5,23] Interestingly, BPA-E2 mixture shows a drastic increase in fluorescence signal compared to just single agent BPA. The PC50 of BPA-E2 mixture is much lower than that of BPA alone (4.77×10^{-14} M and 1.57×10^{-10} M, respectively). This reduction in PC_{50} makes the mixture of BPA-E2 even as potent as compared to E2 alone. This result is consistent with previously published work using the traditional E-screen method.[24] Other tested binary mixtures of DCHP-E2 and BaP-E2 show an opposite trend with BPA-E2 mixture. While BPA-E2 mixture indicates a highly synergistic effect, DCHP-E2 and BaP-E2 show antagonistic effects, where their PC_{50} values could not be determined (Figure 5.3). The binary mixture of E2 and another phthalate derivative, butylbenzyl phthalate, was shown to be antagonistic in previous work.[24] However, to the best of our knowledge, the mixture

behaviors of DCHP-E2 and BaP-E2 are not previously reported in the literatures and are new findings enabled by our technology.

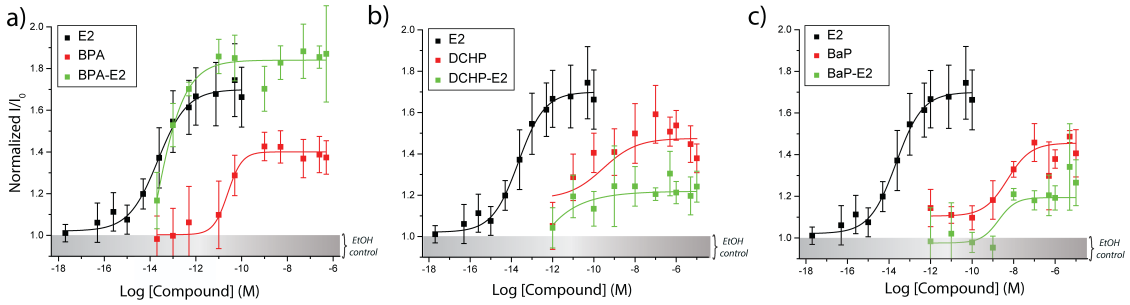

d)

Chemical name	Abbrev.	Test concentration range (M)	PC_{50} – individuals (M)	PC_{50} – binary mixtures (M)	Mixture behavior
17β-Estradiol	E2	$2 \times 10^{-18} - 1 \times 10^{-10}$	2.43×10^{-14}	N/A	N/A
Bis-Phenol A	BPA	$2 \times 10^{-14} - 5 \times 10^{-7}$	1.57×10^{-10}	4.77×10^{-14}	Synergistic
Dicyclohexylphthalate	DCHP	$1 \times 10^{-12} - 1 \times 10^{-5}$	8.76×10^{-10}	N/A	Antagonistic
Benzo(a)pyrene	BaP	$1 \times 10^{-12} - 1 \times 10^{-5}$	2.25×10^{-8}	N/A	Antagonistic

Figure 5.3. Fluorescence response from nanosensor BenzNP-GFP for binary mixture effects of 1 fM 17β-Estradiol (E2) with (a) Bis-Phenol A, (b) Dicyclohexylphthalate, (c) Benzo(a)pyrene. Each data point is the mean value of four replicates per treatment (n=4). d) PC_{50} values for individual compounds and binary mixtures with 1 fM E2. PC_{50} value is the concentration of compound x with 50% activity of the positive control (17β-Estradiol, E2).

Our sensor can rapidly detect cellular responses from ultra-low levels of estrogenic agents, raising the question of what phenotypic change was being detected. Estrogenic EDCs trigger cells to proliferate, which should result in an elevated population of S-phase cells. The S-phase cell population can be measured by flow cytometry. This method has been previously described as flow cytometric E-screen assay, and was validated using a range of estrogenic compounds.6 In our study, cells were treated with different concentrations of E2 and BPA for 24 hours, then trypsinized and washed with PBS. Ethanol was used to stabilize these cells at 4°C. After 2 hours, cells were stained with Propidium Iodine/RNAse solution before running flow cytometry. As

observed in sensor response of E2 and BPA-treated cells, higher concentrations of E2 and BPA induced more S-phase cell population, which become significant at 2.5×10^{-14} M and 1×10^{-11} M, respectively (Figure 5.4a). We observed a similar trend in the increased S-phase population as seen with the nanosensor BenzNP-GFP response. This increase in S-phase is eliminated when cells were treated with the co-incubation of E2 or BPA with the anti-estrogen ICI 182,780 (Figure 5.4b). The direct correlation between our sensing studies and the cytometric data provides solid evidence that our sensor is responsive to cell cycle changes.

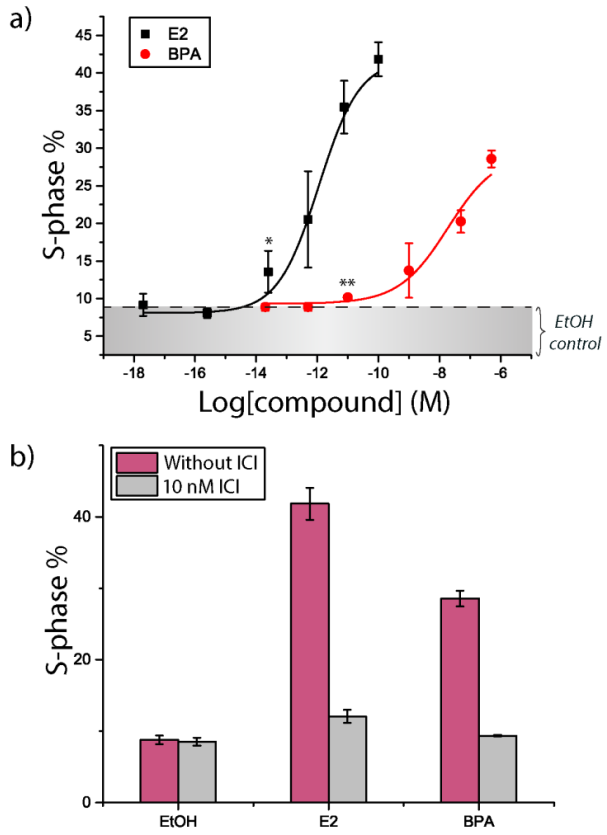

Figure 5.4. (a) E2 and BPA effects on S-phase cell population of MCF-7 measured by flow cytometry. The S-phase percentage of MCF-7 cells increases as the concentration of E2 or BPA increases. (b) Co-incubation effect of E2 and BPA with ICI 182,780, an estrogen receptor antagonist, on S-phase cell population. The proliferation effect of MCF-7 cells when treated with E2 or BPA is inhibited in the presence of 10 nM of ICI 182,780. Each data point is the mean value of three replicates per treatment (n=3).

5.4. Conclusions

We have demonstrated the usefulness of our simple nanosensor, BenzNP-GFP, for detecting low dose effects of estrogenic EDCs. This technique is rapid, versatile and only involves one step process of adding the nanosensor solution into the EDC-treated cells. We have successfully detected the estrogenic activity of an endogenous (E2) and other xenogenous agents (BPA, DCHP and BaP) on MCF-7 cells at ultra low concentrations (femto and picomolar ranges). The ease of performing this cell-based assay using BenzNP-GFP complex has made it possible to test the effects of EDCs at a broader range of concentrations. Whereas, a sensitive flow cytometry method still limits number of samples one can perform due to multistep processing procedure. Significantly, this nanosensor can also be used to detect EDC mixture effect, eliminating the lengthy processing time comes with infinite number of possible combinatorial EDC mixtures. Studying the combination behaviors is a step forward to better reflect the effects of EDCs in a more complex system, such as *in vivo.* Such complexity can be complicated by the pre-existence of endogenous estrogen, which when mixed with other xenogenous substances, might be drastically different compared to single agent itself as observed in our study.

5.5. Experimental section

5.5.1. Nanosensor (BenzNP and GFP) fabrication. To determine the appropriate ratio of BenzNP and GFP for the assay, different concentrations of BenzNP were first titrated with 150 nM GFP to find out at which concentration of BenzNP, GFP

intensity can be quenched. Final concentrations of 100 nM BenzNP and 150 nM GFP were used for all assays. The appropriate ratio of BenzNP and GFP was mixed with 5mM Phosphate buffer (5mM PB) for 30 minutes to form nanosensor complexes and quench the fluorescence intensity of GFP. This mixture was then added to cell microplate for estrogenic activity detection.

5.5.2. Cell culture. For routine cell culture, MCF-7 cells were maintained in Dulbecco's Minimum Essential Medium (DMEM) with phenol red as pH indicator, supplemented with 10% Fetal Bovine Serum and 1% antibiotics. Cells were grown in a humidified atmosphere containing 5% CO2 at 37 °C. For estrogenic activity experiments, MCF-7 cells were cultured in low steroid conditions with charcoal dextran treated fetal bovine serum (CDFBS) in order to minimize estrogenic activity of serum and arrest all cells at G_0/G_1 phase. More specifically, cells were transferred to DMEM-F12 (phenol red free due to its known estrogenic activity) media, supplemented with 5% CDFBS and 1% antibiotics for 3 days. After that, cells were seeded on 96-well plate for experiments using only 2.5% CDFBS DMEM-F12 media to avoid cell overgrown and enhance estrogenic effect in a serum deprived environment.

5.5.3. Cell number titration. a series of cell number from 2,000 to 10,000 cells were plated on 96-well plate overnight (Figure 5.5). BenzNP-GFP complex solution with co-incubation of Hoechst 33342 was added to the 96-well plate after one time washing with Phosphate Buffer Saline (PBS). Alamar Blue/cell media solution was prepared in the ratio of 1/10. This mixture was incubated with cells for approximately 3 hours before being read out at EX560/EM590.

5.5.4. Cell-based assay for estrogenic activity detection. 10,000 cells were seeded on 96-well plate in 2.5% CDFBS DMEM-F12 media overnight. A series of E2 or BPA concentrations were prepared in 2.5% CBFBS DMEM-F12 media with 0.1% EtOH. Cells were washed with PBS and treated with these concentrations for 24 hours. After that, cells were washed one more time with PBS. Appropriate ratio of BenzNP-GFP nanosensor was mixed with 10 μg/ml of Hoechst 33342 and added into 96-well plate for 15 minute incubation time. The GFP and Hoechst fluorescence were measured with EX/EM wavelengths of 475/495 nm and 355/460 nm on a Molecular Devices SpectraMax M3 microplate reader at 25 °C. Normalization of fluorescence intensity was done by I/I_0, where I is the final fluorescence intensity and I_0 is the initial fluorescence intensity of the sensor.

5.5.6. Flow cytometry and cell cycle analysis. Serum deprived cells were seeded on 6-well plate at a density of 180,000cells/well in CDFBS DMEM-F12. Six concentrations of E2 and six concentrations of BPA (three replicates each treatment) were incubated with cells for 24 hours. The highest concentration of E2 (1×10^{-10} M) and BPA (5×10^{-7} M) were mixed with 10 nM ER inhibitor (ICI 182,780) to co-incubate with cells, also for 24 hours. Cells were washed with PBS once before being trypsinized and transferred into 1.5 ml eppendorf tubes. 1000 μL of culturing media was added into each tube to stop the trypsin activity. Samples were centrifuged at 3000 rpm for 5 minutes and the supernatant was discarded. 150 μL of PBS was added into each tube to resuspend cells into solution. 350 μL of EtOH was added to stabilize cells at 4°C for two hours. Cells were then centrifuged again to discard the supernatant before staining with PI/RNAse mixed with PBS at 1:1. Flow cytometric measurements for cell samples were

performed using a LSRFortessa 3 Laser, HTS flow cytometer (BD Biosciences). The data was then analyzed using FlowJo 7.6 using Watson Pragmatic model for cell cycle analysis.

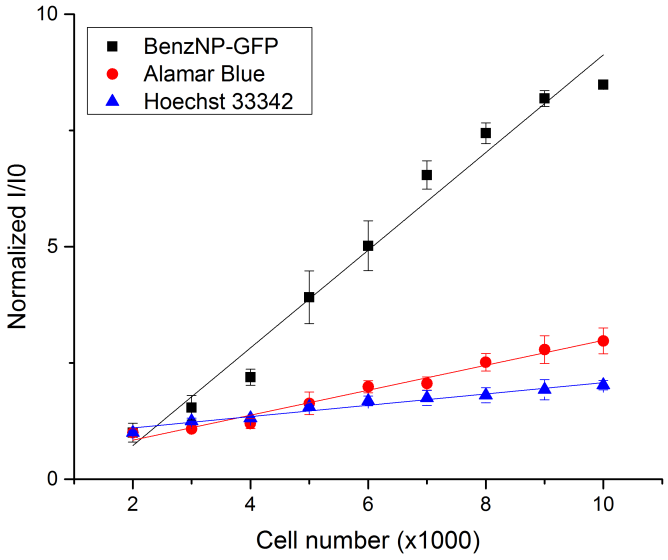

Figure 5.5. Response of different sensing systems (BenzNP-GFP sensor, Alamar Blue, and Hoechst 33342) with different cell numbers from 2k to 10k MCF-7 cells. BenzNP-GFP complex is more sensitive to cell numbers than Alamar Blue and Hoechst 33342.

5.6. References

(1) Colborn, T.; Saal, F. S. V.; Soto, A. M. *Environ. Health Perspect.* **1993**, *101*, 378-384.

(2) Guillette, L. J.; Gunderson, M. P. *Reproduction* **2001**, *122*, 857-864.

(3) McLachlan, J. A.; Simpson, E.; Martin, M. *Best Pract. Res. Clin. Endocrinol. Metab.* **2006**, *20*, 63-75.

(4) Tyler, C. R.; Jobling, S.; Sumpter, J. P. *Crit. Rev. Toxicol.* **1998**, *28*, 319-361.

(5) Vanparys, C.; Depiereux, S.; Nadzialek, S.; Robbens, J.; Blust, R.; Kestemont, P.; De Coen, W. *Sci. Total. Environ.***2010**, *408*, 4451-4460.

(6) Vanparys, C.; Maras, M.; Lenjou, M.; Robbens, J.; Van Bockstaele, D.; Blust, R.; De Coen, W. *Toxicol. In Vitro* **2006**, *20*, 1238-1248.

(7) Vandenberg, L. N.; Ehrlich, S.; Belcher, S. M.; Ben-Jonathan, N.; Dolinoy, D. C.; Hugo, E. R.; Hunt, P. A.; Newbold, R. R.; Rubin, B. S.; Saili, K. S.; Soto, A. M.; Wang, H.-S.; vom Saal, F. S. *Endocrine Disruptors* **2013**, *1*, e26490.

(8) Zacharewski, T. *Environ. Sci. Technol.* **1997**, *31*, 613-623.

(9) Furst, A. L.; Hoepker, A. C.; Francis, M. B. *ACS Cent. Sci.* **2017**.

(10) Yang, O.; Kim, H. L.; Weon, J. I. *J. Cancer Prev.* **2015**, *20*, 12-24.

(11) Shanle, E. K.; Xu, W. *Chem. Res. Toxicol.* **2011**, *24*, 6-19.

(12) Bajaj, A.; Rana, S.; Miranda, O. R.; Yawe, J. C.; Jerry, D. J.; Bunz, U. H. F.; Rotello, V. M. *Chem. Sci.* **2010**, *1*, 134-138.

(13) Le, N. D. B.; Rana, S.; Rotello, V. M. *Expert Rev. Mol. Diagn.* **2013**, *13*, 111-113.

(14) Rana, S.; LeNgoc, D. B.; Mout, R.; Saha, K.; Tonga, G. Y.; BainRobert, E. S.; Miranda, O. R.; Rotello, C. M.; Rotello, V. M. *Nat. Nano.* **2015**, *10*, 65-69.

(15) Wiskur, S. L.; Ait-Haddou, H.; Lavigne, J. J.; Anslyn, E. V. *Acc.Chem. Res.* **2001**, *34*, 963-972.

(16) Nguyen, B. T.; Anslyn, E. V. *Coord. Chem. Rev.* **2006**, *250*, 3118-3127.

(17) Rana, S.; Le, N. D. B.; Mout, R.; Duncan, B.; Elci, S. G.; Saha, K.; Rotello, V. M. *Acs Cent. Sci.* **2015**, *1*, 191-197.

(18) Zhu, Y. L.; Wang, A. T.; Liu, M. C.; Zwart, A.; Lee, R. Y.; Gallagher, A.; Wang, Y.; Miller, W. R.; Dixon, J. M.; Clarke, R. *Int. J. Oncol.* **2006**, *29*, 1581-1589.

(19) Soto, A. M.; Sonnenschein, C.; Chung, K. L.; Fernandez, M. F.; Olea, N.; Serrano, F. O. *Environ. Health. Perspect.* **1995**, *103*, 113-122.

(20) Metz, C. M. *Workplace Health Saf.* **2016**, *64*, 28-36.

(21) Vandenberg, L. N.; Colborn, T.; Hayes, T. B.; Heindel, J. J.; Jacobs, D. R.; Lee, D. H.; Shioda, T.; Soto, A. M.; vom Saal, F. S.; Welshons, W. V.; Zoeller, R. T.; Myers, J. P. *Endocr. Rev.* **2012**, *33*, 378-455.

(22) Hong, E. J.; Ji, Y. K.; Choi, K. C.; Manabe, N.; Jeung, E. B. *J. Reprod. Dev.* **2005**, *51*, 253-263.

(23) OECD (Organisation for Economic Co-operation and Development), 2008. OECD Guideline for the testing of chemicals. Draft proposal for a new guideline 4XX: The stably transfected human estrogen receptor-α transcriptional activation assay for detection of estrogenic agonist-activity of chemicals

(24) Suzuki, T.; Ide, K.; Ishida, M. *J. Pharm. Pharmacol.* **2001**, *53*, 1549-1554.

CHAPTER 6

SENSING BY SMELL: NANOPARTICLE-ENZYME SENSORS FOR RAPID AND SENSITIVE DETECTION OF BACTERIA WITH OLFACTORY OUTPUT

6.1. Abstract

We present here a highly efficient sensor for bacteria that provides an olfactory output, allowing detection without the use of instrumentation, and with a modality that does not require visual identification. The sensor platform uses nanoparticles to reversibly complex and inhibits lipase. These complexes are disrupted in the presence of bacteria, restoring enzyme activity and generating scent from odorless pro-fragrance substrate molecules. This system provides rapid (15 min) sensing and very high sensitivity (10^2 cfu/mL) detection of bacteria using the human sense of smell as an output.

6.2. Introduction

The human olfactory system has evolved to detect extremely low concentrations of volatile organic compounds present in complex environments.[1] Humans can discriminate more than 1 trillion olfactory stimuli, several orders of magnitude greater than their capability in visual discrimination.[2] This sensitivity and versatility makes olfaction a promising platform for biotechnological applications,[3] however there have been few examples of the application of translation of sensor responses to olfactory outputs. [4-7]

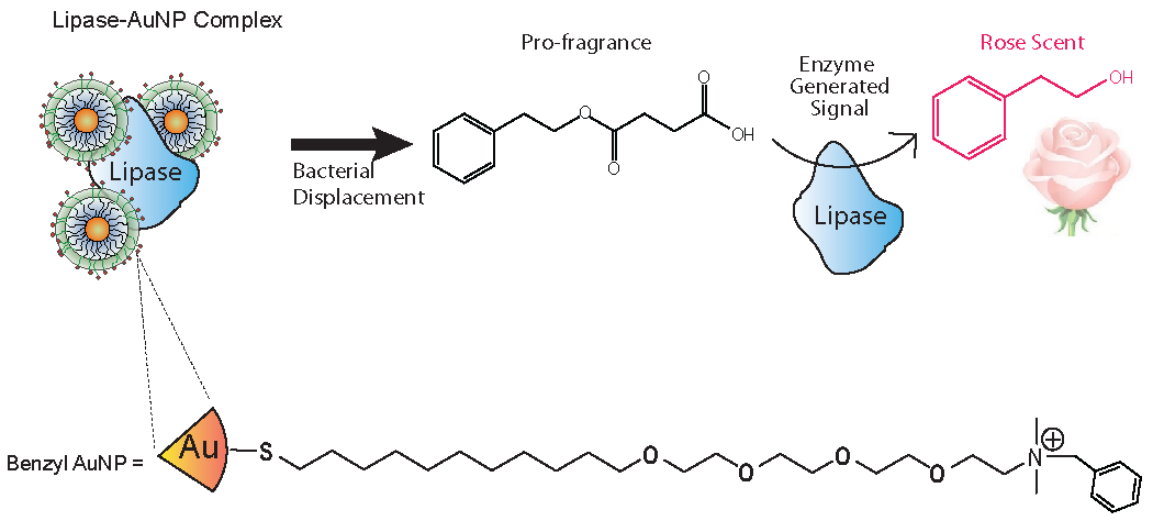

Figure 6.1. Schematic representation of sensor elements used in this study. Cationic AuNPs bind with the anionic enzyme inhibiting the catalysis of the pro-fragrance into scent. Bacteria present in solution compete for the AuNP surface and displace the enzyme inducing the production of the rose fragrance.

Nanotechnology provides new opportunities to redefine the bounds of human perception.[8] There have been a wide variety of examples where the intrinsic properties of nanomaterials have been used to generate visual output,[9,10] with additional examples of nanomaterials modulating other colorimetric processes.[11-13] Engineered nanomaterials have also been shown to influence the behavior of fragrance molecules.[14] In a recent study, Weder *et al.* demonstrated cellulose nanocrystals functionalized with pro-fragrance molecules that could be used to control the production of volatile compounds.[4] These covalently bound complexes remain odorless until functional groups are cleaved in response to specific external stimuli, generating pungent aroma molecules.[5] Taken together, we hypothesized that pro-fragrances in combination with surface-engineered nanomaterials could provide reactive constructs to transduce molecular interactions into outputs that could be 'read out' through our sense of smell, providing a useful sensor

modality for detection of bacteria that provides a potential strategy for combatting the threat of bacterial drinking water contamination that contributes to over 1.5 million deaths worldwide a year.[15,16]

We use a supramolecular-based approach to generate an effective smell-based sensor platform for bacteria. The system is comprised of three tunable components: 1) surface functionalized gold nanoparticles (AuNP), 2) pro-fragrance molecules, and 3) enzymes to cleave the pro-fragrances to generate the olfactory output (Figure 6.1). In this sensor, the surface moieties of the nanoparticles behave as both selective recognition elements for analytes present in solution and to reversibly inhibit the complexed enzymes.[13] The pro-fragrance molecules[17] provide a 'turn-on' response for the sensor system, going from odorless to strongly odiferous upon cleavage by the enzyme. Finally, the enzyme provides a strategy for amplifying the output, generating multiple fragrance molecules per recognition event.[18] Bringing these components together provides a sensitive sensor system for bacteria, allowing human subjects to rapidly detect bacteria in solution at levels as low as 10^2 cfu/mL, a relevant limit of detection for overall bacterial load in drinking water, and consistent with other recently published sensor systems.[19-22]

6.3. Results and Discussion

Our sensor design uses nanoparticles to both recognize the bacteria and to inhibit the fragrance-generating enzyme. We chose AuNPs possessing ligands with terminal benzyl headgroups, as these nanoparticles have been shown to interact strongly with the anionic cell surface of bacteria. [23,24] We used the robust and industrially used *Candida Rugosa* lipase as the enzymatic amplifier, [25] relying on the negative charge of the protein

to provide electrostatic complementarity with the cationic nanoparticle, and hence inhibiting catalysis.[11,26,27] Given the ability of human olfaction to discern an enormous variety of scents, we had a wide range of pro-fragrance options to choose from. We ultimately chose the succinic acid ester of phenylethyl alcohol (SAEPE) as our substrate/pro-fragrance, due to the low odor threshold of phenylethyl alcohol,[28] coupled with the orthogonality of the pleasant rose scent with odors commonly found in contaminated drinking water.

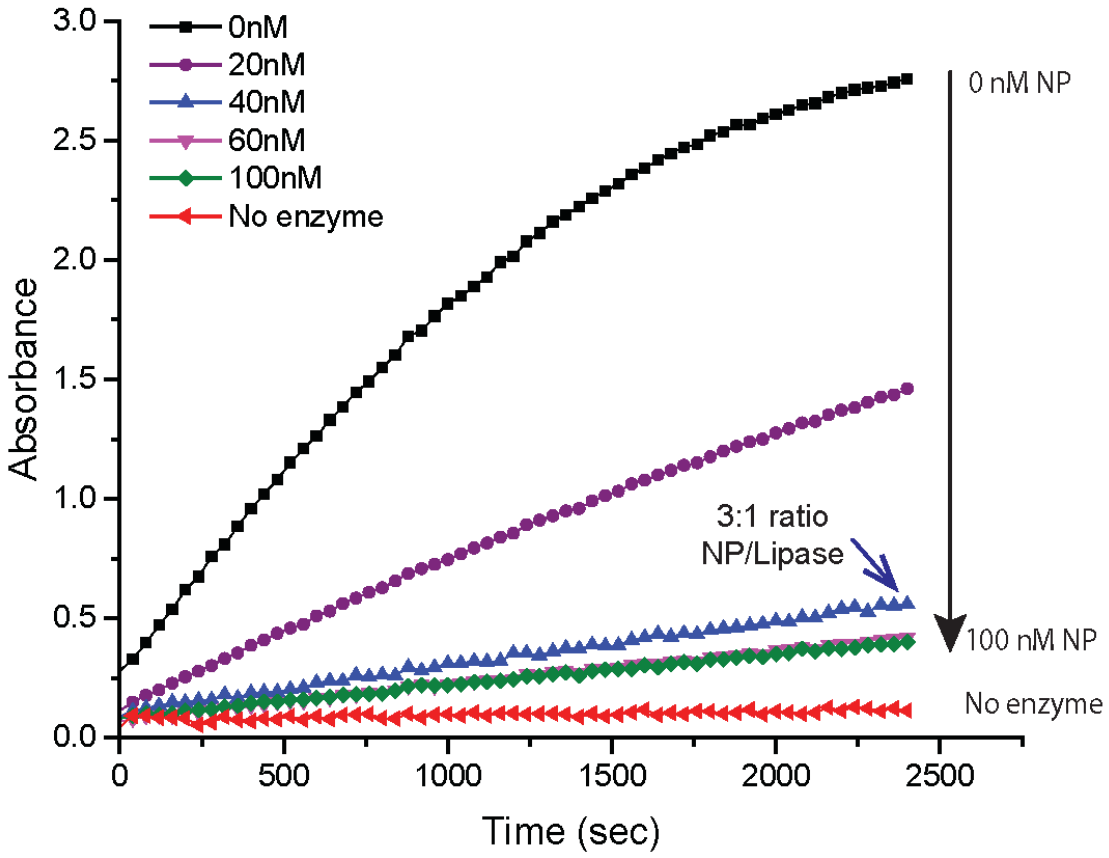

Figure 6.2. Lipase inhibition assay in the presence of benzyl AuNP. Lipase (15 nM) was incubated with a series of benzyl AuNP concentrations before adding the colorimetric substrate p-NPB (0.6 mM).

We initially performed a colorimetric assay to optimize the AuNP:lipase ratio required for inhibition. These studies were performed using p-nitrophenylbutyrate (pNPB) in sodium phosphate buffer solution (5 mM, pH 7.4). As shown in Figure 6.2, an approximately 3:1 AuNP to lipase ratio provided essentially complete inhibition of the lipase. This AuNP:lipase ratio was used to generate the nanozyme complex for all further studies. This colorimetric assay was able to detect both Gram positive and negative bacteria, including: *E. coli, B. subtilis, M. luteus,* and *P. aeruginosa* (Figure 6.3), indicating the generality of the enzyme activation process.

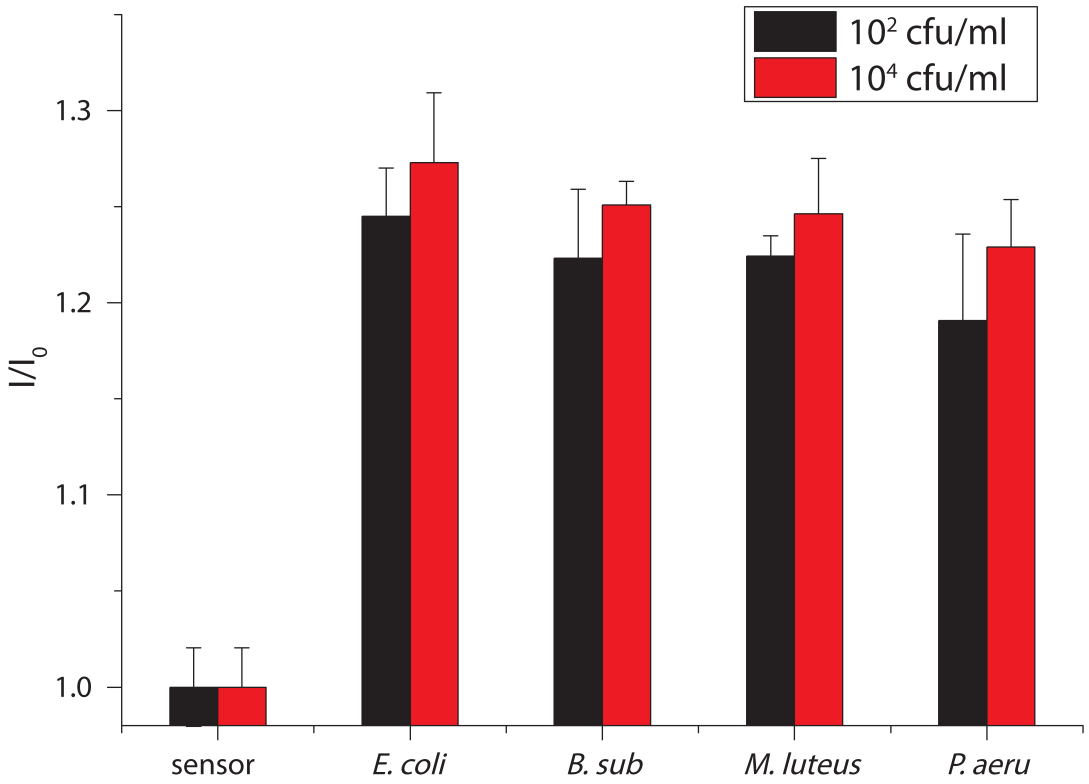

Figure 6.3 Detection of bacteria using the nanozyme complex with colorimetric substrate p-nitrophenylbutyrate (pNPB) in sodium phosphate buffer solution (5 mM, pH 7.4). I_0 is the initial absorbance of the nanozyme complex without bacteria and I is the final absorbance of the nanozyme complex in the presence of bacteria after 30 minutes of incubation. *E. coli, B. sub, M. luteus, P. aeru.*

We next turned to bacterial sensing using the enzyme platform, beginning with an instrument-based analytical strategy. These studies used *E. coli* as a non-pathogenic "safe" bacteria strain to minimize health concerns in both the instrumental and human studies.[29] Solutions of the sensor elements were incubated for 30 minutes prior to the addition of the pro-fragrance. We then used headspace gas chromatography to quantify the production of scent generated by our bacterial sensor.[30] The concentration of the volatile product present in the headspace of the sample vial was quantified according to an external calibration curve (see Supporting Information). As shown in Figure 6.4, the uninhibited lipase cleaves significantly more pro-fragrance than the nanoparticle-enzyme complex and controls. Significantly, no signal was observed using the substrate alone and bacteria, indicating that the bacteria do not hydrolyze the pro-fragrance in the timeframe studied. As expected, the sensor system generated measurable and distinctly different signals in the presence of 10^4 and 10^6 cfu/mL of *E. coli*.

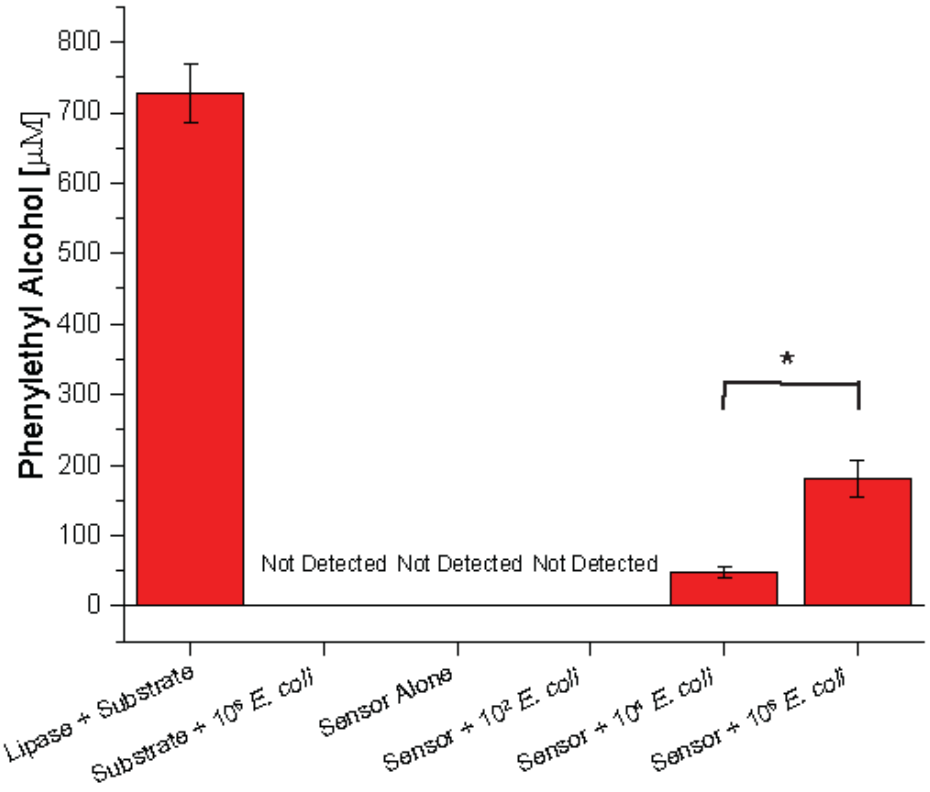

Figure 6.4. Headspace gas chromatography analysis of sensor response to increasing concentrations of bacteria. Samples were prepared in triplicate. Error bars represent standard deviations of the measurements. *= $p< 0.05$, ***=$p<0.001$.

Having established the generation of fragrance output, we next determined the ability of humans to serve as "detectors". Ten volunteers were asked to smell glass vials at two time points: 1 minute as a control, and 15 minutes for sensing, with the interval chosen to ensure olfactory clearance.[31] They ranked the samples in order from least/no smell (1) to strongest smell (5), and the raw ranking order data were analyzed using the Kruskal-Wallace H-test. Initial studies focused on the sensitivity of the scent response. As expected, participants were able to detect the phenylethyl alcohol at both time points (Figure 6.5a). In contrast, the enzyme-substrate pair was not detected at 1 minute, but

readily discerned at 15 minutes. In our sensing studies, no significant difference in response was observed across conditions at 1 minute under any conditions; however after 15 minutes participants were successfully able to detect *E. coli* concentrations at both 10^2 and 10^4 cfu/mL (Figure 6.5b) with high significance relative to the controls. Interestingly, 10^2 cfu/mL of *E. coli* did not produce a detectable signal using gas chromatography, demonstrating that human olfaction was more sensitive than the chromatographic method.

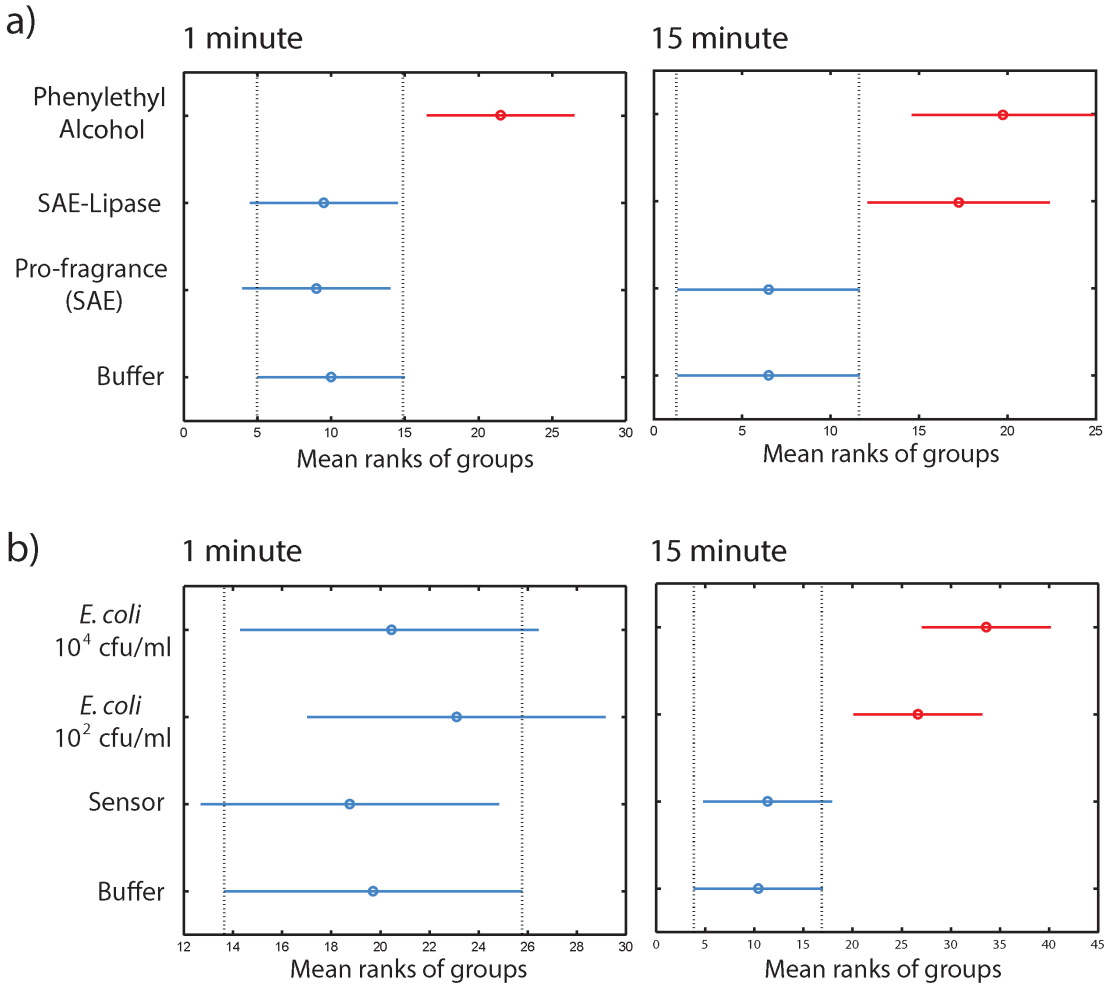

Figure 6.5. Human olfactory detection studies. (a) Lipase activity test in the presence of the pro-fragrance SAEPE was carried out with six participants. SAEPE only and 5 mM Phosphate buffer were used as the negative control. The hydrolyzed form of SAEPE was

used as the positive control (strong standard). Hydrolyzed SAEPE and SAEPE in the presence of uninhibited lipase are significantly different from the negative controls SAEPE alone ($p<0.01$ and $p<0.01$, respectively) after 15 minutes. (b) With ten participants, olfactory detection of *E. coli* at 10^2 and 10^4 cfu/mL were compared to the controls of just buffer and sensor only after 15 minutes. The olfactory signals from the vials which contained 10^2 and 10^4 cfu/mL of *E. coli* are significantly different from the signal from the sensor-only vial ($p<0.001$ and $p<0.0001$, respectively).

6.4. Conclusions

In summary, we report here the development of a supramolecular-based sensor that uses the human olfactory system to read out the response. This sensor was able to detect bacteria with high sensitivity. These studies demonstrate that by controlling the behavior of responsive nanomaterials at the molecular level, we can alter how human beings observe their surroundings in a manner that is otherwise impossible. We believe this responsive strategy can be broadly applied to other surface functionalized nanoparticles and enzymes to provide sensing of a wide variety of analytes, with the availability of an almost limitless number of aroma profiles providing versatility unavailable with other transduction strategies.

6.5. Experimental section

6.5.1. Bacteria Growth Conditions. Bacteria were cultured in LB medium at 37 °C and 275 rpm until stationary phase. The cultures were then harvested by centrifugation and washed with 0.85 % sodium chloride solution for three times. Concentrations of resuspended bacterial solution were determined by optical density

measured at 600 nm. 5 mM sodium phosphate buffer was used to make dilutions of bacterial solutions.

6.5.2. Plate Reader Assay. Lipase inhibition assay was done at 25 °C with the final concentrations in Costar clear 96 well plate of 15 nM lipase, 0.6 mM pNPB, and 20, 40, 60, 80, 100 nM benzyl AuNP. Lipase and benzyl AuNP were first incubated for 30 minutes in 96 well plate to insure their interaction reaches equilibrium, then 10 μL of substrate p-NPB was added into the well. The activity of lipase was monitored every 30 seconds for a total of 40 minutes time frame at the absorbance of 405 nm.

6.5.3. Human Trial Assays.

Olfactory detection of lipase activity: Four different solutions were made in 20 mL glass vials with a final volume of 1 mL each. The volume of 1 mL was chosen to maintain the easy-to-use format of the sensor for eventual on-site detection use. 5 mM sodium phosphate buffer and 4 mM SAEPE were used as the negative controls and the rose scent (2-Phenylethyl alcohol) was used as the positive control, a strong standard. The activity of lipase was assessed by incubating 100 nM of lipase with 4 mM of SAEPE for 20 minutes. The participants were asked to smell these samples and rank them in the order from 1 to 5 with 1 has the lightest smell and 5 has the strongest smell.

Olfactory detection to determine the threshold of phenylethyl alcohol: Serial dilutions of phenylethyl alcohol were prepared and detected by five volunteers to establish the threshold of the rose fragrance. 'Yes' indicates that the volunteer was able to smell the fragrance and 'No' indicates that no fragrance was detected. The threshold of phenylethyl alcohol detected by volunteers was determined to be in μM range, which is consistent with previous report (Table 6.1).[28]

Table 6.1. Serial dilutions of phenylethyl alcohol detected by five volunteers.

Vial #	Type	**Conc. (M)**	**1**	**2**	**3**	**4**	**5**	Percentage (%)
1	Fragrance	0.05	Yes	Yes	Yes	Yes	Yes	100
2	Fragrance	0.01	Yes	Yes	Yes	Yes	Yes	100
3	Fragrance	0.005	Yes	Yes	Yes	Yes	Yes	100
4	Fragrance	0.001	Yes	Yes	Yes	Yes	Yes	100
5	Fragrance	0.0005	Yes	Yes	Yes	Yes	Yes	100
6	Fragrance	0.0001	Yes	Yes	Yes	Yes	Yes	100
7	Fragrance	0.00005	Yes	Yes	Yes	Yes	Yes	100
8	Buffer	0	No	No	No	No	No	100
9	Buffer	0	No	No	No	No	No	100

Olfactory detection of *E. coli*: The same procedure was followed as above for buffer and sensor samples. For the *E. coli*-containing vials, 100 nM lipase was incubated with 300 nM benzyl AuNP for 30 minutes, and then 10 μL of *E. coli* was added into each vial so that the final concentrations of *E. coli* in each vial are 10^2 and 10^4 cfu/mL.

6.5.4. Gas Chromatography Head-Space Analysis. Headspace phenylethyl alcohol was measured using a gas chromatography (model GC-17A, Shimadzu Co., Tokyo, Japan) equipped with a solid-phase microextraction (SPME) auto injector (model AOC-5000, Shimadzu Co., Tokyo, Japan). Samples (1 mL) in 20 mL glass vials capped with aluminum caps with polytetrafluoroethylene (PTFE)/silicone septa. Samples were prepared using 500 nM lipase, 1.5 μM benzyl AuNP, and 4 mM of SAEPE. A 50/3 μm divinylbenzene (DVB)/carboxen/polydimethylsiloxane (PDMS) stable flex (SPME) fiber (Supelco Co., Bellefonte, PA) was then inserted into the vial headspace for 2 min to absorb volatiles. The fiber was transferred to the GC injector port (250 °C) for 3 min. The injection port was operated in split mode, and the split ratio was set at 20:1.

Volatiles were separated on a fused-silica capillary Equity-1 Supelco column (30 × 0.25 mm inner diameter × 25 μm) coated with 100% PDMS at an initial oven temperature of 70 °C to final temperature of 220 °C over 10 min (step rate 15 °C/min). A flame ionization detector was used at a temperature of 250 °C. Phenylethyl alcohol concentrations were determined from peak areas using a standard curve made from dilutions of phenylethyl alcohol in 5 mM sodium phosphate buffer. Each measurement was performed in triplicate and results were expressed as mean values ± standard deviation.

6.5.5. Kruskal-Wallace H-test. Kruskal-Wallis test is a non-parametric version of one-way ANOVA which is applied when the assumption of normal (Gaussian) distribution is not met. This test can compare the medians of multiple samples to determine if they come from the same population or not. This methodology uses ranks of the data to compare the test statistics. To do so, the results from all groups are pooled and arranged in rank order from smallest to largest. The numeric index of this ordering is then used to evaluate the null hypothesis (sample are coming from the same distribution) using chi-square statistics. MATLAB software (MATLAB and Statistics Toolbox Release 2012b, The MathWorks, Inc., Natick, Massachusetts, United States) was used to perform Kruskal-Wallis test.[32,33]

6.6. Reference

(1) Sela, L.; Sobel, N. *Exp. Brain Res.* **2010**, *205*, 13-29.

(2) Bushdid, C.; Magnasco, M. O.; Vosshall, L. B.; Keller, A. *Science* **2014**, *343*, 1370-1372.

(3) Hellwig, M.; Henle, T. *Angew. Chemie Int. Ed.* **2014**, *53*, 10316-10329.

(4) Kuhnt, T.; Herrmann, A.; Benczedi, D.; Foster, E. J.; Weder, C. *Polym. Chem.* **2015**, *6*, 6553-6562.

(5) Kuhnt, T.; Herrmann, A.; Benczedi, D.; Weder, C.; Foster, E. J. *RSC Ad.* **2014**, *4*, 50882-50890.

(6) Xu, Y. Q.; Zhang, Z. Y.; Ali, M. M.; Sauder, J.; Deng, X. D.; Giang, K.; Aguirre, S. D.; Pelton, R.; Li, Y. F.; Filipe, C. D. M. *Angew. Chem. Int. Ed.* **2014**, *53*, 2620-2622.

(7) Mohapatra, H.; Phillips, S. T. *Angew. Chem. Int. Ed.* **2012**, *51*, 11145-11148.

(8) Whitesides, G. M. *Angew. Chemie Int. Ed.* **2015**, *54*, 3196-3209.

(9) Elghanian, R.; Storhoff, J. J.; Mucic, R. C.; Letsinger, R. L.; Mirkin, C. A. *Science* **1997**, *277*, 1078-1081.

(10) De la Rica, R.; Stevens, M. M. *Nat. Nanotechnol.* **2012**, *7*, 821-824.

(11) Miranda, O. R.; Chen, H. T.; You, C. C.; Mortenson, D. E.; Yang, X. C.; Bunz, U. H. F.; Rotello, V. M. *J. Am. Chem. Soc.* **2010**, *132*, 5285-5289.

(12) Jiang, Z. W.; Le, N. D. B.; Gupta, A.; Rotello, V. M. *Chem. Soc. Rev.* **2015**, *44*, 4264-4274.

(13) Miranda, O. R.; Li, X. N.; Garcia-Gonzalez, L.; Zhu, Z. J.; Yan, B.; Bunz, U. H. F.; Rotello, V. M. *J. Am. Chem. Soc.* **2011**, *133*, 9650-9653.

(14) Duncan, B.; Landis, R. F.; Jerri, H. A.; Normand, V.; Benczedi, D.; Ouali, L.; Rotello, V. M. *Small* **2015**, *11*, 1302-1309.

(15) WHO, UNICEF (2014) Progress on Drinking Water and Sanitation: 2014 Update. Geneva, Switzerland: WHO Press.

(16) WHO (2011) Guidelines for Drinking-Water Quality -4th ed. Geneva, Switzerland: WHO Press.

(17) Herrmann, A. *Angew. Chem. Int. Ed. Engl.* **2007**, *46*, 5836-5863.

(18) Duncan, B.; Le, N. D. B.; Alexander, C.; Gupta, A.; Tonga G. Y.; Yazdani, M.; Landis, R. F.; Wang, L. S.; Yan, B.; Burmaoglu, S.; Li X.; Rotello, V. M. *ACS Nano* **2017**, *11,* 5339-5343.

(19) Tripathi, S. M.; Bock, W. J.; Mikulic, P.; Chinnappan, R.; Ng, A.; Tolba, M.; Zourob, M. *Biosens. Bioelectron.* **2012**, *35*, 308-312.

(20) Wang, Y.; Knoll, W.; Dostalek, J. *Anal. Chem.* **2012**, *84*, 8345-8350.

(21) Chang, J. B.; Mao, S.; Zhang, Y.; Cui, S. M.; Zhou, G. H.; Wu, X. G.; Yang, C. H.; Chen, J. H. *Nanoscale* **2013**, *5*, 3620-3626.

(22) Bartram, J.; Cotruvo, J.; Exner, M.; Fricker, C.; Glasmacher, A. *Int. J. Food Microbiol.* **2004**, *92*, 241-247.

(23) Li, X. N.; Robinson, S. M.; Gupta, A.; Saha, K.; Jiang, Z. W.; Moyano, D. F.; Sahar, A.; Riley, M. A.; Rotello, V. M. *ACS Nano* **2014**, *8*, 10682-10686.

(24) Miller, K. P.; Wang, L.; Benicewicz, B. C.; Decho, A. W. *Chem. Soc. Rev.* **2015**, *44*, 7787-7807.

(25) Jeong, Y.; Duncan, B.; Park, M. H.; Kim, C.; Rotello, V. M. *Chem. Commun. (Camb).* **2011**, *47*, 12077-12079.

(26) Rana, S.; Le, N. D. B.; Mout, R.; Saha, K.; Tonga, G. Y.; Bain, R. E. S.; Miranda, O. R.; Rotello, C. M.; Rotello, V. M. *Nat. Nanotechnol.* **2015**, *10*, 65-69.

(27) Rana, S.; Le, N. D. B.; Mout, R.; Duncan, B.; Elci, S. G.; Saha, K.; Rotello, V. M. *Acs Cent. Sci.* **2015**, *1*, 191-197.

(28) Tsukatani, T.; Miwa, T.; Furukawa, M.; Costanzo, R. M. *Chem. Senses* **2003**, *28*, 25-32.

(29) Yang, W.; Zerbe, H.; Petzl, W.; Brunner, R. M.; Guenther, J.; Draing, C.; von Aulocke, S.; Schuberth, H. J.; Seyfert, H. M. *Mol. Immunol.* **2008**, *45*, 1385-1397.

(30) Poole, C. F. *Gas Chromatography*. Waltham: Elsevier. 2012. Print.

(31) Philpott, C. M.; Wolstenholme, C. R.; Goodenough, P. C.; Clark, A.; Murty, G. E. *J. Laryngol. Otol.* **2008**, *122*, 912-917.

(32) McDonald, John H. Handbook of Biological Statistics. Baltimore, MD: Sparky House Publishing, 2009. Print.

(33) Miller, J. C and J. N Miller. Statistics for Analytical Chemistry. Chichester: E. Horwood, 1984. Print.

CHAPTER 7

FUTURE TRENDS IN CHEMICAL-NOSE SENSING

Chemical-nose sensors have been proven to be an effective approach for complex mixture identification. This method truly shines when the knowledge of the biomarker in the mixture of interest is poorly characterized.

For cancer diagnostic applications, chemical-nose sensors hold great promise to be transformed into useful point-of-care tests (PoC) due to their simplistic design and rapid detection capability. These features are desired for the development of PoC tests to meet the ASSURED guidelines established by the World Health Organization. PoC tests using chemical-nose approach are even more valuable in settings that have limited access to clinical facilities such as suburband areas, especially in developing countries.

For environmental toxicity testing, chemical-nose sensors are the "first line of defense" as it can act as a primary screening tool to identify which compound or mixture can potentially pose a threat to humans and the environment. Using this approach, ~72,000 uncatagorized compounds can be rapidly screened and narrowed down to the most harmful compounds, without the costly and time-consuming process such as the screening program assays established by the Environmental Protection Agency (EPA). Further testing is required to gain detailed insights about the mechanisms of action for these compounds or mixtures. In addition, many compounds are only toxic after being metabolized. Therefore, testing only the parent molecules can yield false negative results. To cover the wide range of toxicity, *in-vivo* tests are desirable. However, to reduce the cost, other *in-vitro* tests that can capture the metabolisms of compounds of interest are

more suitable for primary screening. These tests could potentially utilize liver cells or organ-on-the-chip technology to screen the metabolites of the parent compounds.

Chemical-nose sensor demonstrated its usefulness in the bacterial detection application, where a general 'yes' or 'no' answer to the bacterial existence in drinking water is typically sufficient for in-the-field testing. However, if we want to extend the use of the chemical-nose sensing approach to other specific settings in bacterial detection such as food quality control, restaurants, and hospitals, more vigorous sensing tests need to be developed. These 'nose' tests should be more specific toward mixtures of bacteria in general, and not respond to any other analytes such as other food ingredients or sanitizing agents. For this purpose, 'nose' sensors are required to establish a base line describing the common background found in those specific settings. This is a requirement that is not essential for bacterial detection in drinking water due to its relatively simple environment (not many compounds or organisms exist in drinking water).

Chemical-nose sensors offer a new pathway for point-of-care testing thanks to their simplistic design and relatively low-cost materials. However, to successfully implement this sensing approach for PoC testing, much more effort needs to be contributed in this field to increase the sample size and extend the analyte map. This will lead to big data trends in chemical-nose sensing, which requires more data scientists to validate 'nose' tests using appropriate statistical analysis, including machine learning approaches, something with which not all biologists and chemists are comfortable handling. Taken together, the success of 'nose' sensor in the PoC testing field will require the convergence of interdisciplinary knowledge in biology, chemistry and statistics.

Advances in pattern recognition sensing will then be truly transformative, making rapid and highly personalized diagnosis a reality.

BIBLIOGRAPHY

Ábalos, T.; Jiménez, D.; Martínez-Máñez, R.; Ros-Lis, J. V.; Royo, S.; Sancenóna, F.; Soto, J.; Costero, A. M.; Gil, S.; Parra, M. *Tetrahedron Lett.* **2009**, *50*, 3885–3888.

Abbani, M. A.; Mallick, P.; Vogelsang, M. S. *Mass Spectrometry Based Proteomics in Cancer Research*, Springer, New York, **2010**.

Acimovic, S. S.; Ortega, M. A.; Sanz, V.; Berthelot, J.; Garcia-Cordero, J. L.; Renger, J.; Maerkl, S. J.; Kreuzer, M. P.; Quidant, R. *Nano Lett.* **2014**, *14*, 2636-2641.

Ai, H. W.; Shaner, N. C.; Cheng, Z. H.; Tsien, R. Y.; Campbell, R. E. *Biochemistry* **2007**, *46*, 5904-5910.

aMedina, D. *J. Cell. Biochem.* **1993**, 155–155.

Azuma, Y.; Taniguchi, A.; Matsumoto, K. *Glycoconj. J.* **2000**, *17*, 301-306.

Baggerly, K. A.; Morris, J. S.; Coombes, K. R. *Bioinformatics* **2004**, *20*, 777-U710.

Bajaj, A.; Miranda, O. R., Kim, I.-B.; Phillips, R. L.; Jerry, D. J.; Bunz, U. H. F.; Rotello, V. M. *Proc. Natl. Acad. Sci.* **2009**, *106*, 10912–10916.

Bajaj, A.; Miranda, O. R.; Phillips, R.; Kim, I. B.; Jerry, D. J.; Bunz, U. H. F.; Rotello, V. M. *J. Am. Chem. Soc.* **2010**, *132*, 1018-1022.

Bajaj, A.; Rana, S.; Miranda, O. R.; Yawe, J. C.; Jerry, D. J.; Bunz, U. H. F.; Rotello, V. M. *Chem. Sci.* **2010**, *1*, 134-138.

Baker, S. G. *J. Natl. Cancer Inst.* **2003**, *95*, 511-515.

Bamrungsap, S.; Chen, T.; Shukoor, M. I.; Chen, Z.; Sefah, K.; Chen, Y.; Tan, W. H. *Acs Nano* **2012**, *6*, 3974-3981.

Barash, O.; Peled, N.; Hirsch, F. R.; Haick, H. *Small* **2009**, *5*, 2618-2624.

Barash, O.; Peled, N.; Tisch, U.; Bunn, P. A.; Hirsch, F. R.; Haick, H. *Nanomedicine-Nanotech. Bio. Med.***2012**, *8*, 580-589.

Bartram, J.; Cotruvo, J.; Exner, M.; Fricker, C.; Glasmacher, A. *Int. J. Food Microbiol.* **2004**, *92*, 241-247.

Bhasikuttan, A. C.; Mohanty, J.; Nau, W. M.; Pal, H. *Angew.Chem.* **2007**, 119, 4198–4200.

Brereton, R. G. Data analysis for the laboratory and chemical plant. John Wiley & Sons Ltd, England, UK (2003).

Broza, Y. Y.; Haick, H. *Nanomedicine* **2013**, *8*, 785-806.

Buck, L. B. *Angew. Chem. Int. Ed.* **2005**, *44*, 6128-6140.

Bushdid, C.; Magnasco, M. O.; Vosshall, L. B.; Keller, A. *Science* **2014**, *343*, 1370-1372.
Butcher, R. A.; Schreiber, S. L. *Curr. Opin. Chem. Biol.* **2005**, *9*, 25-30.

Cao, L.; Isaacs, L. *Supramol. Chem.* **2014**, *26*, 251-258.

Carroll, P.; Schreuder, L. J.; Muwanguzi-Karugaba, J.; Wiles, S.; Robertson, B. D.; Ripoll, J.; Ward, T. H.; Bancroft, G. J.; Schaible, U. E.; Parish, T. *PLoS One* **2010**, *5*.

Chan, L. P.; Chou, T. H.; Ding, H. Y.; Chen, P. R.; Chiang, F. Y.; Kuo, P. L.; Liang, C. H. *BBA-Gen. Subjects* **2012**, *1820*, 1081-1091.

Chandler, D. *Nature* **2005**, *437*, 640−647.

Chang, J. B.; Mao, S.; Zhang, Y.; Cui, S. M.; Zhou, G. H.; Wu, X. G.; Yang, C. H.; Chen, J. H. *Nanoscale* **2013**, *5*, 3620-3626.

Chen, L. H.; Xu, S.; McBranch, D.; Whitten, D. *J. Am. Chem. Soc.* **2000**, *122*, 9302-9303.

Chinai, J. M.; Taylor, A. B.; Ryno, L. M.; Hargreaves, N. D.; Morris, C. A.; Hart, P. J. Urbach, A. R. *J. Am. Chem. Soc.* **2011**, 133, 8810–8813.

Chinen, A. B.; Guan, C. M.; Ferrer, J. R.; Barnaby, S. N.; Merkel, T. J.; Mirkin, C. A. *Chem. Rev.* **2015**, *115*, 10530-10574. **2014**, *13*, 4120-4130.

Choi, H. S.; Liu, W.; Misra, P.; Tanaka, E.; Zimmer, J. P.; Ipe, B. I.; Bawendi, M. G.; Frangioni, J. V. *Nat. Biotechnol.* **2007**, *25*, 1165-1170.

Choi, Y. E.; Kwak, J. W.; Park, J. W. *Sensors* **2010**, *10*, 428-455.

Chou, S. S.; De, M.; Luo, J.; Rotello, V. M.; Huang, J.; Dravid, V. P. *J. Am. Chem. Soc.* **2012**, *134*, 16725–16733.

Chuah, B. Y. S.; Putti, T.; Salto-Tellez, M.; Charlton, A.; Iau, P.; Buhari, S. A.; Wong, C. I.; Tan, S. H.; Wong, A. L. A.; Chan, C. W.; Goh, B. C.; Lee, S. C. *Ann. Oncol.* **2011**, *22*, 1748-1754.

Colborn, T.; Saal, F. S. V.; Soto, A. M. *Environ. Health Perspect.* **1993**, *101*, 378-384.

Dancey, J. E.; Chen, H. X. *Nature Rev. Drug Discov.* **2006**, *5*, 649-659.

De Castro, D. G.; Clarke, P. A.; Al-Lazikani, B.; Workman, P. *Clin. Pharm. Ther.* **2013**, *93*, 252-259.

De la Rica, R.; Stevens, M. M. *Nat. Nanotechnol.* **2012**, *7*, 821-824.

De, M.; Rana, S.; Akpinar, H.; Miranda, O. R.; Arvizo, R. R.; Bunz, U. H. F.; Rotello, V. M. *Nat. Chem.* **2009**, *1*, 461–465.

De, M.; Rana, S.; Rotello, V. M. *Macromol. Biosci.* **2009**, *9*, 174-178.

Diamandis, E. P. *Mol. Cell. Proteomics* **2004***, 3*, 367–378.

Downey, C. M.; Aghaei, M.; Schwendener, R. A.; Jirik, F. R. *Plos One* **2014**, *9*. e99988.

Duncan, B.; Landis, R. F.; Jerri, H. A.; Normand, V.; Benczedi, D.; Ouali, L.; Rotello, V. M. *Small* **2015**, *11*, 1302-1309.

Duncan, B.; Le, N. D. B.; Alexander, C.; Gupta, A.; Tonga G. Y.; Yazdani, M.; Landis, R. F.; Wang, L. S.; Yan, B.; Burmaoglu, S.; Li X.; Rotello, V. M. *ACS Nano* **2017**, *11,* 5339-5343.

Dunphy, K. A.; Seo, J. H.; Kim, D. J.; Roberts, A. L.; Tao, L. W.; DiRenzo, J.; Balboni, A. L.; Crisi, G. M.; Hagen, M. J.; Chandrasekaran, T.; Gauger, K. J.; Schneider, S. S.; Jerry, D. J. *Cancer Cell Int.* **2013**, *13*.

El-Boubbou, K.; Zhu, D. C.; Vasileiou, C.; Borhan, B.; Prosperi, D.; Li, W.; Huang, X. *J. Am. Chem. Soc.* **2010**, *132*, 4490–4499.

Elghanian, R.; Storhoff, J. J.; Mucic, R. C.; Letsinger, R. L.; Mirkin, C. A. *Science* **1997**, *277*, 1078-1081.

Esser, B.; Swager, T. M. *Angew. Chem., Int. Ed.* **2010**, *49*, 8872–8875.

Everley, P. A.; Krijgsveld, J.; Zetter, B. R.; Gygi, S. P. *Mol. Cell. Proteomics* **2004**, *3*, 729-735.

Feng, Y.; Mitchison, T. J.; Bender, A.; Young, D. W.; Tallarico, J. A. *Nature Rev. Drug Discov.* **2009**, *8*, 567-578.

Fernández-Olavarría, A.; Mosquera-Pérez, R.; Díaz-Sánchez, R.-M.; Serrera-Figallo, M.-A.; Gutiérrez-Pérez, J.-L.; Torres-Lagares, D. *J. Clin. Exp. Dent.* **2016**, *8*, e184-e193.

Folmer-Andersen, J. F.; Kitamura, M.; Anslyn, E. V. *J. Am. Chem. Soc.* **2006**, *128*, 5652-5653.

Freeman, W. A.; Mock, W. L.; Shih, N.-Y. *J. Am. Chem. Soc.* **1981**, *103*, 7367-7368.

Furst, A. L.; Hoepker, A. C.; Francis, M. B. *ACS Cent. Sci.* **2017**.

Geva-Zatorsky, N.; Dekel, E.; Cohen, A. A.; Danon, T.; Cohen, L.; Alon, U. *Cell* **2010**, *140*, 643-651.

Gharbi, S.; Gaffney, P.; Yang, A.; M. J. Zvelebil, Cramer, R.; Waterfield, M. D.; Timms, J. F. *Mol. Cell. Proteomics* **2002**,*1*, 91-98.

Gottesman, M. M. *Ann. Rev. Med.* **2002**, *53*, 615-627.

Grana-Suarez, L.; Verboom, W.; Huskens, J. *Chem. Commun.* **2014**, *50*, 7280-7282.

Greco, W. R.; Bravo, G.; Parsons, J. C. *Pharmacol. Rev.* **1995**, *47*, 331-385.

Guillette, L. J.; Gunderson, M. P. *Reproduction* **2001**, *122*, 857-864.

Hakim, M.; Broza, Y. Y.; Barash, O.; Peled, N.; Phillips, M.; Amann, A.; Haick, H. Chem. Rev. 2012, 112, 5949-5966.

Hakim, M.; Broza, Y. Y.; Barash, O.; Peled, N.; Phillips, M.; Amann, A.; Haick, H. *Chemical Reviews* **2012**, *112*, 5949-5966.

Han, J. S.; Bender, M.; Hahn, S.; Seehafer, K.; Bunz, U. H. F. *Chem. Eur. J.* **2016**, *22*, 3230-3233.

Han, J. S.; Wang, B. H.; Bender, M.; Kushida, S.; Seehafer, K.; Bunz, U. H. F. *ACS Appl. Mater. Interf.* **2017**, *9*, 790-797.

Han, J. S.; Wang, B. H.; Bender, M.; Pfisterer, J.; Huang, W.; Seehafer, K.; Yazdani, M.; Rotello, V. M.; Rotello, C. M.; Bunz, U. H. F. *Polym. Chem.* **2017**, *8*, 2723-2732.

Han, J. S.; Wang, B. H.; Bender, M.; Seehafer, K.; Bunz, U. H. F. *Analyst* **2017**, *142*, 537-543.

Han, J. S.; Wang, B. H.; Bender, M.; Seehafer, K.; Bunz, U. H. F. *ACS Appl. Mater. Interfaces* **2016**, *8*, 20415-20421.

Han, J. S.; Wang, B. H.; Bender, M.; Seehafer, K.; Bunz, U. H. F. Analyst 2017, 142, 537-543.

Han, J.; Bender, M.; Seehafer, K.; Bunz, U. H. F. *Angew. Chem. Int. Ed.* **2016**, *55*, 7689-7692.

Hanash, S. M. *Electrophoresis* **2000**, *21*, 1202-1209.

Hanash, S.; Taguchi, A. *Nature Reviews Cancer* **2010**, *10*, 652-660.

Hardin, J.; Rocke, D. M. *J. Comput. Graph. Stat.* **2005**, *14*, 928-946.

Heilig, B.; Hufner, M.; Dorken, B.; Schmidtgayk, H. *Klin. Wochenschr.* **1986**, *64*, 776-780.

Hellwig, M.; Henle, T. *Angew. Chemie Int. Ed.* **2014**, *53*, 10316-10329.

Herrmann, A. *Angew. Chem. Int. Ed. Engl.* **2007**, *46*, 5836-5863.
Hong, E. J.; Ji, Y. K.; Choi, K. C.; Manabe, N.; Jeung, E. B. *J. Reprod. Dev.* **2005**, *51*, 253-263.

Hostetler, M. J.; Wingate, J. E.; Zhong, C. J.; Harris, J. E.; Vachet, R. W.; Clark, M.

https://www.theguardian.com/us-news/2015/mar/09/dog-detects-thyroid-cancer-research

Hu, Q.-D.; Tang, G.-P.; Chu, P. K. *Acc. Chem. Res.* **2014**, *47*, 2017–2025.

Jeong, Y.; Duncan, B.; Park, M. H.; Kim, C.; Rotello, V. M. *Chem. Commun. (Camb).* **2011**, *47*, 12077-12079.

Jia, J.; Zhu, F.; Ma, X. H.; Cao, Z. W. W.; Li, Y. X. X.; Chen, Y. Z. *Nature Rev. Drug Discov.* **2009**, *8*, 111-128.

Jiang, H.; Pritchard, J. R.; Williams, R. T.; Lauffenburger, D. A.; Hemann, M. T. *Nature Chem. Biol.* **2011**, *7*, 92-100.

Jiang, Z. W.; Le, N. D. B.; Gupta, A.; Rotello, V. M. *Chem. Soc. Rev.* **2015**, *44*, 4264-4274.

Jiménez, D.; Martínez-Máñez, R.; Sancenón, F.; Ros-Lis, J. V.; Soto, J.; Benito, Á.; García-Breijo, E. *Eur. J. Inorg. Chem.* **2005,** *2005***,** 2393–2403.

Jiménez, D.; Martínez-Máñez, R.; Sancenón, F.; Soto, J. *Tetrahedron Lett.* **2004**, *45*, 1257–1259.

Katada, S.; Hirokawa, T.; Oka, Y.; Suwa, M.; Touhara, K. *J. Neurosci.* **2005**, *25*, 1806-1815.

Kemp, H. Ann. Clin. Biochem. **2013**, *50*, 632-632.

Kemp, H. *Ann. Clin. Biochem.* **2013**, *50*, 632-632.

Kim, C.; Tonga, G. Y.; Yan, B.; Kim, C. S.; Kim, S. T.; Park, M.-H.; Zhu, Z.; Duncan, B.; Creran, B.; Rotello, V. M. *Org. Biomol. Chem.* **2015**, *13*, 2474-2479.

Kingsmore, S. F. *Nat. Rev. Drug Discov.* **2006**, *5*, 310-320.

Kittrell, F. S.; Oborn, C. J.; Medina, D. *Cancer Res.* **1992**, *52*, 1924-1932.

Kong, H.; Liu, D.; Zhang, S. C.; Zhang, X. R. *Anal. Chem.* **2011**, *83*, 1867–1870.

Kong, H.; Liu, D.; Zhang, S. C.; Zhang, X. R. *Analytical Chemistry* **2011**, *83*, 1867-1870.

Kosaka, P. M.; Pini, V.; Ruz, J. J.; da Silva, R. A.; Gonzalez, M. U.; Ramos, D.; Calleja, M.; Tamayo, J. *Nat. Nanotechnol.* **2014**, *9*, 1047-1053

Krutzik, P. O.; Crane, J. M.; Clutter, M. R.; Nolan, G. P. *Nat. Chem. Biol.* **2008**, *4*, 132-142.

Kuhnt, T.; Herrmann, A.; Benczedi, D.; Foster, E. J.; Weder, C. *Polym. Chem.* **2015**, *6*, 6553-6562.
Kuhnt, T.; Herrmann, A.; Benczedi, D.; Weder, C.; Foster, E. J. *RSC Ad.* **2014**, *4*, 50882-50890.
Kumar, V.; Anslyn, E. V. *J. Am. Chem. Soc.* **2013**, *135*, 6338–6344.

Kwong, G. A.; von Maltzahn, G.; Murugappan, G.; Abudayyeh, O.; Mo, S.; Papayannopoulos, I. A.; Sverdlov, D. Y.; Liu, S. B.; Warren, A. D.; Popov, Y.; Schuppan, D.; Bhatia, S. N. *Nat. Biotechnol.* **2013**, *31*, 63-70.

Lamb, J.; Crawford, E. D.; Peck, D.; Modell, J. W.; Blat, I. C.; Wrobel, M. J.; Lerner, J.; Brunet, J. P.; Subramanian, A.; Ross, K. N.; Reich, M.; Hieronymus, H.; Wei, G.;

Armstrong, S. A.; Haggarty, S. J.; Clemons, P. A.; Wei, R.; Carr, S. A.; Lander, E. S.; Golub, T. R. *Science* **2006**, *313*, 1929-1935.

Lavigne, J. J.; Savoy, S.; Clevenger, M. B.; Ritchie, J. E.; McDoniel, B.; Yoo, S. J.; Anslyn, E. V.; McDevitt, J. T.; Shear, J. B.; Neikirk, D. *J. Am. Chem. Soc.* **1998**, *120*, 6429-6430.

Le, N. D. B.; Rana, S.; Rotello, V. M. *Expert Rev. Mol. Diagn.* **2013**, *13*, 111-113.

Le, N. D. B.; Tonga, G. Y.; Mout, R.; Kim, S. T.; Wille, M. E.; Rana, S.; Dunphy, K. A.; Jerry, D. J.; Yazdani, M.; Ramanathan, R.; Rotello, C. M.; Rotello V. M. *J. Am. Chem. Soc.* **2017**, *139*, 8008-8012.

Le, N. D. B.; Yazdani, M.; Rotello, V. M. *Nanomedicine* **2014**, *9*, 1487-1498.

Lee, J. W.; Samal, S.; Selvapalam, N.; Kim, H.-J.; Kim, K. *Acc. Chem. Res.* **2003**, *36*, 621–630.

Li, X. N.; Robinson, S. M.; Gupta, A.; Saha, K.; Jiang, Z. W.; Moyano, D. F.; Sahar, A.; Riley, M. A.; Rotello, V. M. *ACS Nano* **2014**, *8*, 10682-10686.
Li, X.; Kong, H.; Mout, R.; Saha, K.; Moyano, D. F.; Robinson, S. M.; Rana, S.; Zhang, X.; Riley, M. A.; Rotello, V. M. *ACS Nano* **2014**, *8*, 12014-12019.

Lilja, H.; Ulmert, D.; Vickers, A. J. *Nat. Rev. Cancer* **2008**, *8*.

Liu, B.; Bazan, G. C. *Chem. Mater.* **2004**, *16*, 4467-4476.

Loewe, S. *Arzneimittelforschung* **1953**, *3*, 285-290.

Logsdon, L. A.; Schardon, C. L.; Ramalingam, V.; Kwee, S. K.; Urbach, A. R. *J. Am. Chem. Soc.* **2011**, *133*, 17087-17092.

Lord, H.; Yu, Y. F.; Segal, A.; Pawliszyn, *J. Anal. Chem.* **2002**, *74*, 5650-5657.

Love, J. C.; Estroff, L. A.; Kriebel, J. K.; Nuzzo, R. G.; Whitesides, G. M. Chem.

Maibach, Howard I., Farzam Gorouhi, and Maibach. *Evidence Based Dermatology*. N.p.: People's Medical House USA Ltd (PMPH), 2011. Print.

Marom, O.; Nakhoul, F.; Tisch, U.; Shiban, A.; Abassi, Z.; Haick, H. *Nanomedicine* **2012**, *7*, 639-650.

Masson, E.; Ling, X.; Joseph, R.; Kyeremeh-Mensah, L.; Lu, X. *RSC Adv.* **2012**, *2*, 1213–1247.

McDonald, John H. Handbook of Biological Statistics. Baltimore, MD: Sparky House Publishing, 2009. Print.

McLachlan, J. A.; Simpson, E.; Martin, M. *Best Pract. Res. Clin. Endocrinol. Metab.* **2006**, *20*, 63-75.

McQuade, D. T.; Pullen, A. E.; Swager, T. M. *Chem. Rev.* **2000**, *100*, 2537-2574.

Metz, C. M. *Workplace Health Saf.* **2016**, *64*, 28-36.

Miller, J. C and J. N Miller. Statistics for Analytical Chemistry. Chichester: E. Horwood, 1984. Print.

Miller, K. P.; Wang, L.; Benicewicz, B. C.; Decho, A. W. *Chem. Soc. Rev.* **2015**, *44*, 7787-7807.
Miranda, O. R.; Chen, H. T.; You, C. C.; Mortenson, D. E.; Yang, X. C.; Bunz, U. H. F.; Rotello, V. M. *J. Am. Chem. Soc.* **2010**, *132*, 5285-5289.

Miranda, O. R.; Creran, B.; Rotello, V. M. *Curr. Opin. Chem. Biol.* **2010**, *14*, 728–736.

Miranda, O. R.; Li, X. N.; Garcia-Gonzalez, L.; Zhu, Z. J.; Yan, B.; Bunz, U. H. F.; Rotello, V. M. *J. Am. Chem. Soc.* **2011**, *133*, 9650-9653.

Misek, D. E.; Kim, E. H. *Int. J. Proteomics* **2011**, *2011*, 343582.

Mohapatra, H.; Phillips, S. T. *Angew. Chem. Int. Ed.* **2012**, *51*, 11145-11148.

Mulvaney, S. P.; Musick, M. D.; Keating, C. D.; Natan, M. J. *Langmuir* **2003**, *19*, 4784-4790.

Nandakumar, D. N.; Nagaraj, V. A.; Vathsala, P. G.; Rangarajan, P.; Padmanaban, G. *Antimicrob. Agents Chemother.* **2006**, *50*, 1859-1860.

Nandwana, V.; Mout, R.; Yeh, Y. C.; Dickert, S.; Tuominen, M. T.; Rotello, V. M. *J. Inorg. Organomet. Polym. Mater.* **2013**, *23*, 227-232.

Nature Med. **2010**, *16*, 347-347.

Nguyen, B. T.; Anslyn, E. V. *Coord. Chem. Rev.* **2006**, *250*, 3118-3127.

Nicholson, J. K.; Connelly, J.; Lindon, J. C.; Holmes, E. *Nature Rev. Drug Discov.* **2002**, *1*, 153-161.

O'Dwyer, D.; Ralton, L. D.; O'Shea, A.; Murray, G. I. *Plos One* **2011**, *6*.

Obeid, M.; Tesniere, A.; Ghiringhelli, F.; Fimia, G. M.; Apetoh, L.; Perfettini, J. L.; Castedo, M.; Mignot, G.; Panaretakis, T.; Casares, N.; Metivier, D.; Larochette, N.; van Endert, P.; Ciccosanti, F.; Piacentini, M.; Zitvogel, L.; Kroemer, G. *Nat. Med.* **2007**, *13*, 54-61.

OECD (Organisation for Economic Co-operation and Development), 2008. OECD Guideline for the testing of chemicals. Draft proposal for a new guideline 4XX: The stably transfected human estrogen receptor-α transcriptional activation assay for detection of estrogenic agonist-activity of chemicals.

Olansky, L.; Kennedy, L. *Diabetes Care* **2010**, *33*, 948-949.

Pai, N. P.; Vadnais, C.; Denkinger, C.; Engel, N.; Pai, M. *PLoS Med*. **2012**, *9*.

Palacios, M. A.; Nishiyabu, R.; Marquez, M.; Anzenbacher, P. *J. Am. Chem. Soc.* **2007**, *129*, 7538–7544.

Parsons, A. B.; Lopez, A.; Givoni, I. E.; Williams, D. E.; Gray, C. A.; Porter, J.; Chua, G.; Sopko, R.; Brost, R. L.; Ho, C. H.; Wang, J. Y.; Ketela, T.; Brenner, C.; Brill, J. A.; Fernandez, G. E.; Lorenz, T. C.; Payne, G. S.; Ishihara, S.; Ohya, Y.; Andrews, B.; Hughes, T. R.; Frey, B. J.; Graham, T. R.; Andersen, R. J.; Boone, C. *Cell* **2006**, *126*, 611-625.

Pei, H.; Li, H. J.; Lv., M.; Wang, J.; Gao, J.; Lu, J.; Li, Y.; Huang, Q.; Hu, J.; Fan, C. *J. Am. Chem. Soc.* **2012**, *134*, 13843–13849.

Peng, G.; Hakim, M.; Broza, Y. Y.; Billan, S.; Abdah-Bortnyak, R.; Kuten, A.; Tisch, U.; Haick, H. *Br. J. Cancer* **2010**, *103*, 542-551.

Peng, G.; Tisch, U.; Adams, O.; Hakim, M.; Shehada, N.; Broza, Y. Y.; Billan, S.; Abdah-Bortnyak, R.; Kuten, A.; Haick, H. *Nat. Nanotechnol.* **2009**, *4*, 669-673.

Peng, G.; Trock, E.; Haick, H. *Nano Lett.* **2008**, *8*, 3631-3635.

Perlman, Z. E.; Slack, M. D.; Feng, Y.; Mitchison, T. J.; Wu, L. F.; Altschuler, S. J. *Science* **2004**, *306*, 1194-1198.

Persaud, K.; Dodd, G. *Nature* **1982**, *299*, 352-355.

Phillips, R. L.; Miranda, O. R.; You, C.-C.; Rotello, V. M.; Bunz, U. H. F. *Angew. Chem. Int. Ed.* **2008**, *47*, 2590–2594.

Phillips, R. L.; Miranda, O. R.; Mortenson, D. E.; Subramani, C.; Rotello, V. M.; Bunz, U. H. F. *Soft Matter* **2009**, *5*, 607-612.

Philpott, C. M.; Wolstenholme, C. R.; Goodenough, P. C.; Clark, A.; Murty, G. E. *J. Laryngol. Otol.* **2008**, *122*, 912-917.
Poole, C. F. *Gas Chromatography*. Waltham: Elsevier. 2012. Print.

Pritchard, J. R.; Bruno, P. M.; Gilbert, L. A.; Capron, K. L.; Lauffenburger, D. A.; Hemann, M. T. *Proc. Natl. Acad. Sci. U.S.A.* **2013**, *110*, E170-E179.

Pritchard, J. R.; Bruno, P. M.; Hemann, M. T.; Lauffenburger, D. A. *Mol. Biosyst.* **2013**, *9*, 1604-1619.

Qian, X. M.; Peng, X. H.; Ansari, D. O.; Yin-Goen, Q.; Chen, G. Z.; Shin, D. M.; Yang, L.; Young, A. N.; Wang, M. D.; Nie, S. M. *Nat. Biotechnol.* **2008**, *26*, 83-90.

R Development Core Team (2010). *R: A language and environment for statistical computing. R Foundation for Statistical Computing*, Vienna, Austria. ISBN 3-900051-07-0, URL http://www.R-project.org.

R.; Londono, J. D.; Green, S. J.; Stokes, J. J.; Wignall, G. D. et al. *Langmuir* **1998**, *14*,

Rana, S.; Elci, S. G.; Mout, R.; Singla, A. K.; Yazdani, M.; Bender, M.; Bajaj, A.; Saha, K.; Bunz, U. H. F.; Jirik, F. R.; Rotello, V. M. *J. Am. Chem. Soc.* **2016**, *138*, 4522-4529.

Rana, S.; Le, N. D. B.; Mout, R.; Duncan, B.; Elci, S. G.; Saha, K.; Rotello, V. M. *Acs Cent. Sci.* **2015**, *1*, 191-197.

Rana, S.; Le, N. D. B.; Mout, R.; Saha, K.; Tonga, G. Y.; Bain, R. E. S.; Miranda, O. R.; Rotello, C. M.; Rotello, V. M. *Nat. Nanotechnol.* **2015**, *10*, 65–69.

Rana, S.; Le, N.D. B.; Mout, R.; Duncan, B.; Elci, S. G.; Saha, K.; Rotello, V. M. *ACS Cent. Sci.* **2015**, *1*, 191–197.

Rana, S.; Singla, A. K.; Bajaj, A.; Elci, S. G.; Miranda, O. R.; Mout, R.; Yan, B.; Jirik, F. R.; Rotello, V. M. *Acs Nano* **2012**, *6*, 8233-8240.

Reil, A.; Wesche, J.; Greinacher, A.; Bux, J. *Transfusion* **2011**, *51*, 18-24.

Reis-Filho, J. S.; Tutt, A. N. J. *Histopathology* **2008**, *52*, 108-118.

Rich, R. L.; Myszka, D. G. *J. Mol. Recogn.* **2008**, *21*, 355-400.

Rihel, J.; Prober, D. A.; Arvanites, A.; Lam, K.; Zimmerman, S.; Jang, S.; Haggarty, S. J.; Kokel, D.; Rubin, L. L.; Peterson, R. T.; Schier, A. F. *Science* **2010**, *327*, 348-351.

Rosi, N.; Mirkin, C. A. *Chem. Rev.* **2005**, *105*, 1547-1562.

Rusling, J. F.; Kumar, C. V.; Gutkind, J. S.; Patel, V. *Analyst* **2010**, *135*, 2496-2511.

Saha, K.; Kim, S. T.; Yan, B.; Miranda, O. R.; Alfonso, F. S.; Shlosman, D.; Rotello, V. M. *Small* **2013**, *9*, 300-305.

Sanchez, J. M.; Sacks, R. D. *Anal. Chem.* **2003**, *75*, 2231-2236.

Schirle, M.; Bantscheff, M.; Kuster, B. *Chem. Biol.* **2012**, *19*, 72-84.

Schmittel, M.; Lin, H.-W. *Angew. Chem. Int. Ed.* **2007**, *46*, 893–896.

Sela, L.; Sobel, N. *Exp. Brain Res.* **2010**, *205*, 13-29.
Sha, M. Y.; Xu, H. X.; Natan, M. J.; Cromer, R. J. Am. Chem. Soc. 2008, 130, 17214-17215.

Sha, M. Y.; Xu, H. X.; Natan, M. J.; Cromer, R. *J. Am. Chem. Soc.* **2008**, *130*, 17214-17215.

Shaner, N. C.; Steinbach, P. A.; Tsien, R. Y. *Nature Methods* **2005**, *2*, 905-909.

Shanle, E. K.; Xu, W. *Chem. Res. Toxicol.* **2011**, *24*, 6-19.

Shapiro, D. E. *Statistical Methods in Medical Research* **1999**, *8*, 113-134.

Shin, J.; Choi, S. J.; Lee, I.; Youn, D. Y.; Park, C. O.; Lee, J. H.; Tuller, H. L.; Kim, I. D. *Adv. Funct. Mater.* **2013**, *23*, 2357-2367.

Shuster, G.; Gallimidi, Z.; Reiss, A. H.; Dovgolevsky, E.; Billan, S.; Abdah-Bortnyak, R.; Kuten, A.; Engel, A.; Shiban, A.; Tisch, U.; Haick, H. *Breast Cancer Res. Treat.* **2011**, *126*, 791-796.

Šimundić, A.-M. *EJIFCC* **2009**, *19*, 203-211.

Singla, A. K.; Downey, C. M.; Bebb, G. D.; Jirik, F. R. *Oncoscience* **2015**, *2*, 263-271.

Soto, A. M.; Sonnenschein, C.; Chung, K. L.; Fernandez, M. F.; Olea, N.; Serrano, F. O. *Environ. Health. Perspect.* **1995**, *103*, 113-122.

Srinivas, P. R.; Kramer, B. S.; Srivastava, S. Lancet Oncol. 2001, 2, 698-704.

Srinivas, P. R.; Kramer, B. S.; Srivastava, S. *Lancet Oncology* **2001**, *2*, 698-704.

St John, A.; Price, C. P. *Clin. Biochem. Rev.* **2014**, *35*, 155-167.

St John, A.; Price, C. P. Clin. Biochem. Rev. 2014, 35, 155-167.

St John, A.; Price, C. P. *The Clinical Biochemist Reviews* **2014**, *35*, 155-167.

Suzuki, T.; Ide, K.; Ishida, M. *J. Pharm. Pharmacol.* **2001**, *53*, 1549-1554.

Tanaka, M.; Bateman, R.; Rauh, D.; Vaisberg, E.; Ramachandani, S.; Zhang, C.; Hansen, K. C.; Burlingame, A. L.; Trautman, J. K.; Shokat, K. M.; Adams, C. L. *PLoS Biol.* **2005**, *3*, 764-776.

Tao, Y.; Ran, X.; Ren, J.; Qu, X. *Small* **2014**, *10*, 3667–3671.

Tisch, U.; Haick, H. *Mrs Bulletin* **2010**, *35*, 797-803.

Tisch, U.; Schlesinger, I.; Ionescu, R.; Nassar, M.; Axelrod, N.; Robertman, D.; Tessler, Y.; Azar, F.; Marmur, A.; Aharon-Peretz, J.; Haick, H. *Nanomedicine* **2013**, *8*, 43-56.

Tripathi, S. M.; Bock, W. J.; Mikulic, P.; Chinnappan, R.; Ng, A.; Tolba, M.; Zourob, M. *Biosens. Bioelectron.* **2012**, *35*, 308-312.

Tsukatani, T.; Miwa, T.; Furukawa, M.; Costanzo, R. M. *Chem. Senses* **2003**, *28*, 25-32.

Turner, A. P. F.; Magan, N. *Nature Rev. Microbiol.* **2004,** *2*, 161-166.

Tyler, C. R.; Jobling, S.; Sumpter, J. P. *Crit. Rev. Toxicol.* **1998**, *28*, 319-361.

Van de Stolpe, A.; Den Toonder, J. M. J. *Cancers* **2014**, *6*, 1195-1207.

Vandenberg, L. N.; Colborn, T.; Hayes, T. B.; Heindel, J. J.; Jacobs, D. R.; Lee, D. H.; Shioda, T.; Soto, A. M.; vom Saal, F. S.; Welshons, W. V.; Zoeller, R. T.; Myers, J. P. *Endocr. Rev.* **2012**, *33*, 378-455.

Vandenberg, L. N.; Ehrlich, S.; Belcher, S. M.; Ben-Jonathan, N.; Dolinoy, D. C.; Hugo, E. R.; Hunt, P. A.; Newbold, R. R.; Rubin, B. S.; Saili, K. S.; Soto, A. M.; Wang, H.-S.; vom Saal, F. S. *Endocrine Disruptors* **2013**, *1*, e26490.

Vanparys, C.; Depiereux, S.; Nadzialek, S.; Robbens, J.; Blust, R.; Kestemont, P.; De Coen, W. *Sci. Total. Environ.***2010**, *408*, 4451-4460.

Vanparys, C.; Maras, M.; Lenjou, M.; Robbens, J.; Van Bockstaele, D.; Blust, R.; De Coen, W. *Toxicol. In Vitro* **2006**, *20*, 1238-1248.

Venables, W. N. & Ripley, B. D. (2002). *Modern Applied Statistics with S*. Fourth Edition. Springer, New York. ISBN 0-387-95457-0.

Vermes, I.; Haanen, C.; Reutelingsperger, C. *J. Immunol. Methods* **2000**, *243*, 167-190.

Wang, B.; Han, J.; Bender, M.; Seehafer, K.; Bunz, U. H. F. Macromolecules 2017.

Wang, P.; Song, C. H.; Xie, W. H.; Ye, H.; Wang, K. J.; Dai, L. P.; Zhang, Y.; Zhang, J. Y. *Journal of Immunology Research* **2014**.

Wang, Y.; Knoll, W.; Dostalek, J. *Anal. Chem.* **2012**, *84*, 8345-8350.

Wenz, G.; Han, B. H.; Müller, A. *Chem. Rev.* **2006**, *106*, 782−817.

Werner, S.; Chen, H.; Butt, J.; Michel, A.; Knebel, P.; Holleczek, B.; Zornig, I.; Eichmuller, S. B.; Jager, D.; Pawlita, M.; Waterboer, T.; Brenner, H. *Scientific Reports* **2016**, *6*.

Whitesides, G. M. *Angew. Chemie Int. Ed.* **2015**, *54*, 3196-3209.
WHO (2011) Guidelines for Drinking-Water Quality -4th ed. Geneva, Switzerland: WHO Press.

WHO, UNICEF (2014) Progress on Drinking Water and Sanitation: 2014 Update. Geneva, Switzerland: WHO Press.

Wiskur, S. L.; Floriano, P. N.; Anslyn, E. V.; McDevitt, J. T. *Angew. Chem. Int. Ed.* **2003**, *42*, 2070-2072.

Wold, S.; Esbensen, K.; Geladi, P. Principal component analysis. Chemom. *Intell. Lab. Syst.* 2(1–3), 37–52 (1987).

Wright, A. T.; Anslyn, E. V. *Chem. Soc. Rev.* **2006**, *35*, 14-28.

Wright, A. T.; Zhong, Z. L.; Anslyn, E. V. *Angew. Chem. Int. Ed.* **2005**, *44*, 5679-5682.

Wu, P.; Miao, L.-N.; Wang, H.-F.; Shao, X.-G.; Yan, X.-P. *Angew. Chem. Int. Ed.* **2011**, *50*, 8118–8121.

Wulfkuhle, J. D.; Liotta, L. A.; Petricoin, E. F. *Nat. Rev. Cancer* **2003**, *3*, 267-275.

Xu, Q.; Zhang, Y.; Tang, B.; Zhang, C.-Y. *Anal. Chem.* **2016**, *88*, 2051-2058.

Xu, X.-D.; Zhao, L.; Qu, Q.; Wang, J.-G.; Shi, H.; Zhao, Y. *ACS Appl. Mater. Interfaces* **2015**, *7*, 17371–17380.

Xu, Y. Q.; Zhang, Z. Y.; Ali, M. M.; Sauder, J.; Deng, X. D.; Giang, K.; Aguirre, S. D.; Pelton, R.; Li, Y. F.; Filipe, C. D. M. *Angew. Chem. Int. Ed.* **2014**, *53*, 2620-2622.

Xu, Z. Q.; Broza, Y. Y.; Ionsecu, R.; Tisch, U.; Ding, L.; Liu, H.; Song, Q.; Pan, Y. Y.; Xiong, F. X.; Gu, K. S.; Sun, G. P.; Chen, Z. D.; Leja, M.; Haick, H. *Br. J. Cancer* **2013**, *108*, 941-950.

Yang, O.; Kim, H. L.; Weon, J. I. *J. Cancer Prev.* **2015**, *20*, 12-24.

Yang, S. K.; Ambade, A. V.; Weck, M. *J. Am. Chem. Soc.* **2010**, *132*, 1637-1645.

Yang, W.; Zerbe, H.; Petzl, W.; Brunner, R. M.; Guenther, J.; Draing, C.; von Aulocke, S.; Schuberth, H. J.; Seyfert, H. M. *Mol. Immunol.* **2008**, *45*, 1385-1397.

Yeh, Y.-C.; Rana, S.; Mout, R.; Yan, B.; Alfonso, F. S.; Rotello, V. M. *Chem. Commun.* **2014**, 50, 5565-5568.

Yoon, H. I.; Kwon, O.-R.; Kang, K. N.; Shin, Y. S.; Shin, H. S.; Yeon, E. H.; Kwon, K. Y.; Hwang, I.; Jeon, Y. K.; Kim, Y.; Kim, C. W. *Journal of Cancer Prevention* **2016**, *21*, 187-193.

You, C-C.; Miranda, O. R.; Gider, B.; Ghosh, P. S.; Kim, IK-B.; Erdogan, B.; Krovi, S. A.; Bunz, U. H. F.; Rotello, V. M. *Nat. Nanotechnol.* **2007**, *2*, 318–323.

You, C. C.; De, M.; Han, G.; Rotello, V. M. *J. Am. Chem. Soc.* **2005**, *127*, 12873-12881.

Young, D. W.; Bender, A.; Hoyt, J.; McWhinnie, E.; Chirn, G. W.; Tao, C. Y.; Tallarico, J. A.; Labow, M.; Jenkins, J. L.; Mitchison, T. J.; Feng, Y. *Nature Chem. Biol.* **2008**, *4*, 59-68.

Yuan, Z.; Du, Y.; Tseng, Y.-T.; Peng, M.; Cai, N.; He, Y.; Chang, H.-T.; Yeung, E. S. *Anal. Chem.* **2015**, *87*, 4253–4259.

Zacharewski, T. *Environ. Sci. Technol.* **1997**, *31*, 613-623.

Zhao, J.; Zhang, Y. M.; Sun, H. L.; Chang, X. Y.; Liu, Y. *Chem. Eur. J.* **2014**, *20*, 15108-15115.

Zhou, H.; Baldini, L.; Hong, J.; Wilson, A. J.; Hamilton, A. D. *J. Am. Chem. Soc.* **2006**, *128*, 2421–2425.

Zhu, J. J.; Djukovic, D.; Deng, L. L.; Gu, H. W.; Himmati, F.; Chiorean, E. G.; Raftery, D. *J. Proteome Res.* **2014**, *13*, 4120-4130.

Zhu, Y. L.; Wang, A. T.; Liu, M. C.; Zwart, A.; Lee, R. Y.; Gallagher, A.; Wang, Y.; Miller, W. R.; Dixon, J. M.; Clarke, R. *Int. J. Oncol.* **2006**, *29*, 1581-1589.